

*International Journal of*  
Numerical Methods  
for Heat & Fluid  
Flow

**Boundary element method**

**Part I: heat transfer**

Guest Editor: Professor Luiz C. Wrobel



---

# International Journal of Numerical Methods for Heat & Fluid Flow

ISSN 0961-5539

Volume 13  
Number 5  
2003

Boundary element method. Part I : heat transfer

Guest Editor

Professor Luiz C. Wrobel

<b>Access this journal online</b> _____	<b>523</b>
<b>Editorial advisory board</b> _____	<b>524</b>
<b>Abstracts and keywords</b> _____	<b>525</b>
<b>Preface</b> _____	<b>527</b>
<b>A comparison of different regularization methods for a Cauchy problem in anisotropic heat conduction</b> <i>N.S. Mera, L. Elliott, D.B. Ingham and D. Lesnic</i> _____	<b>528</b>
<b>Inverse analysis of continuous casting processes</b> <i>Iwona Nowak, Andrzej J. Nowak and Luiz C. Wrobel</i> _____	<b>547</b>
<b>Optimization of a window frame by BEM and genetic algorithm</b> <i>Malgorzata Król and Ryszard A. Bialecki</i> _____	<b>565</b>
<b>BEM/FVM conjugate heat transfer analysis of a three-dimensional film cooled turbine blade</b> <i>A. Kassab, E. Divo, J. Heidmann, E. Steinthorsson and F. Rodriguez</i> _____	<b>581</b>

---

## CONTENTS

---

### Access this journal electronically

The current and past volumes of this journal are available at

**[www.emeraldinsight.com/ft](http://www.emeraldinsight.com/ft)**

You can access over 100 additional Emerald journals, each with a comprehensive searchable archive of articles (many dating back to 1989), a detailed classification system and links to referenced material.

See previous issue contents for full details of what your access includes.



---

**CONTENTS***continued*

<b>RBF interpolation of boundary values in the BEM for heat transfer problems</b>	
<i>Nam Mai-Duy and Thanh Tran-Cong</i> _____	<b>611</b>
<b>Dual reciprocity boundary element analysis of transient advection-diffusion</b>	
<i>Krishna M. Singh and Masataka Tanaka</i> _____	<b>633</b>
<b>Awards for Excellence</b> _____	<b>647</b>

# Access this journal online

[www.emeraldinsight.com/hff.htm](http://www.emeraldinsight.com/hff.htm)



As a subscriber to this journal, you can benefit from instant, electronic access to the content of this title. Your access includes a variety of features that increase the value of your journal subscription.

## Automatic permission to make up to 25 copies of individual articles

This facility can be used for teaching purposes, training courses, meetings or seminars. This only applies to articles of which Emerald owns copyright. For further details visit [www.emeraldinsight.com/copyright](http://www.emeraldinsight.com/copyright)

## How to access this journal electronically

To benefit from electronic access to this journal you first need to register on the Internet. Registration is simple and full instructions are available online at [www.emeraldinsight.com/register](http://www.emeraldinsight.com/register) Once completed, your institution will have instant access to the journal content from [www.emeraldinsight.com](http://www.emeraldinsight.com) or via the journal homepage [www.emeraldinsight.com/hff.htm](http://www.emeraldinsight.com/hff.htm)

Our liberal institution-wide licence allows everyone within your institution to access your journal electronically, thus making your subscription more cost-effective. Our Web site has been designed to provide you with a comprehensive, simple system that needs only minimum administration. Access is available via IP authentication or username and password.

## Key features of Emerald electronic journals

### Online Publishing and Archiving

You can gain access to past volumes as well as new material from this journal on the Internet via Emerald Fulltext. You can browse or search the database for relevant articles.

### Key Reading

This feature provides abstracts of articles chosen by the journal editor on the basis of their subject-matter. These are selected to provide readers with current awareness of interesting articles from other publications within the same field.

### Reference Linking

Direct links are provided from the journal article references to abstracts of the most influential articles cited (where possible this is to the full text of the article).

### E-mail an Article

This facility allows you to e-mail relevant and interesting articles in PDF format to another PC for later use, reference or printing purposes.

## Additional Complementary Services Available

Your access includes a variety of features that add to the functionality and value of your journal subscription:

### E-mail Services

Emerald's range of free e-mail alerting services is designed to deliver personal notification of news and features in a number of different interest areas.

### Research Register

Located at [www.emeraldinsight.com/researchregister](http://www.emeraldinsight.com/researchregister), the Emerald Research Register is an Internet research forum where you and your readers can identify information on research activity world-wide. This feature is invaluable if you are seeking information or wish to disseminate information about your own research.

### Support Resources

Comprehensive librarian and user toolkits have been created to help you get the most from your journal subscription. For further information about what is available visit [www.emeraldinsight.com/usertoolkit](http://www.emeraldinsight.com/usertoolkit)

### Choice of Access

Electronic access to this journal is available via a number of channels, enabling end users and libraries to reach the content through their preferred delivery system. The Emerald Fulltext Web site – [www.emeraldinsight.com/ft](http://www.emeraldinsight.com/ft) – is the recommended means of electronic access, as it provides fully searchable and high value-added access to the complete content of the journal.

Subscribers can also access and search the article content of this journal through the following journal delivery services:

#### EBSCOhost EJS

[journals.ebsco.com](http://journals.ebsco.com)

#### Huber E-Journals

[e-journals.hanshuber.com/english/index.htm](http://e-journals.hanshuber.com/english/index.htm)

#### Minerva

[www.minerva.at](http://www.minerva.at)

#### OCLC Firstsearch Electronic Collections Online

[www.uk.oclc.org/oclc/menu/eco.htm](http://www.uk.oclc.org/oclc/menu/eco.htm)

#### RoweCom's Information Quest

[www.informationquest.com](http://www.informationquest.com)

#### SilverPlatter

[www.silverplatter.com](http://www.silverplatter.com)

#### SwetsBlackwell's SwetsWise

[www.swetswise.com](http://www.swetswise.com)

## Emerald Customer Support Services

For customer service and technical help, contact:

E-mail [support@emeraldinsight.com](mailto:support@emeraldinsight.com)

Tel +44 (0) 1274 785278

Fax +44 (0) 1274 785204



EDITORIAL ADVISORY BOARD

**M. Bellet**

CEMEF, Ecole Nationale Supérieure des Mines de Paris,  
Sophia Antipolis, Valbonne 06560, France

**G.F. Carey**

College of Engineering, University of Texas at Austin,  
Austin, Texas 78712-1085, USA

**R. Codina**

Resistencia de los Materiales y Estructuras en Ingeniería,  
Universitat Politècnica de Catalunya, Jordi Girona 1-3,  
Edifici C1, 08034 Barcelona, Spain

**Gianni Comini**

Dipt di Energetica e Macchine, Università degli Studi di  
Udine, Via delle Scienze 208, Udine 33100, Italy

**R.M. Cotta**

Department of Mechanical Engineering, EE/COPPE/UF RJ,  
CX Postal 68503, Cicade Universitaria, Rio de Janeiro, RJ,  
Brazil

**Marcela Cruchaga**

Departamento de Ingeniería Mecánica, Universidad de  
Santiago de Chile, Santiago de Chile

**G. De Vahl Davis**

University of New South Wales, Sydney, NSW,  
Australia 2052

**E. Dick**

Department of Machinery, State University of Ghent, Sint  
Pietersnieuwstraat 41, B-9000 Ghent, Belgium

**Amir Faghri**

Mechanical Engineering Department, University of  
Connecticut, 191 Auditorium Road, U-139, Storrs,  
Connecticut 06269-3139, USA

**D. Gethin**

Department of Mechanical Engineering, University of  
Wales Swansea, Singleton Park, Swansea SA2 8PP, UK

**Dan Givoli**

Faculty of Aerospace Engineering, Technion – Israel  
Institute of Technology, 32000, Haifa, Israel

**M.A. Hogge**

L.T.A.S. Thermomécanique, University of Liège, Rue E  
Solvay 21, B-4000 Liège, Belgium

**D.B. Ingham**

Department of Applied Mathematical Studies, University  
of Leeds, Leeds LS2 9JT, UK

**Y. Jaluria**

Department of Mechanical & Aerospace Engineering,  
Rutgers University, PO Box 909, Piscataway, New Jersey  
08855, USA

**M.A. Keavey**

Nuclear Electric plc, Berkeley Nuclear Laboratories,  
Berkeley, Gloucester GL13 9PB, UK

**T.G. Keith Jr**

Department of Mechanical Engineering, The University of  
Toledo, Toledo, Ohio 43606, USA

**R.E. Khayat**

Dept of Mechanical & Materials Engineering, University of  
Western Ontario, London, Ontario, Canada N6A 5B9

**R. Lohner**

GMU/CSI, MS 5C3 Dept of Civil Engineering, George  
Mason University, Fairfax, VA 22030-4444, USA

**N.C. Markatos**

Department of Chemical Engineering, National Technical  
University of Athens, 9 Heron Polytechniou Str., Zografou  
Campus, GR-157 73 Athens, Greece

**K. Morgan**

Department of Civil Engineering, University College of  
Swansea, Swansea SA2 8PP, UK

**M. Napolitano**

Istituto di Macchine ed Energetica, Politecnico di Bari, Via  
Re David 200, I-70125 Bari, Italy

**C. Nonino**

Dipartimento di Energetica e Macchine, Università degli  
Studi di Udine, Via delle Scienze 208, 33100 Udine, Italy

**J. Peiro**

Dept of Aeronautics, Imperial College of Science & Tech,  
Prince Consort Road, London SW7 2BY

**F.G. Rammerstorfer**

Institut für Leichtbau und Flugzeugbau, Technische  
Universität Wien, Gusshausstrasse 27-29 317, A-1040  
Wien, Austria

**R.S. Ransing**

Dept of Mechanical Engineering, University of Wales  
Swansea, Singleton Park, Swansea SA2 8PP

**B. Sarler**

Faculty of Mechanical Engineering, University of  
Ljubljana, Askerceva 6, 1000 Ljubljana, Slovenia

**K.N. Seetharamu**

School of Mechanical Engineering, University of Science  
Malaysia (KCP), Tronoh, Malaysia

**Wei Shyy**

Department of Mechanical and Aerospace Engineering,  
University of Florida, Gainesville, Florida, USA

**D.B. Spalding**

CHAM, Bakery House, 40 High Street, Wimbledon Village,  
London SW19 5AU, UK

**B. Sundén**

Lund Institute of Technology, Heat Transfer Division, Box  
118, S-221 00 Lund, Sweden

**K.K. Tamma**

Department of Mechanical Engineering, 125 Mech. Engrg,  
University of Minnesota, 111 Church Street SE,  
Minneapolis, Minnesota 55455, USA

**J.A. Visser**

Department of Mechanical Engineering, University of  
Pretoria, Pretoria 0002, South Africa

**V.R. Voller**

Civil Engineering, University of Minnesota, 500 Pillsbury  
Drive, Minneapolis, Minnesota 55455-0220, USA

**L.C. Wrobel**

Department of Mechanical Engineering, Brunel University,  
Uxbridge 4BS 3PH, UK

**A comparison of different regularization methods for a Cauchy problem in anisotropic heat conduction**

*N.S. Mera, L. Elliott, D.B. Ingham and D. Lesnic*

**Keywords** Boundary element method, Heat conduction

In this paper various regularization methods are numerically implemented using the boundary element method (BEM) in order to solve the Cauchy steady-state heat conduction problem in an anisotropic medium. The convergence and the stability of the numerical methods are investigated and compared. The numerical results obtained confirm that stable numerical results can be obtained by various regularization methods but if high accuracy is required for the temperature, or if the heat flux is also required, then care must be taken when choosing the regularization method since the numerical results are substantially improved by choosing the appropriate method.

**Inverse analysis of continuous casting processes**

*Iwona Nowak, Andrzej J. Nowak and Luiz C. Wrobel*

**Keywords** Inverse problems, Boundary element method, Sensitivity, Casting, Metals

This paper discusses an algorithm for phase change front identification in continuous casting. The problem is formulated as an inverse geometry problem, and the solution procedure utilizes temperature measurements inside the solid phase and sensitivity coefficients. The proposed algorithms make use of the boundary element method, with cubic boundary elements and Bezier splines employed for modelling the interface between the solid and liquid phases. A case study of continuous casting of copper is solved to demonstrate the main features of the proposed algorithms.

**Optimization of a window frame by BEM and genetic algorithm**

*Malgorzata Król and Ryszard A. Bialecki*

**Keywords** Boundary elements, Genetic algorithms, Heat transfer, Windows  
Genetic algorithms and boundary elements have been used to find an optimal design of a

plastic window frame with air chambers and steel stiffeners. The objective function has been defined as minimum heat loss subject to a constraint of prescribed stiffness and weight of the steel insert.

**BEM/FVM conjugate heat transfer analysis of a three-dimensional film cooled turbine blade**

*A. Kassab, E. Divo, J. Heidmann, E. Steinthorsson and F. Rodriguez*

**Keywords** Heat transfer, Coupled phenomena, Boundary elements, Finite volume

We report on the progress in the development and application of a coupled boundary element/finite volume method temperature-forward/flux-back algorithm developed to solve conjugate heat transfer arising in 3D film-cooled turbine blades. We adopt a loosely coupled strategy where each set of field equations is solved to provide boundary conditions for the other. Iteration is carried out until interfacial continuity of temperature and heat flux is enforced. The NASA-Glenn explicit finite volume Navier-Stokes code Glenn-HT is coupled to a 3D BEM steady state heat conduction solver. Results from a CHT simulation of a 3D film-cooled blade section are compared with those obtained from the standard two temperature model, revealing that a significant difference in the level and distribution of metal temperatures is found between the two. Finally, current developments of an iterative strategy accommodating large numbers of unknowns by a domain decomposition approach is presented. An iterative scheme is developed along with a physically-based initial guess and a coarse grid solution to provide a good starting point for the iteration. Results from a 3D simulation show the process that converges efficiently and offers substantial computational and storage savings.

**RBF interpolation of boundary values in the BEM for heat transfer problems**

*Nam Mai-Duy and Thanh Tran-Cong*

**Keywords** Boundary element method, Boundary integral equation, Heat transfer

This paper is concerned with the application of radial basis function networks (RBFNs) as

interpolation functions for all boundary values in the boundary element method (BEM) for the numerical solution of heat transfer problems. The quality of the estimate of boundary integrals is greatly affected by the type of functions used to interpolate the temperature, its normal derivative and the geometry along the boundary from the nodal values. In this paper, instead of conventional Lagrange polynomials, interpolation functions representing these variables are based on the "universal approximator" RBFNs, resulting in much better estimates. The proposed method is verified on problems with different variations of temperature on the boundary from linear level to higher orders. Numerical results obtained show that the BEM with indirect RBFN (IRBFN) interpolation performs much better than the one with linear or quadratic elements in terms of accuracy and convergence rate. For example, for the solution of Laplace's equation in 2D, the BEM can achieve the norm of error of the boundary solution of  $O(10^{-5})$  by using IRBFN interpolation while quadratic BEM can achieve a norm only of  $O(10^{-2})$  with the same boundary points employed. The IRBFN-BEM also appears to have achieved a higher efficiency. Furthermore, the convergence rates are of  $O(h^{1.38})$  and  $O(h^{4.78})$  for the quadratic BEM and the IRBFN-based

BEM, respectively, where  $h$  is the nodal spacing.

### **Dual reciprocity boundary element analysis of transient advection-diffusion**

*Krishna M. Singh and Masataka Tanaka*

**Keywords** Boundary element method, Plates, Approximation concepts

This paper presents an application of the dual reciprocity boundary element method (DRBEM) to transient advection-diffusion problems. Radial basis functions and augmented thin plate splines (TPS) have been used as coordinate functions in DRBEM approximation in addition to the ones previously used in the literature. Linear multistep methods have been used for time integration of differential algebraic boundary element system. Numerical results are presented for the standard test problem of advection-diffusion of a sharp front. Use of TPS yields the most accurate results. Further, considerable damping is seen in the results with one step backward difference method, whereas higher order methods produce perceptible numerical dispersion for advection-dominated problems.

---

# Preface

Preface

This special issue of the *International Journal of Numerical Methods for Heat & Fluid Flow* comprises six papers dealing with the novel formulations and applications of the boundary element method (BEM) for heat transfer problems. The BEM is now a well-established numerical technique for the analysis of many engineering problems. The basis of the technique is to transform the original partial differential equation of the problem into an equivalent integral equation by means of the Green's theorems and fundamental solutions (or Green's functions). The resulting boundary integral equation only requires discretisation along the boundaries and surface integrations, providing some modelling advantages.

527

---

The first three papers in this issue all deal with the application of inverse analysis and optimisation techniques to heat conduction problems, reflecting an area of growing popularity of the BEM. Mera *et al.* discusses different regularization methods for a Cauchy problem in anisotropic heat conduction, Nowak *et al.* deals with the inverse analysis of continuous casting processes, while Krol and Bialecki derive a formulation based on genetic algorithms for the optimisation of a window frame design. The next paper by Kassab *et al.* develops a coupled BEM/FVM formulation for the conjugate heat transfer analysis of a three-dimensional film cooled turbine blade, and demonstrates the efficiency of such a combination. The final two papers, by Mai-Duy and Tran-Cong, and Singh, and Tanaka, show novel BEM formulations for the efficient and accurate evaluation of the boundary integrals, and for the numerical treatment of transient advection-diffusion problems, respectively.

I am indebted to the authors for their contributions to this special issue, and for their cooperation and support. It is hoped that this volume will contribute to increasing the awareness of the journal readership to this powerful numerical technique which presents a number of advantages for the solution of several heat transfer problems, particularly those involving moving boundaries and inverse analysis.

**Professor Luiz Wrobel**  
*Brunel University*



HF  
13,5

528

Received December 2001  
Revised July 2002  
Accepted January 2003

# A comparison of different regularization methods for a Cauchy problem in anisotropic heat conduction

N.S. Mera, L. Elliott, D.B. Ingham and D. Lesnic  
*Department of Applied Mathematics, University of Leeds, UK*

**Keywords** *Boundary element method, Heat conduction*

**Abstract** *In this paper, various regularization methods are numerically implemented using the boundary element method (BEM) in order to solve the Cauchy steady-state heat conduction problem in an anisotropic medium. The convergence and the stability of the numerical methods are investigated and compared. The numerical results obtained confirm that stable numerical results can be obtained by various regularization methods, but if high accuracy is required for the temperature, or if the heat flux is also required, then care must be taken when choosing the regularization method since the numerical results are substantially improved by choosing the appropriate method.*

## 1. Introduction

Many natural and man-made materials cannot be considered isotropic and the dependence of the thermal conductivity with direction has to be taken into account in the modelling of the heat transfer. For example, crystals, wood, sedimentary rocks, metals that have undergone heavy cold pressing, laminated sheets, composites, cables, heat shielding materials for space vehicles, fibre reinforced structures, and many others are examples of anisotropic materials. Composites are of special interest to the aerospace industry because of their strength and reduced weight. Therefore, heat conduction in anisotropic materials has numerous important applications in various branches of science and engineering and hence its understanding is of great importance.

If the temperature or the heat flux on the surface of a solid  $\Omega$  is given, then the temperature distribution in the domain can be calculated, provided the temperature is specified at least at one point. However, in the direct problem, many experimental impediments may arise in measuring or in the enforcing of the given boundary conditions. There are many practical applications which arise in engineering where a part of the boundary is not accessible for temperature or heat flux measurements. For example, the temperature or the heat flux measurement may be seriously affected by the presence of the sensor and hence there is a loss of accuracy in the measurement, or, more simply, the surface of the body may be unsuitable for attaching a sensor to measure



---

the temperature or the heat flux. The situation when neither the temperature nor the heat flux can be prescribed on a part of the boundary while both of them are known on the other part leads in the mathematical formulation to an ill-posed problem which is termed as “the Cauchy problem”.

This problem is much more difficult to solve both numerically and analytically since its solution does not depend continuously on the prescribed boundary conditions. Violation of the stability of the solution creates serious numerical problems since the system of linear algebraic equations obtained by discretising the problem is ill-conditioned. Therefore, a direct method to solve this problem cannot be used since such an approach would produce a highly unstable solution. A remedy for this is the use of regularization methods which attempt to find the right compromise between accuracy and stability.

Currently, there are various methods to deal with ill-posed problems. However, their performance depends on the particular problem being solved. Therefore, it is the purpose of this paper to investigate and compare several regularization methods for a Cauchy anisotropic heat conduction problem. There are different methods to solve an ill-posed problem such as the Cauchy problem. One approach is to use the general regularization methods such as Tikhonov regularization, truncated singular value decomposition, conjugate gradient method, etc. On the other hand, specific regularization methods can be developed for particular problems in order to make use of the maximum amount of information available. The use of any extra information available for a specific problem is particularly important in choosing the regularization parameter of the method employed. Both general regularization and specific regularization methods developed for the Cauchy problems are considered in this paper.

These methods are investigated and compared in order to reveal their performance and limitation. All the methods employed are numerically implemented using the boundary element method (BEM) since it was found that this method performs better for linear partial differential equations with constant coefficients than other domain discretisation methods. Numerical results are given in order to illustrate and compare the convergence, accuracy and stability of the methods employed.

## 2. Mathematical formulation

Consider an anisotropic medium in an open bounded domain  $\Omega \subset \mathbb{R}^2$  and assume that  $\Omega$  is bounded by a curve  $\Gamma$  which may consist of several segments, each being sufficiently smooth in the sense of Liapunov. We also assume that the boundary consists of two parts,  $\partial\Omega = \Gamma = \Gamma_1 \cup \Gamma_2$ , where  $\Gamma_1, \Gamma_2 \neq \emptyset$  and  $\Gamma_1 \cap \Gamma_2 = \emptyset$ . In this study, we refer to steady heat conduction applications in anisotropic homogeneous media and we assume that heat generation is absent. Hence the function  $T$ , which denotes the temperature distribution in  $\Omega$ , satisfies the anisotropic steady-state heat conduction equation, namely,

$$LT = \sum_{i,j=1}^2 k_{ij} \frac{\partial^2 T}{\partial x_i \partial x_j} = 0, \quad \underline{x} \in \Omega \quad (1)$$

where  $k_{ij}$  is the constant thermal conductivity tensor which is assumed to be symmetric and positive-definite so that equation (1) is of the elliptic type. When  $k_{ij} = \delta_{ij}$ , where  $\delta_{ij}$  is the Kronecker delta symbol, we obtain the isotropic case and  $T$  satisfies the Laplace equation

$$\nabla^2 T(\underline{x}) = 0, \quad \underline{x} \in \Omega \quad (2)$$

In the direct problem formulation, if the temperature and/or heat flux on the boundary  $\Gamma$  is given then the temperature distribution in the domain can be calculated, provided that the temperature is specified at least at one point. However, many experimental impediments may arise in measuring or enforcing a complete boundary specification over the whole boundary  $\Gamma$ . The situation when neither the temperature nor the heat flux can be prescribed on a part of the boundary while both of them are known on the other part leads to the mathematical formulation of an inverse problem consisting of equation (1) which has to be solved subject to the boundary conditions

$$T(\underline{x}) = f(\underline{x}) \quad \text{for } \underline{x} \in \Gamma_1 \quad (3)$$

$$\frac{\partial T}{\partial \nu^+}(\underline{x}) = q(\underline{x}) \quad \text{for } \underline{x} \in \Gamma_1 \quad (4)$$

where  $f, q$  are prescribed functions,  $\partial/\partial \nu^+$  is given by

$$\frac{\partial}{\partial \nu^+} = \sum_{i,j=1}^2 k_{ij} \cos(\nu, x_i) \frac{\partial}{\partial x_j} \quad (5)$$

and  $\cos(\nu, x_i)$  are the direction cosines of the outward normal vector  $\nu$  to the boundary  $\Gamma$ . In the above formulation of the boundary conditions (3) and (4) it can be seen that the boundary  $\Gamma_1$  is overspecified by prescribing both the temperature  $f$  and the heat flux  $q$ , whilst the boundary  $\Gamma_2$  is underspecified since both the temperature  $T|_{\Gamma_2}$  and the heat flux

$$\frac{\partial T}{\partial \nu^+} |_{\Gamma_2}$$

are unknown and have to be determined.

This problem, termed the Cauchy problem, is much more difficult to solve both analytically and numerically than the direct problem since the solution does not satisfy the general conditions of well-posedness. Although the problem may have a unique solution, it is well-known (Hadamard, 1923) that

this solution is unstable with respect to the small perturbations in the data on  $\Gamma_1$ . Thus, the problem is ill-posed and we cannot use a direct approach, e.g. Gaussian elimination method, to solve the system of linear equations which arise from discretising the partial differential equations (1) or (2) and the boundary conditions (3) and (4). Therefore, regularization methods are required in order to accurately solve this Cauchy problem.

### 3. Regularization methods

#### 3.1 Truncated singular value decomposition

Consider the ill-conditioned system of equations

$$\mathbb{C}\underline{X} = \underline{d} \quad (6)$$

where  $\mathbb{C} \in \mathbb{R}^{M \times N}$ ,  $\underline{X} \in \mathbb{R}^N$ ,  $\underline{d} \in \mathbb{R}^M$  and  $M \geq N$ .

The singular value decomposition (SVD) of the matrix  $\mathbb{C} \in \mathbb{R}^{M \times N}$  is given by

$$\mathbb{C} = \mathbb{W}\mathbb{X}\mathbb{V}^T = \sum_{i=1}^N \underline{w}_i \sigma_i \underline{v}_i^T \quad (7)$$

where  $\mathbb{W} = \text{col}[\underline{w}_1, \dots, \underline{w}_M] \in \mathbb{R}^{M \times M}$ , and  $\mathbb{V} = \text{col}[\underline{v}_1, \dots, \underline{v}_N] \in \mathbb{R}^{N \times N}$  are orthogonal matrices

$$\mathbb{X} = \begin{pmatrix} \mathbb{S} \\ 0_{M-N} \end{pmatrix} \quad \text{if } M > N$$

$$\mathbb{X} = \mathbb{S} \quad \text{if } M = N$$

and the diagonal matrix  $\mathbb{S} = \text{diag}[\sigma_1, \dots, \sigma_N]$  has a non-negative diagonal elements ordered such that

$$\sigma_1 \geq \sigma_2 \geq \sigma_3 \geq \dots \geq \sigma_N \geq 0 \quad (8)$$

The non-negative quantities  $\sigma_i$  are called the *singular values of the matrix*  $\mathbb{C}$ . The number of positive singular values of  $\mathbb{C}$  is equal to the rank of the matrix  $\mathbb{C}$ . In the ideal setting, without perturbation and rounding errors, the treatment of the ill-conditioned system of equation (6) is straightforward, namely, we simply ignore the SVD components associated with the zero singular values and compute the solution of the system by means of

$$\underline{X} = \sum_{i=1}^{\text{rank}(\mathbb{C})} \frac{\underline{w}_i^T \underline{d}}{\sigma_i} \underline{v}_i \quad (9)$$

In practice, noise is always present in the problem and the vector  $\underline{d}$  and the matrix  $\mathbb{C}$  are only known approximately. Therefore, if some of the singular

values of  $\mathbb{C}$  are non-zero, but very small, instability arises due to division by these small singular values in expression (9). One way to overcome this instability is to modify the inverses of the singular values in expression (9) by multiplying them by a *regularizing filter function*  $f_\lambda(\sigma_i)$  for which the product  $f_\lambda(\sigma)/\sigma \rightarrow 0$  as  $\sigma \rightarrow 0$ . This filters out the components of the sum (9) corresponding to small singular values and yields an approximation for the solution of the problem with the representation

$$\underline{X}_\lambda = \sum_{i=1}^{\text{rank}(\mathbb{C})} \frac{f_\lambda(\sigma_i)}{\sigma_i} (\underline{w}_i^T \underline{d}) \underline{v}_i \quad (10)$$

To obtain some degree of accuracy, one must retain singular components corresponding to large singular values. This is done by taking  $f_\lambda(\sigma) \approx 1$  for large values of  $\sigma$ . An example of such a filter function is

$$f_\lambda(\sigma) = \begin{cases} 1 & \text{if } \sigma^2 > \lambda \\ 0 & \text{if } \sigma^2 \leq \lambda \end{cases} \quad (11)$$

The approximation (10) then takes the form

$$\underline{X}_\lambda = \sum_{\sigma_i^2 > \lambda} \frac{1}{\sigma_i} (\underline{w}_i^T \underline{d}) \underline{v}_i \quad (12)$$

and it is known as the truncated singular value decomposition (TSVD) solution of the problem (6). For different filter functions,  $f_\lambda$ , different regularization methods are obtained, see Section 3.2. A stable and accurate solution is then obtained by matching the regularization parameter  $\lambda$  to the level of the noise present in the problem to be solved.

### 3.2 Tikhonov regularization

In this section, we give a brief description of the Tikhonov regularization method. For further details on this method, we refer the reader to Tikhonov and Arsenin (1977) and Tikhonov *et al.* (1995).

Again consider the ill-conditioned system of equation (6). The Tikhonov regularized solution of the ill-conditioned system (6) is given by

$$\underline{X}_\lambda : T_\lambda(\underline{X}_\lambda) = \min \{ T_\lambda(\underline{X}) | \underline{X} \in \mathbb{R}^N \} \quad (13)$$

where  $T_\lambda$  represents the Tikhonov functional given by

$$T_\lambda(\underline{X}) = \|\mathbb{C}\underline{X} - \underline{d}\|_2^2 + \lambda^2 \|\mathbb{L}\underline{X}\|_2^2 \quad (14)$$

and  $\mathbb{L} \in \mathbb{R}^{N \times N}$  induces the smoothing norm  $\|\mathbb{L}\underline{X}\|_2$  with  $\lambda \in \mathbb{R}$ , the regularization parameter to be chosen. The problem is in the standard form,

also referred to as Tikhonov regularization of order zero, if the matrix  $\mathbb{L}$  is the identity matrix  $\mathbb{I}_N \in \mathbb{R}^{N \times N}$ .

Formally, the Tikhonov regularized solution  $\underline{X}_\lambda$  is given as the solution of the regularized equation

$$(\mathbb{C}^T \mathbb{C} + \lambda^2 \mathbb{L}^T \mathbb{L}) \underline{X} = \mathbb{C}^T \underline{d} \quad (15)$$

However, the best way to solve equation (13) numerically is to treat it as a least squares problem of the form

$$\underline{X}_\lambda : T_\lambda(\underline{X}_\lambda) = \min_{\underline{X} \in \mathbb{R}^N} \left\| \begin{pmatrix} \mathbb{C} \\ \lambda \mathbb{L} \end{pmatrix} \underline{X} - \begin{pmatrix} \underline{d} \\ 0 \end{pmatrix} \right\|_2 \quad (16)$$

Regularization is necessary when solving inverse problems because the simple least squares solution obtained when  $\lambda = 0$  is completely dominated by the contributions from the data and rounding errors. By adding regularization, we are able to damp out these contributions and maintain the norm  $\|\mathbb{L} \underline{X}\|_2$  to be of reasonable size. If too much regularization, or smoothing, is imposed on the solution, then it will not fit the given data  $\underline{d}$  and the residual norm  $\|\mathbb{C} \underline{X} - \underline{d}\|_2$  will be too large. If too little regularization is imposed on the solution, then the fit will be good, but the solution will be dominated by the contributions from the data errors, and hence  $\|\mathbb{L} \underline{X}\|_2$  will be too large. In this paper, we assume that  $\mathbb{L} = \mathbb{I}_N$ , i.e. we consider Tikhonov regularization of order zero.

If we insert the SVD (7) into the least squares formulation (15), then we obtain

$$\mathbb{V}(\mathbb{X}^2 + \lambda^2 \mathbb{I}) \mathbb{V}^T \underline{X}_\lambda = \mathbb{V} \mathbb{X}^T \mathbb{W}^T \underline{d} \quad (17)$$

Solving equation (17) for  $\underline{X}_\lambda$ , we obtain

$$\underline{X}_\lambda = [\mathbb{V}(\mathbb{X}^2 + \lambda^2 \mathbb{I}) \mathbb{V}^T]^\dagger \mathbb{V} \mathbb{X} \mathbb{W}^T \underline{d} = \mathbb{V}(\mathbb{X}^2 + \lambda^2 \mathbb{I})^\dagger \mathbb{X} \mathbb{W}^T \underline{d} \quad (18)$$

where  $^\dagger$  denotes the Moore-Penrose pseudo inverse of a matrix. On substituting the matrices  $\mathbb{W}$ ,  $\mathbb{V}$  and  $\mathbb{X}$  into equation (18), we obtain the regularized solution, as a function of the left and right singular vectors and the singular values, as follows:

$$\underline{X}_\lambda = \sum_{i=1}^N \frac{f_\lambda(\sigma_i)}{\sigma_i} (\underline{w}_i^T \underline{d}) \underline{v}_i \quad (19)$$

where  $f_\lambda$  are the Tikhonov filter factors given by

$$f_\lambda(\sigma_i) = \frac{\sigma_i^2}{\sigma_i^2 + \lambda^2} \quad (20)$$

It should be noted that the Tikhonov filter factors, as defined earlier, depend on both the singular values  $\sigma_i$  and the regularization parameter  $\lambda$ , and  $f_i \approx 1$ , if  $\sigma_i \gg \lambda$ , and  $f_i \approx \sigma_i^2/\lambda^2$ , if  $\sigma_i \ll \lambda$ . In particular, the basic least squares solution  $X_{LS}$  is given by equation (19) with the regularization parameter  $\lambda = 0$  and the Tikhonov filter factors  $f_i = 1$  for  $i=1, \dots, M$ . Hence, comparing the regularized solution  $X_\lambda$  with the least squares solution  $X_{LS}$ , we see that the filter factors practically filter out the contributions to the solution corresponding to small singular values, whilst they leave the SVD components corresponding to large singular values almost unaffected. Moreover, damping sets in for  $\sigma_i \approx \lambda$ .

### 3.3 Conjugate gradient method

In this section, we describe a variational method that can be applied to solve the Cauchy problem. Since the boundary condition at  $\Gamma_2$  is to be determined, we consider it as a control  $v \in L^2(\Gamma_2)$  in a direct problem formulation to fit the Cauchy data  $f \in L^2(\Gamma_1)$ . Thus, we consider the direct problem

$$LT = 0 \tag{21}$$

$$T|_{\Gamma_2} = v \tag{22}$$

$$\frac{\partial T}{\partial \nu^+}|_{\Gamma_1} = q \tag{23}$$

with  $q \in L^2(\Gamma_1)$ . Assuming that  $\Gamma$  is a Lipschitzian boundary consisting of two non-intersecting closed curves,  $\Gamma_1$  and  $\Gamma_2$ , we note that since  $q \in L^2(\Gamma_1)$  and  $v \in L^2(\Gamma_2)$ , there is a unique solution  $T(q,v)$  of the direct problems (21)-(23) (Lions and Magenes, 1972). Then we aim to find  $v$  such that

$$Av := T(q,v)|_{\Gamma_1} = f \tag{24}$$

In doing so, we try to minimise the functional

$$J(v) = \frac{1}{2} \|Av - f\|_{L^2(\Gamma_1)}^2 \tag{25}$$

It has been established (Hao and Lesnic, 2000), that this functional is twice Frechet differentiable and its gradient can be calculated as

$$J'(v) = - \frac{\partial \psi}{\partial \nu^+}|_{\Gamma_2} \tag{26}$$

where  $\psi$  is the solution of the adjoint problem

$$L\psi = 0 \tag{27}$$

$$\psi|_{\Gamma_2} = 0 \tag{28}$$

$$\frac{\partial \psi}{\partial \nu^+}|_{\Gamma_1} = T(q, v)|_{\Gamma_1} - f \tag{29}$$

Thus, the conjugate gradient method applied to our problem has the form of the following algorithm.

- (i) Specify an initial guess  $v_0$  for the temperature on  $\Gamma_2$  and set  $k = 0$ .
- (ii) Solve the direct problems (21)-(23) with  $v = v_k$  and determine the *residual*

$$\tilde{r}_k := Av_k - f \tag{30}$$

- (iii) Determine the gradient  $r_k$  by solving the adjoint problems (27)-(29) with

$$\frac{\partial \psi_k}{\partial \nu^+}|_{\Gamma_1} = \tilde{r}_k \tag{31}$$

then calculate  $d_k = -r_k + \beta_{k-1}d_{k-1}$ , with the convention that  $\beta_{-1} = 0$  and

$$\beta_{k-1} = \frac{\|r_k\|^2}{\|r_{k-1}\|^2} \tag{32}$$

- (iv) Determine  $A_0d_k = T(0, d_k)|_{\Gamma_1}$  by solving the problems (21)-(23) with  $q = 0$  and  $v = d_k$ ,

$$v_{k+1} = v_k + \xi_k d_k, \tag{33}$$

$$\xi_k = \frac{\|r_k\|^2}{\|A_0d_k\|^2} = \frac{\|r_k\|^2}{\|T(0, d_k)|_{\Gamma_1}\|^2} \tag{34}$$

- (v) Increase  $k$  by one and go to (ii) until a prescribed stopping criterion is satisfied.

It is known that, in general, the conjugate gradient method produces a stable solution for ill-posed problems, provided that a regularizing stopping criterion is used. The performance of this method for the Cauchy problem for anisotropic heat conduction is investigated and compared with other regularization methods in Section 5.

### 3.4 An alternating iterative algorithm

Apart from general regularization methods, which can be applied for solving any ill-posed problems, typical solution methods may be developed for particular ill-posed problems. In this section, we describe such a particular regularization algorithm developed for Cauchy problems. The algorithm uses

the fact that a part of the boundary is overspecified and the remainder is unspecified in order to reduce the ill-posed problem to a sequence of well-posed problems by alternating the given data on the overspecified part of the boundary. This iterative algorithm was first proposed by Kozlov and Mazya (1990) and consists of the following steps.

- (i) Specify an initial boundary temperature guess  $u_0$  on  $\Gamma_2$ .
- (ii) Solve the mixed well-posed direct problem

$$\sum_{i,j=1}^2 k_{ij} \frac{\partial^2 T^{(0)}}{\partial x_i \partial x_j} = 0 \quad (35)$$

$$T^{(0)}|_{\Gamma_2} = u_0; \quad \frac{\partial T^{(0)}}{\partial \nu^+}|_{\Gamma_1} = q \quad (36)$$

to determine  $T^{(0)}(\underline{x})$  for  $\underline{x} \in \Omega$  and  $\nu_0 = \frac{\partial T^{(0)}}{\partial \nu^+}|_{\Gamma_2}$ .

- (iii) (a) If the approximation  $T^{(2k)}$  is constructed, solve the mixed well-posed direct problem

$$\sum_{i,j=1}^2 k_{ij} \frac{\partial^2 T^{(2k+1)}}{\partial x_i \partial x_j} = 0 \quad (37)$$

$$T^{(2k+1)}|_{\Gamma_1} = f; \quad \frac{\partial T^{(2k+1)}}{\partial \nu^+}|_{\Gamma_2} = \nu_k \quad (38)$$

to determine  $T^{(2k+1)}(\underline{x})$  for  $\underline{x} \in \Omega$  and  $u_{k+1} = T^{(2k+1)}|_{\Gamma_0}$ .

- (b) Having constructed  $T^{(2k+1)}$ , solve the mixed well-posed direct problem

$$\sum_{i,j=1}^2 k_{ij} \frac{\partial^2 T^{(2k+2)}}{\partial x_i \partial x_j} = 0 \quad (39)$$

$$T^{(2k+2)}|_{\Gamma_2} = u_{k+1}; \quad \frac{\partial T^{(2k+2)}}{\partial \nu^+}|_{\Gamma_1} = q \quad (40)$$

to determine  $T^{(2k+2)}(\underline{x})$  for  $\underline{x} \in \Omega$  and

$$\nu_{k+1} = \frac{\partial T^{(2k+2)}}{\partial \nu^+}|_{\Gamma_2}$$

- (iv) Repeat step (iii) for  $k \geq 0$  until a prescribed stopping criterion is satisfied.

According to Kozlov and Mazya (1990), the above algorithm produces two sequences of approximate solutions, namely  $\{T^{(2k)}(x)\}_{k \geq 0}$  and  $\{T^{(2k+1)}(x)\}_{k \geq 0}$ , which both converge in  $H^1(\Omega)$  to the solution  $T$  of the Cauchy problem given by equations (1), (3) and (4) for any initial guess  $u_0 \in H^{1/2}(\Gamma_2)$ .

We note that, provided the initial guess  $u_0$  is in  $H^{1/2}(\Gamma_2)$  and the boundary data  $f$  and  $q$  are in  $H^{1/2}(\Gamma_1)$  and  $H^{1/2}(\Gamma_1)^*$ , respectively, the problems given at step (iii) of the algorithm are both well-posed and uniquely solvable in  $H^1(\Omega)$  (Lions and Magenes, 1972). These intermediate mixed well-posed problems are solved using the BEM described in Section 4.

The same conclusions about the convergence and the regularizing character are obtained, if at the step (i) we specify an initial guess for the heat flux  $\nu_0 \in H^{1/2}(\Gamma_2)^*$ , instead of an initial guess for the temperature  $u_0 \in H^{1/2}(\Gamma_2)$ , and we modify accordingly the steps (ii) and (iii) such that the mixed problems are solved. The algorithm did not converge, if in the steps (ii) and (iii) the mixed problems were replaced by Dirichlet or Neumann problems. In addition, the Neumann direct problem itself is ill-posed due to the non-uniqueness or non-existence of the solution, if the integral of the heat flux  $q$  over the boundary  $\Gamma$  vanishes or not, respectively.

A detailed numerical implementation of this algorithm may be found in Mera *et al.* (2000), where it was shown that, if a regularizing stopping criterion is used, then the iterative algorithm produces a convergent and stable numerical solution for the Cauchy problem considered. Therefore, only those features necessary to compare this iterative algorithm with other regularization methods are presented in this paper.

#### 4. The BEM

BEM (Chang *et al.*, 1973; Wrobel, 2002) is used to discretise the Cauchy problem considered. One way of dealing with the anisotropy is to transform the governing partial differential equation (1) into its canonical form by changing the spatial coordinates. However, after the transformation, the domain deforms and rotates and the boundary conditions become, in general, more complicated than the original ones. Therefore, rather than adopt this approach, we use the fundamental solution for the differential operator  $L$  of the equation (1) in its original form. By using the fundamental solution of the heat equation and Green's identities, the governing partial differential equation (1) is transformed into the following integral equation (Chang *et al.*, 1973)

$$\eta(\underline{x})T(\underline{x}) = \int_{\Gamma} \left[ G(\underline{x}, \underline{x}') \frac{\partial T}{\partial \nu^+}(\underline{x}') - T(\underline{x}') \frac{\partial G}{\partial \nu^+}(\underline{x}, \underline{x}') \right] d\Gamma_{\underline{x}'} \quad (41)$$

where

- (1)  $\underline{x} \in \bar{\Omega}$ ,  $\underline{x}' \in \Gamma$ ,
- (2)  $\eta(\underline{x}) = 1$ , if  $\underline{x} \in \Omega$  and  $\eta(\underline{x}) = \frac{1}{2}$ , if  $\underline{x} \in \Gamma$  (smooth),

- (3)  $d\Gamma_{\underline{x}'}$  denotes the differential increment of  $\Gamma$  at  $\underline{x}'$
- (4)  $G$  is the fundamental solution of equation (1), namely,

$$G(\underline{x}, \underline{x}') = -\frac{|k^{ij}|^{\frac{1}{2}}}{2\pi} \ln(R) \tag{42}$$

where  $k^{ij}$  is the inverse matrix to the matrix  $k_{ij}$  and the geodesic distance  $R$  is defined by

$$R^2 = \sum_{i,j=1}^2 k^{ij}(x_i - x'_i)(x_j - x'_j). \tag{43}$$

In practice, the boundary integral equation (41) may rarely be solved analytically and thus some form of numerical approximation is necessary. Generically, if the boundaries  $\Gamma_1$  and  $\Gamma_2$  are discretised into  $N_1$  and  $N_2$  boundary elements, then equation (41) reduces to solving the following system of linear algebraic equations

$$\mathbb{A}\underline{T}' - \mathbb{B}\underline{T} = 0 \tag{44}$$

where  $\mathbb{A}$  and  $\mathbb{B}$  are matrices which depend solely on the geometry of the boundary  $\Gamma$  and can be calculated analytically. The vectors  $\underline{T}$  and  $\underline{T}'$  are the discretised values of the temperature and heat flux, respectively, which are assumed to be constant over each boundary element and take their values at the midpoint of each element. Equation (44) represents a system of  $N$  linear algebraic equations with  $2N$  unknowns, where  $N = N_1 + N_2$ . The discretisation of the boundary conditions given by equations (3) and (4) provides the values of  $2N_1$  of the unknowns and the problem reduces to solving a system of  $N_1 + N_2$  equations with  $2N_2$  unknowns, which generically can be written as

$$\mathbb{C}\underline{X} = \underline{d} \tag{45}$$

where  $\underline{d}$  is computed using the boundary conditions (3) and (4), the matrix  $\mathbb{C}$  depends solely on the geometry of the boundary  $\Gamma$  and the unknown vector  $\underline{X}$  contains the values of the temperature and the heat flux on the boundary  $\Gamma_1$ . In order to determine the system of equation (45), we need to have  $N_1 \geq N_2$  or  $\text{meas}(\Gamma_1) \geq \text{meas}(\Gamma_2)$ , which is in fact a necessary condition for the Cauchy problem to be numerically identifiable, when the mesh discretisation is uniform.

### 5. Numerical results and discussion

In order to illustrate the performance of the numerical method proposed, we solve a Cauchy problem in a two-dimensional smooth geometry such as the unit disc  $\Omega = \{(x, y) \mid x^2 + y^2 < 1\}$ . We assume that the boundary  $\Gamma = \{(x, y) \mid x^2 + y^2 = 1\}$  of the solution domain is divided into two disjoint

parts, namely,  $\Gamma_1 = \{\underline{x} = (x, y) \mid \underline{x} \in \Gamma, \theta(\underline{x}) \leq \alpha\}$  and  $\Gamma_2 = \{\underline{x} = (x, y) \mid \underline{x} \in \Gamma, \theta(\underline{x}) > \alpha\}$  and where  $\theta(\underline{x})$  is the angular polar coordinate of  $\underline{x}$  and  $\alpha$  is a specified angle in the interval  $(0, 2\pi)$ . In order to illustrate the typical numerical results, we have taken  $\alpha = 3\pi/2$ . Various values may be prescribed for  $\alpha$ , but a necessary condition for the inverse Cauchy problem to be numerically identifiable when a uniform mesh discretisation is adopted is that  $\text{meas}(\Gamma_1) \geq \text{meas}(\Gamma_2)$ , i.e.  $\alpha \geq \pi$ .

The most significant quantity to characterize the anisotropy of a medium is the determinant of the conductivity coefficients, i.e.  $|k_{ij}| = k_{11}k_{22} - k_{12}^2$ . The smaller the value of  $|k_{ij}|$ , the more asymmetric are the temperature fields and the heat flux vectors and the more difficult is the numerical calculation (Chang *et al.*, 1973). We consider a typical benchmark example which governs the steady heat conduction in a two-dimensional anisotropic medium with the thermal conductivity tensor  $k_{ij}$  given by  $k_{11} = 1.0$ ,  $k_{12} = k_{21} = 0.5$  and  $k_{22} = 1.0$ , and the analytical temperature distribution to be retrieved, given by  $T(x, y) = x^2 - 4xy + y^2$ .

### 5.1 Direct approach

The system of linear equation (45) cannot be solved by a direct approach, such as a Gaussian elimination method, since the sensitivity matrix  $\mathbb{C}$  is ill-conditioned. The condition number  $\text{cond}(\mathbb{C}) = \det(\mathbb{C}\mathbb{C}^T)$  of the sensitivity matrix  $\mathbb{C}$  was calculated using the NAG subroutine F03AAF (NAG Fortran Library Manual, 1991), which evaluates the determinant of a matrix using the Crout factorisation method with partial pivoting. The condition number of the system of equation (45) was found to be  $O(10^{-86})$  and  $O(10^{-251})$  for  $N = 40$  and 80 boundary elements while for numbers of boundary elements exceeding  $N = 160$ , the matrix  $(\mathbb{C}\mathbb{C}^T)$  was found to be approximately singular, the value of its determinant becoming uncomputable, thus revealing the high degree of ill-posedness of the Cauchy problem being investigated. Thus, a direct approach to the problem produces a highly unstable solution and that is why regularization methods, such as those presented here, must be used.

### 5.2 Discrepancy principle

The accuracy of the numerical solution  $\underline{X}_\lambda$  obtained by using the regularization methods based on the singular value decomposition of the problem clearly depends on the choice of the parameter  $\lambda$  which is known as the *regularization parameter*. Therefore, in order to obtain an accurate solution for an ill-conditioned problem, it is important to choose the regularization parameter that gives the right balance between the accuracy and the stability of the numerical solution. Currently, there are various criteria available for choosing the regularization parameter, but the most widely used is the *discrepancy principle* of Morozov (1966).

According to this principle, the regularization parameter should be chosen such that

$$\|C\underline{X}_\lambda - \underline{d}\| \approx \delta \quad (46)$$

where  $\delta$  is an estimate of the level of noise present in the problem, i.e.

$$\delta = \|\underline{d} - \underline{d}^\epsilon\| \quad (47)$$

where  $\underline{d}^\epsilon$  is the perturbed value of the right hand side of the system of equation (6).

For the iterative regularization methods, the stability is ensured by stopping the iterative process at the point where the errors in predicting the exact solution start increasing. Thus, regularization is achieved by truncating the iterative process after a specific number of iterations and the number of iterations performed acts as a regularization parameter. Also for these iterative algorithms the discrepancy principle may be used for choosing the regularization parameter by stopping the iterative process when

$$\|C\underline{X}_k - \underline{d}\| \approx \delta \quad (48)$$

where  $\underline{X}_k$  is the numerical solution obtained for the discrete problem (45) by substituting in the vector  $\underline{X}$  the boundary values of the heat flux and of the temperature calculated by the iterative method considered after  $k$  iterations. Thus, for the iterative methods regularization is achieved by matching the number of iterations to the level of noise in the problem. For all the regularization methods considered in this paper, the regularization parameter was chosen using the discrepancy principle.

### 5.3 Comparison of the numerical results

It is the purpose of this section to present and compare the numerical results for the Cauchy problem, obtained using the four regularization methods mentioned earlier. In order to investigate the stability and the regularization properties of the methods considered, the boundary data  $f = T|_{\Gamma_1}$  was perturbed as follows:

$$\tilde{f} = f + \tau \quad (49)$$

where  $\tau$  is a Gaussian random variable with mean zero and standard deviation  $\zeta = (s/100)\max|f|$  generated by the NAG routine G05DDF (NAG Fortran Library Manual, 1991) and  $s$  is the percentage of additive noise included in the input data  $T|_{\Gamma_1}$  in order to simulate the inherent measurement errors.

The numerical results presented in this section were obtained using  $N = 160$  boundary elements. Various number of boundary elements were tested, but it was found that no substantial improvement in the numerical solution is obtained, if the number of boundary elements is increased above  $N = 160$ .

The TSVD and Tikhonov regularization methods were applied to the overdetermined system of linear equation (45) in order to simultaneously retrieve the temperature and the heat flux on the boundary  $\Gamma_2$ . Figure 1(a) and (b) shows the numerical solution obtained by using the TSVD and the Tikhonov

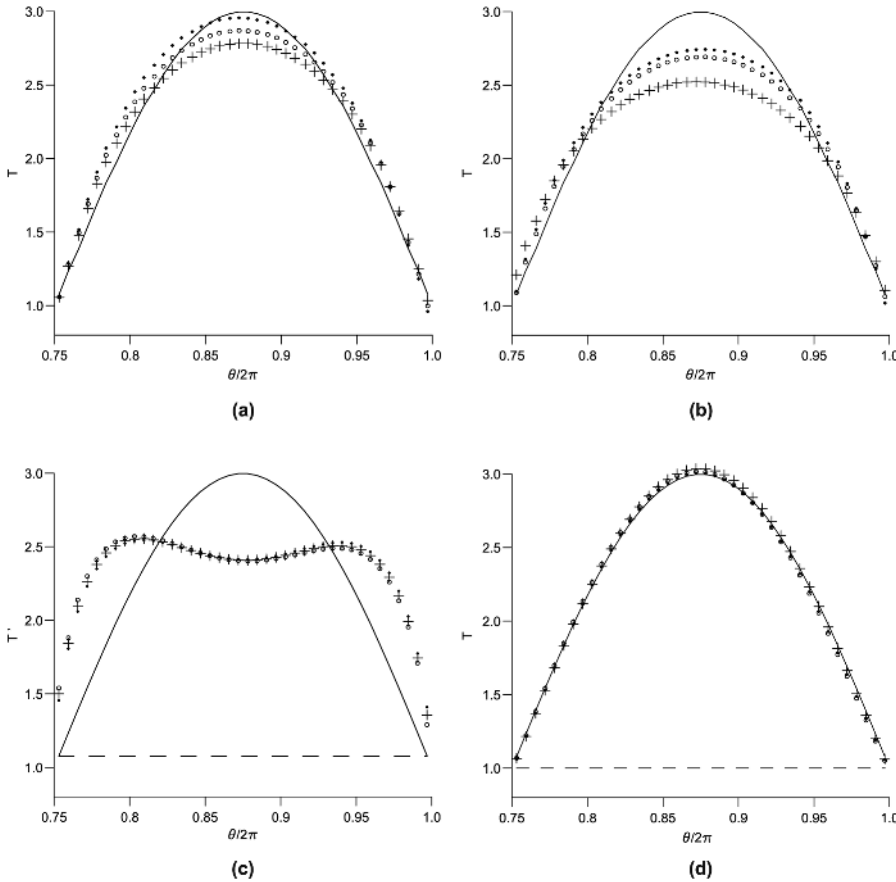


**Figure 1.** The numerical solution for the temperature on the boundary  $\Gamma_2$  obtained by using (a) the SVD method, (b) the Tikhonov regularization method, (c) the conjugate gradient method and (d) the iterative alternating algorithm described in Section 3.4 for  $N=160$  boundary elements and various levels of noise, namely,  $s = 1$  per cent ( $\bullet$ ),  $s = 3$  per cent ( $\circ$ ) and  $s = 5$  per cent ( $+$ ), in comparison with the exact solution ( $-$ )

regularization method, respectively, for the temperature on boundary  $\Gamma_2$  for various levels of noise  $s \in \{1, 3, 5\}$ . It can be seen that as  $s$  decreases, the numerical solution approximates better than the exact solution while remaining stable. If the level of noise is not too big, then the numerical solution obtained by TSVD is a good approximation for the exact solution.

We note that the numerical solution obtained by the Tikhonov regularization method is less accurate than the numerical solution obtained by the TSVD method, but it is still a reasonably good approximation to the exact solution of the problem since we have solved a highly ill-posed problem.

Although, not presented here, it is reported that for both the TSVD and the Tikhonov regularization methods, the discrepancy principle was found to be very efficient in choosing the optimum value of the regularization parameter, i.e. the level of truncation for the singular values of the matrix  $\mathbb{C}$  and

the parameter  $\lambda$ . Numerous other test examples have been investigated and it was found that both the TSVD and the Tikhonov regularization methods produce a convergent and stable solution with respect to decreasing the amount of noise. However, the TSVD was found to produce in general more accurate results than the Tikhonov regularization method.

The conjugate gradient method and the alternating iterative algorithm described in Section 3.4 both require an initial guess to be specified for the temperature on the boundary  $\Gamma_2$ . This initial guess is improved at every iteration and approaches the exact solution. Therefore, the rate of convergence and the accuracy of these methods clearly depend on how close to the exact solution is the initial guess specified. Since the temperature at the end-points of the boundary  $\Gamma_2$  is known, the most natural initial guess is a function, which ensures the continuity of the temperature at these points and is a linear function with respect to the angular polar coordinate  $\theta$ . For the test example considered in this paper, the initial guess is given by the constant function  $u_0 = v_0 = 1$ .

The numerical results for the temperature on the boundary  $\Gamma_2$  obtained by the conjugate gradient method for various levels of noise are presented in Figure 1(c) in comparison with the exact solution and the initial guess specified. It can be seen that the numerical solution is not accurate even for small levels of noise. We note that the test example considered here is a very severe test example for iterative methods since the exact solution is very far from the most natural initial guess available. Numerous test example have been investigated and it was found that the conjugate gradient method produces good results for simple test examples for which the initial guess is not very far from the exact solution. However, for more difficult test examples, as the one presented in this paper, the method failed to produce accurate results for the unspecified boundary data.

A detailed BEM numerical implementation of the alternating iterative algorithm presented in Section 3.4 was given in Mera *et al.* (2000). It was shown that a substantial improvement in the rate of convergence is obtained by relaxing the marching condition

$$u_{k+1} = T^{(2k+1)}|_{\Gamma_2}$$

through

$$u_{k+1} = \varphi T^{(2k+1)}|_{\Gamma_2} + (1 - \varphi)u_k$$

when passing from step iii(a) to iii(b), where  $\varphi$  is a variable relaxation factor with respect to the angular polar coordinate given by

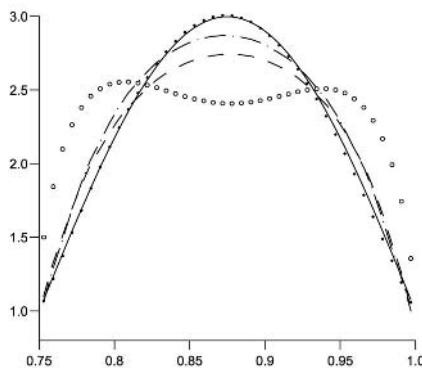
$$\varphi(\theta) = A \sin \left[ \pi \left( \frac{\theta - \alpha}{2\pi - \alpha} \right) \right] \quad (50)$$

and  $A \in [0, 2]$  is a positive constant. This relaxation procedure was found not only to reduce the number of iterations necessary to obtain the convergence but also to substantially increase the accuracy of the numerical solution. We note that the same relaxation procedure was found to be very efficient in increasing the rate of convergence also for the conjugate gradient method.

Figure 1(d) presents the numerical solution for the temperature on the boundary  $\Gamma_2$  obtained using the iterative alternating algorithm presented in Section 3.4 coupled with the relaxation procedure (50) in comparison with the exact solution and the initial guess. It can be seen that even for large amounts of noise added into the input data, there is a very good agreement between the numerical and the exact solution for the problem. Therefore, it can be concluded that this alternating iterative algorithm is very efficient in regularizing the Cauchy problem considered.

We note that for both the conjugate gradient method and for the iterative alternating algorithm presented in Section 3.4, the regularization is achieved by truncating the iterative process at the point where the errors in predicting the exact solution start increasing. Thus, a stable solution is achieved by matching the number of iterations to the level of noise present in the data. Although not presented here, it is reported that the discrepancy principle was found to be efficient in choosing the regularization parameter also for these iterative methods. However, it was found to be more robust for the iterative alternating algorithm than for the conjugate gradient method.

In order to compare the four regularization method considered, Figure 2 graphically shows the numerical solution for the temperature on the boundary obtained with each of these methods for  $N = 160$  boundary elements and  $s = 3$  per cent noise.



**Note:** Obtained by using various regularization methods, namely, the iterative alternating algorithm described in Section 3.4 ( $\bullet$ ), the SVD method ( $-\cdot-\cdot-$ ), the Tikhonov regularization method ( $- - -$ ) and the conjugate gradient method ( $\circ$ ) for  $N = 160$  boundary elements and  $s = 3\%$  noise in comparison with the exact solution ( $—$ )

**Figure 2.**  
The numerical solution for the temperature on the boundary  $\Gamma_2$

It can be seen that the most accurate solution is the one given by the iterative alternating algorithm of Kozlov and Mazya (1990). The TSVD and the Tikhonov regularization methods both give a reasonably good approximation for the temperature on the boundary, but TSVD was in general found to produce more accurate results. The numerical solution obtained by the conjugate gradient method is very poor in comparison with the numerical solutions obtained by the other methods. However, for less severe test examples, it was found that also the conjugate gradient method produces numerical solutions almost as accurate as the numerical solution obtained by the Tikhonov regularization method. The differences between the regularization methods considered are even large, if the numerical solution for the heat flux is sought. Figure 3 presents the numerical solution for the heat flux on the boundary  $\Gamma_2$  obtained with regularization methods for  $N = 160$  boundary elements and  $s = 3$  per cent noise.

Again it can be seen that the TSVD method outperforms the Tikhonov regularization method while both of them produce more accurate results than the conjugate gradient method. However, for all these three methods, the numerical solution for the heat flux is far from the exact solution. In the case of the heat flux, the iterative alternating algorithm of Kozlov and Mazya (1990) was the only method that produced accurate results. It can be seen in Figure 3 that the numerical solution for the heat flux obtained by this algorithm is in a very good agreement with the exact solution while the other methods considered fail to produce accurate results. Numerous other test examples have been investigated and similar conclusions have been drawn.

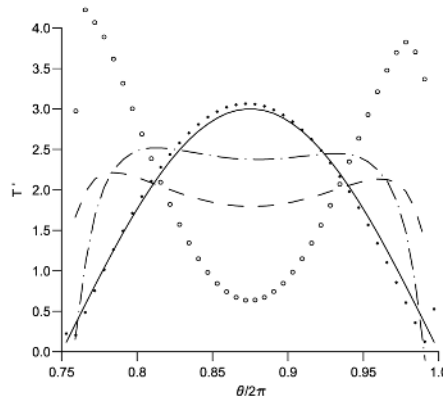


**Figure 3.**  
The numerical solution  
for the heat flux on the  
boundary  $\Gamma_2$

**Note:** Obtained by using various regularization methods, namely, the iterative alternating algorithm described in Section 3.4 (●), the SVD method (— · — · —), the Tikhonov regularization method (---) and the conjugate gradient method (○) for  $N = 160$  boundary elements and  $s = 3\%$  noise in comparison with the exact solution (—)

## 6. Conclusions

In this paper, four regularization methods were investigated and compared for a Cauchy problem in the steady-state anisotropic heat conduction. Three of the methods considered were general regularization methods while the fourth one was an alternating iterative algorithm developed for the Cauchy problems. It was found that the Cauchy problem can be regularized by any of the regularization methods considered since all of them produced a stable numerical solution.

However, the numerical solutions obtained by these methods differ in terms of accuracy. It was found that the TSVD method outperforms the Tikhonov regularization method while the latter outperforms the conjugate gradient method. All these three general regularization methods were outperformed by the iterative alternating algorithm described in Section 3.4. We note that for the severe test example considered, the conjugate gradient method failed to produce an accurate solution both for the temperature and the heat flux. A possible reason for this is that in the conjugate gradient method described in Section 3.3, the boundaries  $\Gamma_1$  and  $\Gamma_2$  should be disjoint non-intersecting closed curves which is not the case for our test example considered. The TSVD method and Tikhonov regularization methods were found to produce reasonably accurate results for the temperature, but they were both found to be less accurate for the heat flux. The iterative alternating algorithm of Kozlov and Mazya (1990) was found to be the only method to produce a good approximation for both the temperature and the heat flux.

Overall, it may be concluded that the Cauchy problem for the anisotropic steady-state heat conduction may be regularized by various methods such as the general regularization methods presented in this paper, but more accurate results are obtained by particular methods such as the iterative alternating algorithm investigated in this paper, which takes into account the particular structure of the problem.

## References

- Chang, Y.P., Kang, C.S. and Chen, D.J. (1973), "The use of fundamental Green's functions for the solution of heat conduction in anisotropic media", *International Journal of Heat and Mass Transfer*, Vol. 16, pp. 1905-18.
- Hadamard, J. (1923), *Lectures on Cauchy Problem in Linear Partial Differential Equations*, Yale University Press, New Heavens.
- Hao, D.N. and Lesnic, D. (2000), "The Cauchy problem for Laplace's equation via the conjugate gradient method", *IMA Journal of Applied Mathematics*, Vol. 65, pp. 199-217.
- Kozlov, V.A. and Mazya, V.G. (1990), "On iterative procedures for solving ill-posed boundary value problems that preserve differential equations", *Leningrad Mathematical Journal*, Vol. 5, pp. 1207-28.
- Lions, J.L. and Magenes, E. (1972), *Non-homogeneous Boundary Value Problems and Their Applications*, Springer-Verlag, Heidelberg.

---

HF  
13,5

Mera, N.S., Elliott, L., Ingham, D.B. and Lesnic, D. (2000), "The boundary element method solution of the Cauchy steady state heat conduction problem in an anisotropic medium", *International Journal for Numerical Methods in Engineering*, Vol. 49, pp. 481-99.

Morozov, V.A. (1966), "On the solution of functional equations by the method of regularization", *Soviet. Math. Dokl.*, Vol. 7, pp. 414-17.

NAG Fortran Library Manual (1991), Mark 15, The Numerical Algorithms Ltd, Oxford.

Tikhonov, A.N. and Arsenin, V.Y. (1977), *Solutions of III-Posed Problems*, Winston-Wiley, Washington DC.

Tikhonov, A.N., Goncharky, A.V., Stepanov, V.V. and Yagola, A.G. (1995), *Numerical Methods for the Solution of III-Posed Problems*, Kluwer Academic Publishers, Dordrecht.

Wrobel, L.C. (2002), *The Boundary Element Method, Applications in Thermo-Fluids and Acoustics*, Wiley, Chichester, Vol. I.

546

---

**Further reading**

Hansen, P.C. (1992), "Analysis of discrete ill-posed problems by means of the *L*-curve", *SIAM Review*, Vol. 34, pp. 561-80.



# Inverse analysis of continuous casting processes

Inverse analysis

Iwona Nowak

*Institute of Mathematics, Technical University of Silesia, Gliwice,  
Konarskiego, Poland*

Andrzej J. Nowak

*Institute of Thermal Technology, Technical University of Silesia, Gliwice,  
Konarskiego, Poland*

Luiz C. Wrobel

*Department of Mechanical Engineering, Brunel University, Uxbridge,  
Middlesex, UK*

547

Received April 2002  
Revised December 2002  
Accepted January 2003

**Keywords** *Inverse problems, Boundary element method, Sensitivity, Casting, Metals*

**Abstract** *This paper discusses an algorithm for phase change front identification in continuous casting. The problem is formulated as an inverse geometry problem, and the solution procedure utilizes temperature measurements inside the solid phase and sensitivity coefficients. The proposed algorithms make use of the boundary element method, with cubic boundary elements and Bezier splines employed for modelling the interface between the solid and liquid phases. A case study of continuous casting of copper is solved to demonstrate the main features of the proposed algorithms.*

## 1. Introduction

The continuous casting process of metals and alloys is a common procedure in the metallurgical industry. Typically, the liquid material flows into the mould (crystallizer), where the walls are cooled by flowing water. The solidifying ingot is then pulled by withdrawal rolls. The side surface of the ingot, below the mould, is very intensively cooled by water flowing out of the mould and sprayed over the surface, outside the crystallizer.

An accurate determination of the interface location between the liquid and solid phases is very important for the quality of the casting material. The estimation of this phase change front location can be found by using *direct modelling techniques* (Crank, 1984) such as the enthalpy method or front tracking algorithms or, as shown in this paper, by solving an *inverse geometry problem*.

Several previous works have dealt with inverse geometry problems (Bénard and Afshari, 1992; Kang and Zabaras, 1995; Nowak *et al.*, 2000; Tanaka *et al.*, 2000; Zabaras, 1990; Zabaras and Ruan, 1989). In particular, Zabaras and Ruan

The financial assistance of the National Committee for Scientific Research, Poland, Grant no. 8 T10B 010 20, is gratefully acknowledged.



---

(1989) developed a formulation based on a deforming finite element method (FEM) and sensitivity coefficients to analyze one-dimensional inverse Stefan problems. Their formulation was applied to study the problem of calculating the position and velocity of the moving interface from the temperature measurements of two or more sensors (thermocouples) located inside the solid phase. Zabarás (1990) extended the deforming FEM formulation to two other problems: the first calculated the boundary heat flux history that would achieve a specified velocity and flux at the freezing front, while the second calculated the boundary heat flux and freezing front position, given the appropriate estimates of the temperature field in a specified number of sensors. Bénard and Afshari (1992) developed a sequential algorithm for the identification of the interface location, for one- and two-dimensional problems, using discrete measurements of temperature and heat flux at the fixed part of the solid boundary. Kang and Zabarás (1995) calculated the optimum history of boundary cooling conditions that resulted in a desired history of the freezing interface location and motion, for a two-dimensional conduction-driven solidification process.

In the present work following Nowak *et al.* (2000) and Tanaka *et al.* (2000), the solution procedure involves the application of the boundary element method (BEM) (Brebbia *et al.*, 1984; Wrobel and Aliabadi, 2002) to estimate the location of the phase change front, making use of temperature measurements inside the solid phase. This front is approximated by Bezier splines, and this is significant for the reduction of the number of design variables and, as a consequence, of the number of required measurements.

Identification of the position of the phase change front requires to build up a series of direct solutions, which gradually approach the correct location. Generally, inverse problems are ill-posed. Thus, there is a problem with the stability and uniqueness of solution (Goldman, 1997). In this paper, it is proposed that the iteration process (necessary because of the non-linear nature of the problem) is preceded by a lumping process. This allows the definition of an initial front position which guarantees convergence of the solution.

The measurements can be obtained by immersing thermocouples into the melt and allowing them to travel with the solidified material, until they are damaged. From certain relationships between time and location of nodes in the continuous casting process, even a limited number of thermocouples can provide a substantial amount of useful information. Alternatively, it is also possible to obtain temperature measurements by using an infrared camera. Although generally more accurate, temperatures have to be measured at the body surface outside the crystallizer, thus at some distance from the phase change front.

It is worth to stress that although temperature measurements in this work are limited only to the solid phase, they carry information on the heat transfer phenomena occurring on the solid-liquid interface. Moreover, mathematical

models available for solids (based on heat conduction) are much more reliable than those for liquids where heat convection generally plays an important role.

## 2. Problem formulation

This section starts with a brief description of the mathematical model of the direct heat transfer problem for continuous casting. This model serves as a basis for the inverse problem that is discussed in detail in the remainder of the section. The direct problem will also be employed to generate simulated temperature measurements for the application of the proposed inverse analysis algorithms.

The mathematical description of the physical problem consists of

- a convection-diffusion equation for the solid part of the ingot:

$$\nabla^2 T(\mathbf{r}) - \frac{1}{a} v_x \frac{\partial T}{\partial x} = 0 \quad (1)$$

where  $T(\mathbf{r})$  is the temperature at point  $\mathbf{r}$ ,  $v_x$  is the casting velocity (assumed to be constant and in the positive  $x$ -direction) and  $a$  is the thermal diffusivity of the solid phase, and

- boundary conditions defining the heat transfer process along the boundaries ABCDO (Figure 1), including the specification of the melting temperature along the phase change front:

$$T(\mathbf{r}) = T_m, \quad \mathbf{r} \in \Gamma_{AB} \quad (2)$$

$$T(\mathbf{r}) = T_s, \quad \mathbf{r} \in \Gamma_{DO} \quad (3)$$

$$-\lambda \frac{\partial T}{\partial n} = q(\mathbf{r}) = 0, \quad \mathbf{r} \in \Gamma_{OA} \quad (4)$$

$$-\lambda \frac{\partial T}{\partial n} = q(\mathbf{r}), \quad \mathbf{r} \in \Gamma_{BC} \quad (5)$$

$$-\lambda \frac{\partial T}{\partial n} = h[T(\mathbf{r}) - T_a], \quad \mathbf{r} \in \Gamma_{CD} \quad (6)$$

where  $T_m$  is the melting temperature,  $T_a$  is the ambient temperature,  $T_s$  is the ingot temperature when leaving the system,  $\lambda$  is the thermal conductivity,  $h$  is the convective heat transfer coefficient and  $q$  is the heat flux.

In the inverse analysis, the location of the phase change front where the temperature is equal to the melting temperature is unknown. This means that the mathematical description is incomplete and needs to be supplemented by

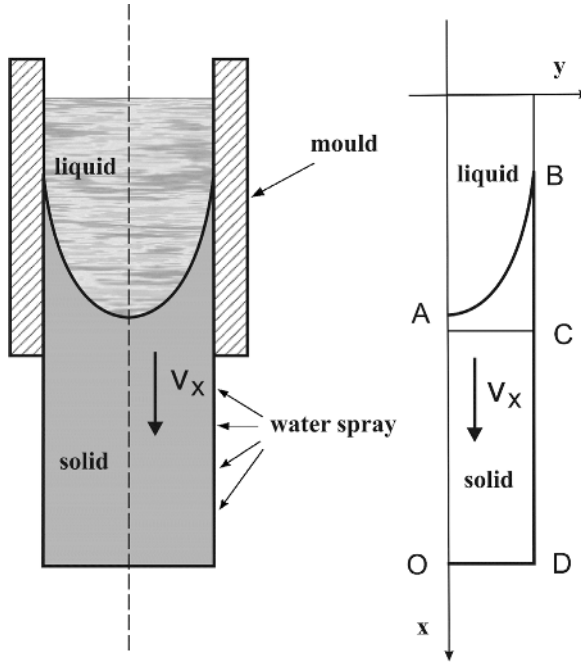


**Figure 1.**  
Schematic of the continuous casting system and the domain under consideration

measurements. Typically, the temperatures  $U_i$  are measured at some points inside the ingot (in case of using thermocouples) or on the surface (if an infrared camera is used). These measurements are collected in a vector  $\mathbf{U}$ .

The objective is to estimate components of vector  $\mathbf{Y}$ , which uniquely describes the phase change front location. In this work, two segments of Bezier splines are used to approximate the interface. This means that vector  $\mathbf{Y}$  contains components of the control points defining the Bezier splines.

The ill-conditioned nature of all inverse problems requires that the number of measurement sensors should be appropriate to make the problem overdetermined. This is achieved by using a number of measurement points greater than the number of design variables. Thus, in general, inverse analysis leads to optimization procedures with least squares calculations of the objective functions  $\Delta$ . However, in the cases studied here, an additional term intended to improve the stability is also introduced (Kurpysz and Nowak, 1995; Nowak, 1997), i.e.

$$\Delta = (\mathbf{T}_{\text{cal}} - \mathbf{U})^T \mathbf{W}^{-1}(\mathbf{T}_{\text{cal}} - \mathbf{U}) + (\mathbf{Y} - \tilde{\mathbf{Y}})^T \mathbf{W}_{\tilde{\mathbf{Y}}}^{-1}(\mathbf{Y} - \tilde{\mathbf{Y}}) \rightarrow \min \quad (7)$$

where vector  $\mathbf{T}_{\text{cal}}$  contains temperatures calculated at temperature sensor locations,  $\mathbf{U}$  stands for the vector of temperature measurements and superscript  $T$  denotes transpose matrices. The symbol  $\mathbf{W}$  denotes

the covariance matrix of measurements. Thus, the contribution of more accurately measured data is stronger than the data obtained with lower accuracy. Known prior estimates of design vector components are collected in vector  $\hat{\mathbf{Y}}$ , and  $\mathbf{W}_Y$  stands for the covariance matrix of prior estimates. The coefficients of matrix  $\mathbf{W}_Y$  have to be large enough to catch the minimum (these coefficients tend to infinity, if prior estimates are not known). It was found that the additional term in the objective function, containing prior estimates, plays a very important role in the inverse analysis, because it considerably improves the stability and accuracy of the inverse procedure.

The present inverse problem is solved by building up a series of direct solutions which gradually approach the correct position of the phase change front. This procedure can be expressed by the following main steps.

- Make the boundary problem well-posed. This means that the mathematical description of the thermal process is completed by assuming arbitrary values  $\mathbf{Y}^*$  (as required by the direct problem).
- Solve the direct problem obtained above and calculate temperatures  $\mathbf{T}^*$  at the sensor locations.
- Compare the above calculated temperatures  $\mathbf{T}^*$  and measured values  $\mathbf{U}$ , and modify the assumed data  $\mathbf{Y}^*$ .

Inverse geometry problems are always non-linear. Thus, an iterative procedure is generally necessary. In this procedure, iterative loops are repeated until the newly obtained vector  $\mathbf{Y}$  minimizes the objective function (7) within a specified accuracy (Beck and Blackwell, 1988; Kurpisz and Nowak, 1995; Nowak, 1997).

Each iteration loop involves the application of sensitivity analysis (Beck and Blackwell, 1988; Nowak, 1997), which utilizes sensitivity coefficients. According to their definition, these coefficients are the derivatives of the temperature at point  $i$  with respect to identified values at point  $j$ , i.e.

$$Z_{ij} = \frac{\partial T_i}{\partial Y_j} \quad (8)$$

and provide a measure of each identified value and an indication of how much it should be modified.

Sensitivity coefficients are obtained by solving a set of auxiliary direct problems in succession. Each of these direct problems arises through differentiation of equation (1) and corresponding boundary conditions (2)-(6) with respect to the particular design variable  $Y_j$ . Thus, the resulting field  $Z_j$  is governed by an equation of the form:

$$\nabla^2 Z_j(\mathbf{r}) - \frac{1}{a} v_x \frac{\partial Z_j}{\partial x} = 0 \quad (9)$$

Differentiation of the boundary conditions (3)-(6) produces conditions of the same type as in the original thermal problem, as follows:

$$Z_j(\mathbf{r}) = 0, \quad \mathbf{r} \in \Gamma_{DO} \quad (10)$$

$$-\lambda \frac{\partial Z_j}{\partial n} = 0, \quad \mathbf{r} \in \Gamma_{OA} \quad (11)$$

$$-\lambda \frac{\partial Z_j}{\partial n} = 0, \quad \mathbf{r} \in \Gamma_{BC} \quad (12)$$

$$-\lambda \frac{\partial Z_j}{\partial n} = hZ_j, \quad \mathbf{r} \in \Gamma_{CD} \quad (13)$$

The boundary condition along the phase change front  $\Gamma_{AB}$  is also obtained by differentiating equation (2):

$$\frac{\partial T}{\partial Y_j} + \frac{\partial T}{\partial x} \frac{\partial x}{\partial Y_j} + \frac{\partial T}{\partial y} \frac{\partial y}{\partial Y_j} = 0 \quad (14)$$

where the derivatives of  $x$  and  $y$  with respect to the design variable  $Y_j$  depend on the particular geometrical representation of the phase change front (Nowak *et al.*, 2000). In this work, two Bezier splines are used, as discussed in more detail later.

Equation (14) can now be rewritten as

$$Z_j = -\frac{\partial T}{\partial x} \frac{\partial x}{\partial Y_j} - \frac{\partial T}{\partial y} \frac{\partial y}{\partial Y_j} \quad (15)$$

or, taking into account Fourier's law,

$$Z_j = -\frac{1}{\lambda} \left( q_x \frac{\partial x}{\partial Y_j} - q_y \frac{\partial y}{\partial Y_j} \right) \quad (16)$$

where  $q_x$  and  $q_y$  are the  $x$ - and  $y$ -components of the heat flux vector.

The Cartesian components of the heat flux vector can be expressed in terms of the tangential and normal components,  $q_\tau$  and  $q_n$ , by the relations:

$$\begin{cases} q_x = -q_n \cos(\alpha) - q_\tau \cos\left(\frac{\pi}{2} + \alpha\right) \\ q_y = -q_n \sin(\alpha) + q_\tau \sin\left(\frac{\pi}{2} + \alpha\right) \end{cases} \quad (17)$$

where  $\cos(\alpha)$  and  $\sin(\alpha)$  are the direction cosines of the normal vector pointing outwards the solid phase (Figure 2).

Taking the above into account, the boundary condition along the phase change front takes the final form: Inverse analysis

$$Z_j = -\frac{1}{\lambda} \left\{ [-q_n \cos(\alpha) + q_\tau \sin(\alpha)] \frac{\partial x}{\partial Y_j} + [q_n \sin(\alpha) - q_\tau \cos(\alpha)] \frac{\partial y}{\partial Y_j} \right\} \tag{18}$$

Solving the above direct problem for the field  $Z_j$ , one can collect results at particular measurement points, i.e.  $Z_{ij}$ ,  $i = 1, 2, \dots$ . Repeating this procedure for all design variables, the whole sensitivity matrix  $\mathbf{Z}$  can then be constructed. This is the most expensive and time consuming stage of the analysis.

Through application of sensitivity analysis and some basic algebraic manipulations (Nowak *et al.*, 2000), minimization of the objective function equation (7) leads to the following set of equations (Nowak, 1997; Nowak *et al.*, 2000):

$$(\mathbf{Z}^T \mathbf{W}^{-1} \mathbf{Z} + \mathbf{W}_Y^{-1}) \mathbf{Y} = \mathbf{Z}^T \mathbf{W}^{-1} (\mathbf{U} - \mathbf{T}^*) + (\mathbf{Z}^T \mathbf{W}^{-1} \mathbf{Z}) \mathbf{Y}^* + \mathbf{W}_Y^{-1} \tilde{\mathbf{Y}} \tag{19}$$

In this work, the BEM is applied for solving both thermal and sensitivity coefficient problems. The main advantage of using this method is the simplification in meshing, as only the boundaries have to be discretized. This is particularly important in inverse geometry problems in which the geometry of the body is changed at each iteration step. Furthermore, the location of the internal measurement sensors does not affect the discretization. Finally, in heat transfer analysis, BEM solutions directly provide temperatures and heat fluxes, both of which are required by inverse solutions. In other words, the numerical differentiation of the temperature field in order to calculate heat fluxes is not needed.

The BEM system of equations for both the thermal and sensitivity coefficient problems has the same form:

$$\mathbf{HT} = \mathbf{GQ} \tag{20}$$

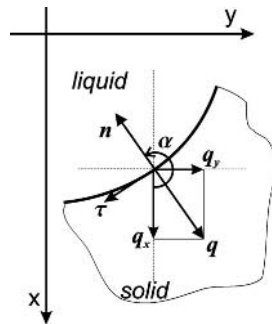


**Figure 2.**  
Geometrical relations on the phase change front

$$\mathbf{HZ}_j = \mathbf{GQ}_j^Z \quad (21)$$

where  $\mathbf{H}$  and  $\mathbf{G}$  stand for the BEM influence matrices. The fundamental solution of the two-dimensional convection-diffusion equation is expressed by the following formula, assuming that the velocity field is constant along the  $x$ -direction:

$$u^* = \frac{1}{2\pi\lambda} \exp\left(-\frac{v_x r_x}{2a}\right) K_0\left(\frac{|v_x|r}{2a}\right) \quad (22)$$

where  $K_0$  stands for the Bessel function of the second kind and zero order and  $r$  is the distance between source and field points, with its component along the  $x$ -axis denoted by  $r_x$ .

### 3. Application of Bezier splines

As noted before, the ill-conditioned nature of all inverse problems requires that they have to be made overdetermined. On the other hand, it is very important to limit the number of sensors, mainly because of the difficulties with measurements acquisition. Application of Bezier splines allows the modelling of the phase change front using a much smaller number of design variables.

The Bezier curve (Draus and Mazur, 1991) is built up of cubic segments. Each of these segments is controlled by four control points  $\mathbf{V}_0, \mathbf{V}_1, \mathbf{V}_2$  and  $\mathbf{V}_3$  (Figure 3). The following formula presents the definition of cubic Bezier segments:

$$\mathbf{P}(u) = (1 - u)^3\mathbf{V}_0 + 3(1 - u)^2u\mathbf{V}_1 + 3(1 - u)u^2\mathbf{V}_2 + u^3\mathbf{V}_3 \quad (23)$$

where  $\mathbf{P}(u)$  stands for a point on the Bezier curve, and  $u$  varies in the range  $\langle 0, 1 \rangle$ . This formula has to be differentiated with respect to the design variable  $Y_j$  (i.e. the  $x$ - and/or  $y$ -coordinate of the given control point) in order to obtain derivatives required in the boundary condition (18).

Numerical experiments have shown that a Bezier curve composed of two cubic segments satisfactorily approximates the phase change front. An extra advantage is that the application of Bezier curves permits to limit the number of identified values. In reality, some of these values (coordinates of Bezier control points) are defined by additional constraints resulting from the physical nature of the problem. These conditions are listed below:

- the  $y$ -coordinates of the first and the last control points of the Bezier curves ( $\mathbf{V}_0^I, \mathbf{V}_3^I$  in Figure 4) are known because those points are located on the ingot surface and symmetry axis, respectively;
- the last control point of the first segment,  $\mathbf{V}_3^I$ , and the first of the second segment,  $\mathbf{V}_0^{II}$ , occupy the same position;

- the smoothness of the curve at the connecting points between two Bezier segments is guaranteed if the appropriate control points are collinear (Draus and Mazur, 1991) (compare with Figure 4);
- the equality of the  $x$ -coordinate of points  $V_2^I$  and  $V_3^I$  ensures the existence of derivatives on the symmetry axis.

Inverse analysis

Because of the above conditions only ten quantities have to be estimated, which fully describe the position of the phase change front. Thus, application of the Bezier functions significantly reduces the number of design variables (Nowak *et al.*, 2000), which also means a reduction in the number of required measurements. Acquiring temperature measurements at points located inside the ingot requires to immerse thermocouples in the solidifying material. This perturbs part of the casted material during measurements. The application of an infrared camera is another method of obtaining measurements. Although the first approach seems to be better, because the measurements location can be closer to the identified values, the second does not destroy any casted material and provides measurements which are generally more accurate. Nevertheless, both methods of measuring temperatures always involve measurement errors, which affect the final results.

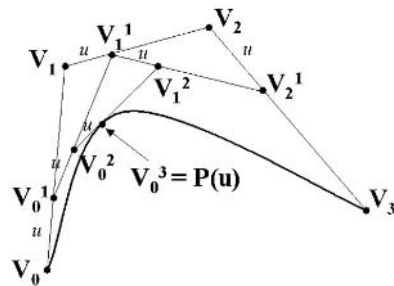


**Figure 3.**  
One Bezier segment and its control points

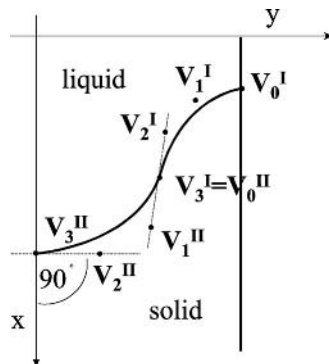


**Figure 4.**  
Identified values in the problem with two Bezier segments

#### 4. Starting point and lumping

Extensive computing of inverse geometry problems showed the great influence of prior estimates and the initial guess on the solution existence and convergence. Contrary to direct problems, the existence of solutions to non-linear inverse problems is not clear. Some starting guesses may not fulfill the conditions for solving the problem. This means that, at the beginning of the iteration process, there is no guarantee that the assumed starting front position (i.e. the starting set of Bezier control points) will lead to the solution.

Because of this, it is proposed (Nowak *et al.*, 2001) that the iteration process is preceded by a kind of *lumping* process. This lumping consists of summing up the coefficients in each row of the main matrix  $\mathbf{A} = \mathbf{Z}^T \mathbf{W}^{-1} \mathbf{Z} + \mathbf{W}_Y^{-1}$  of equation (19) and placing the result on the main diagonal of the square matrix  $\mathbf{L}$ . Thus, matrix  $\mathbf{L}$  takes the following form:

$$\mathbf{L} = \begin{bmatrix} \sum_{j=1}^n \zeta_{1j} & 0 & \dots & 0 \\ 0 & \sum_{j=1}^n \zeta_{2j} & \dots & 0 \\ \vdots & \vdots & & \vdots \\ 0 & 0 & \dots & \sum_{j=1}^n \zeta_{nj} \end{bmatrix} \quad (24)$$

where  $\zeta_{ij}$  is an element of the square matrix  $\mathbf{A}$ . Such matrix decouples the system (19) and each equation may be solved separately.

It was found that replacing matrix  $\mathbf{A}$  in equation (19) by  $\mathbf{L}$  in the first step of the iteration procedure makes the process always convergent. Simultaneously, in the present inverse geometry problem, application of the lumping procedure turns out to be almost always necessary. An inappropriate initial position of the interface without application of lumping usually leads, very quickly, to results contradicting the physics of the problem. The phase change front in successive iterations appears with very sharp corners, and the iterative process eventually diverges. Such a situation is shown in Figure 5.

Searching for a starting position of the identified values is based on an observation of matrix  $\mathbf{L}$ . The largest coefficient on the diagonal of matrix  $\mathbf{L}$  shows the most sensitive initially-assumed design variables. This initially-assumed coordinate could be the reason for the non-existence of solution, and has to be improved. The direction and value of the correction are determined by solving an appropriate equation from the decoupled system (19). Once this

component of vector  $\mathbf{Y}^*$  is corrected, the original system (19) with matrix  $\mathbf{A}$  can be solved iteratively. Inverse analysis

The above algorithm can be further extended in this way, so that not only one component of vector  $\mathbf{Y}^*$  is corrected using matrix  $\mathbf{L}$ , but also all of them. Figure 6 presents a comparison of average errors in subsequent iterations, obtained with the simple and the extended approaches. It can be seen that the final results do not differ significantly. The approach in which all the estimated values are corrected is more time consuming, so the first method seems to be more useful in practical applications.

In the iteration process, it is important that subsequent Bezier control points appear in the correct order. To guarantee the monotonicity of the  $x$ - and  $y$ -coordinates (without which the Bezier segment makes a loop), the size of the vector  $\Delta\mathbf{Y} = \mathbf{Y} - \mathbf{Y}^*$  has to be controlled. If necessary, the calculated vector  $\Delta\mathbf{Y}$  may be reduced until the required criterion is fulfilled.

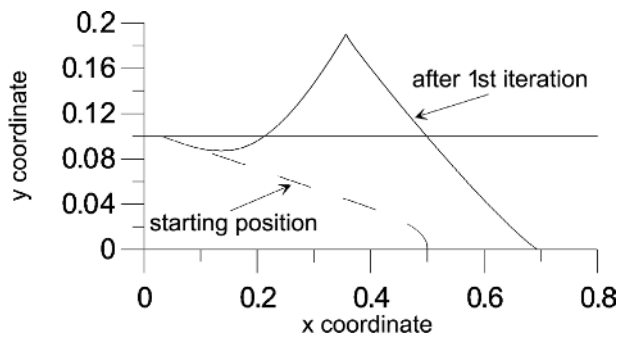


**Figure 5.**  
Estimated curve shape  
without lumping

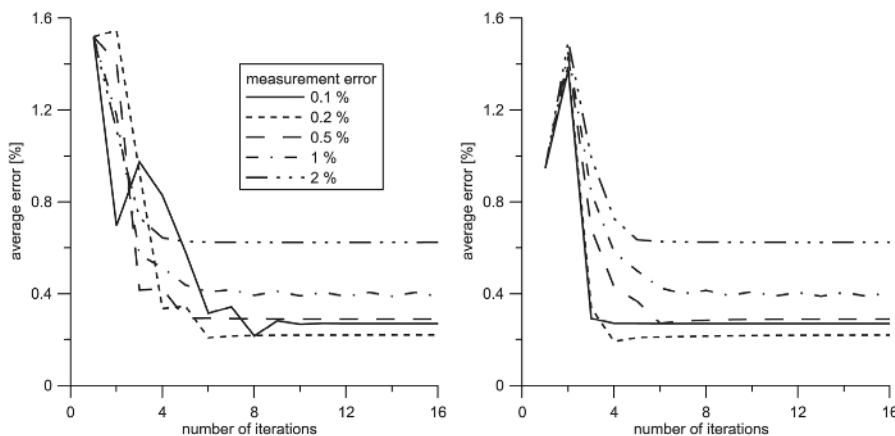


**Figure 6.**  
Comparison of results  
obtained with correcting  
one (left) and all (right)  
estimated values

**5. Influence of the number of measurements and their errors on final results**

In order to demonstrate the main advantages of the lumping algorithm, a two-dimensional continuous casting problem from the copper industry is solved. The following heat fluxes were adopted in these calculations:  $q_{BC} = 4 \times 10^6 \text{ W/m}^2$  and  $q_{CD} = 4,000 (T - T_s) \text{ W/m}^2$ . All the results were obtained for the melting temperature  $T_m = 1,083^\circ\text{C}$ , whereas the end temperature  $T_s$  was assumed to be  $50^\circ\text{C}$ . Temperature measurements were assumed to be read inside the casting material (thermocouples) and along the surface outside the crystallizer (infrared camera).

*5.1 Signals recorded with thermocouples*

First, the influence of measurement errors on the accuracy of the phase change front location was tested. In general, manufacturers provide information on the maximum temperature errors for measurements carried out by thermocouples, for instance less than 2 per cent. In the analyses carried out here, measurement errors were assumed at five levels, to be less than 0.1, 0.2, 0.5, 1 and 2 per cent. In real conditions, the error variation can be approximated by a normal (Gaussian) distribution. In the present paper, measured temperatures were simulated by adding errors to temperatures obtained from the relevant direct solution. The errors are generated by a random generator with normal and/or uniform distribution.

Figure 7 shows the average temperature errors along the estimated phase change interface, for various levels and distributions of measurement errors, where the estimation of the phase change front location was carried out iteratively. This iterative procedure is terminated when the average temperature error stops changing or its changes do not exceed a given tolerance. In the present work, this average error consists of the difference

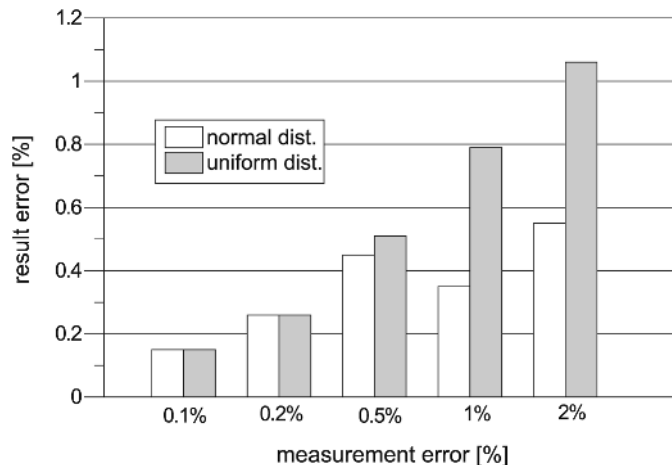


**Figure 7.** Average temperature error along the estimated phase change interface with various levels and distributions of error

between the temperature  $T$  at a node lying on the Bezier curve (solid-liquid boundary) and the melting temperature  $T_m$ , summed over all nodes lying on this interface.

Figure 8 presents the successive locations of the phase change interface and the relevant temperature distribution along this line for normal error distribution and two measurement errors, i.e. 0.5 per cent (case (a)) and 2 per cent (case (b)), respectively.

The influence of the number and location of measurement points was the next issue to investigate. This matter has a significant importance, particularly when the temperature is measured inside the body using thermocouples. In this paper, three different sets of sensors, i.e. sets A, B and C (shown in Figure 9), have been tested. The first and second sets are obtained by immersing five thermocouples in a solidifying material. In set A, the temperature is measured along the estimated boundary, while in set B, sensors are located at the same vertical locations (apart from the bottom one). The last set C consists only of two thermocouples. It can be assumed that each of the thermocouples provide five measurements (at equal time intervals). This means that 25 measurements are obtained for sets A and B, and ten for set C.

For the present problem, the minimum number of measurements necessary to solve the inverse problem is equal to ten. This is because of the application of two Bezier splines to model the phase change front (the number of identified values is equal to ten). Figure 10 shows a comparison of results obtained with

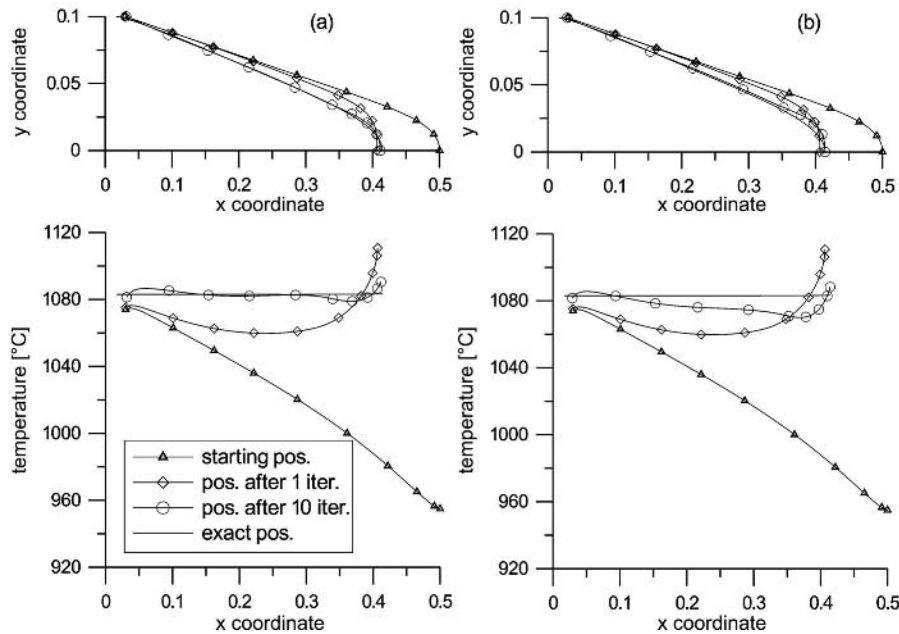


**Figure 8.**  
Location of solid-liquid boundary and temperature distribution along this boundary. (a) mean error 0.5 per cent; (b) mean error 2 per cent

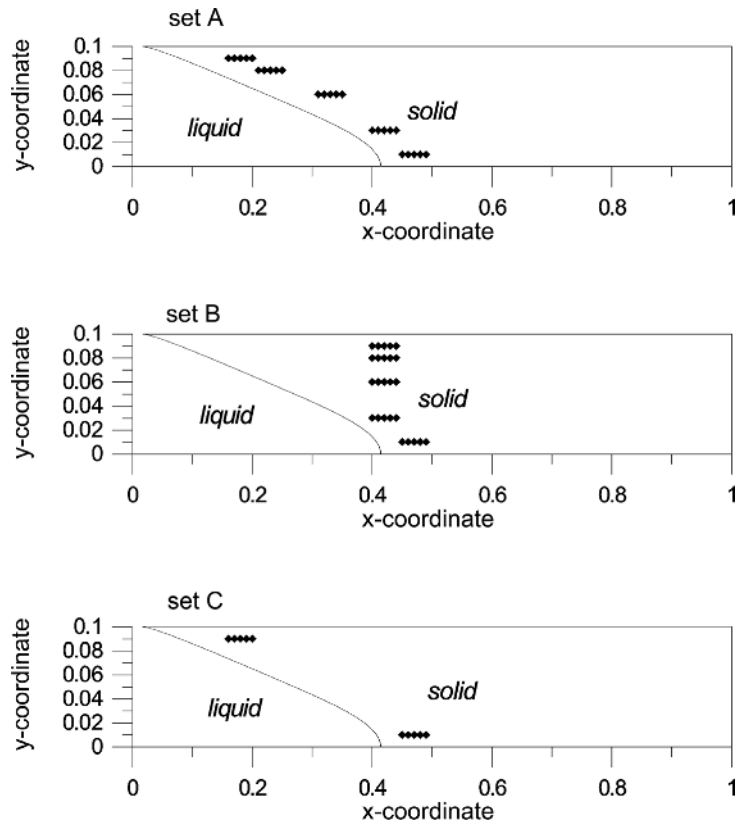


**Figure 9.**  
Three sets of  
temperature sensors

25 measurements for sets A and B, while similar comparisons for sets A and C with ten measurements are shown in Figure 11. In this case, each thermocouple in set A reads only two temperatures. These figures show that the best results are obtained for small measurement errors and sensors placed close to the identified values.

### 5.2 Signals recorded with infrared camera

An infrared camera is an alternative and relatively easy way for obtaining temperature measurements. Furthermore, these cameras measure temperatures with small errors, say 0.2 K. Unfortunately, the temperature has to be measured on the surface of the body outside the crystallizer and therefore, the sensor points are located at some distance from the phase change front. On the other hand, there are no strong limitations on the number of measurement points.

Figures 12 and 13 show results obtained by using an infrared camera for solving inverse geometry thermal problems. The first figure shows successive phase change front locations obtained during the iteration process while in

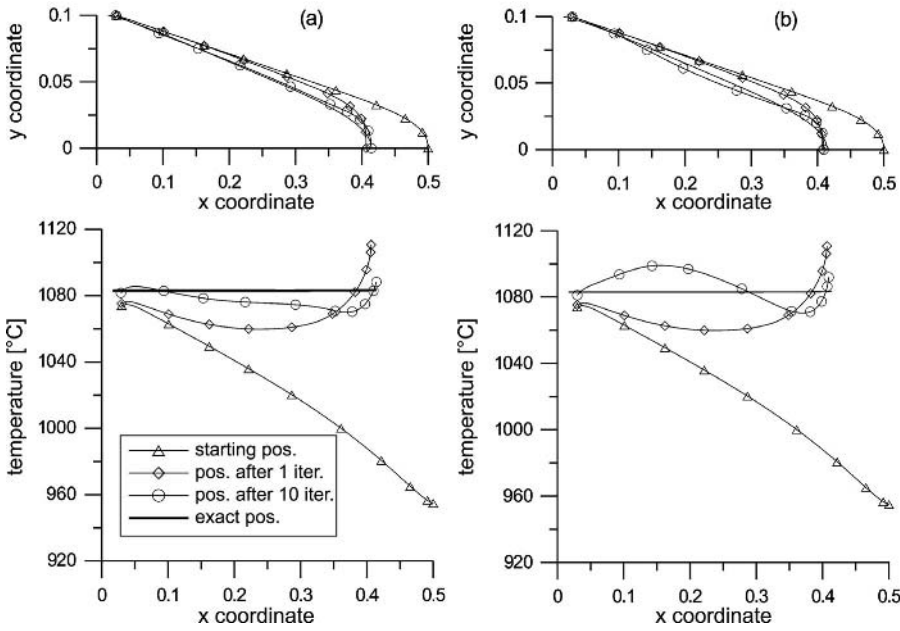


**Figure 10.** Comparison of results for sets A and B (25 measurements). (a) mean error 0.5 per cent; (b) mean error 2 per cent

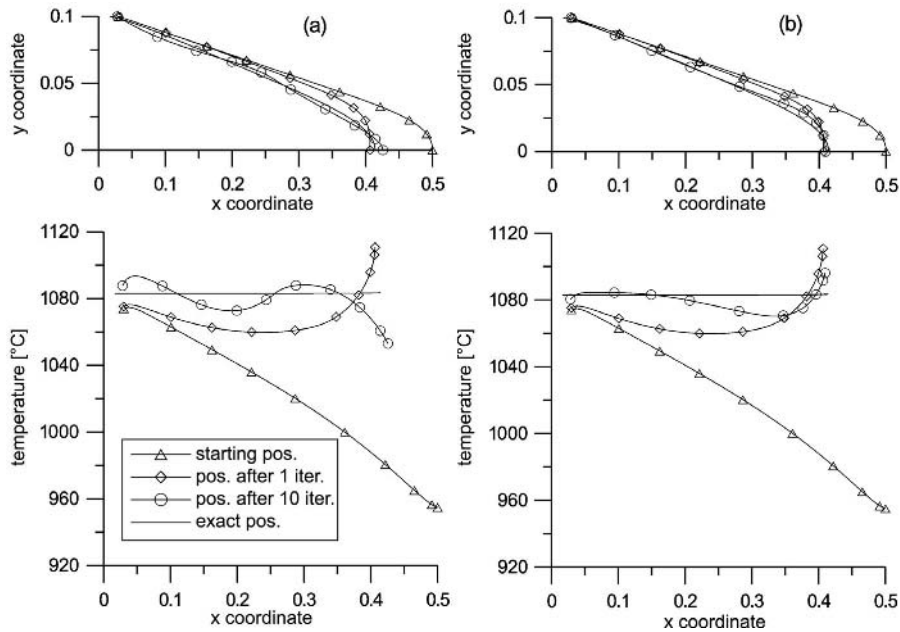


**Figure 11.** Comparison of results for sets A and C (ten measurements). (a) mean error 0.5 per cent; (b) mean error 2 per cent

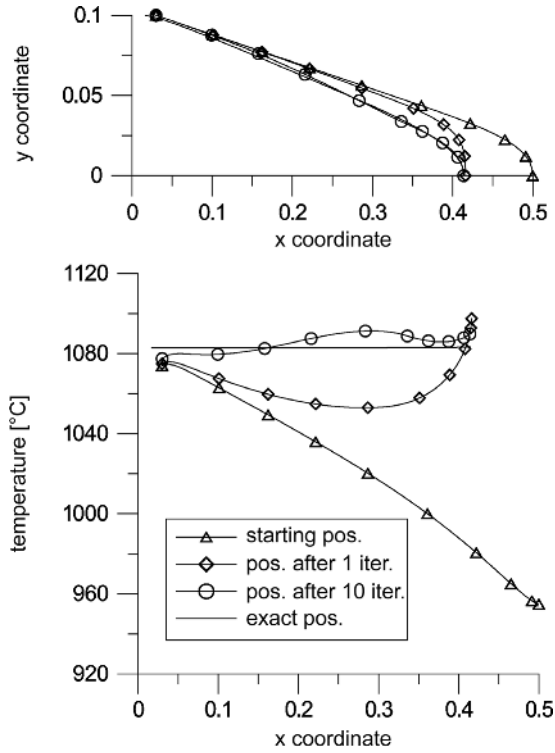


**Figure 12.** Front location and temperature along the interface boundary (40 measurements, maximum error 0.2 per cent)

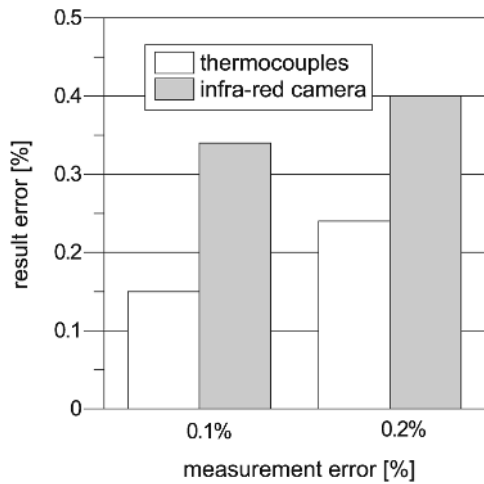


**Figure 13.** Comparison of results obtained for thermocouples (25 measurements) and infrared camera (40 measurements)

the second one, the average error is presented. This error consists of the difference between the temperature  $T$  at a node lying on the Bezier curve (solid-liquid boundary) and the melting temperature  $T_m$ , summed over all nodes lying on this front.

A comparison of both methods (i.e. 25 sensors inside the body and 40 measurements obtained from infrared camera) shows that the results obtained for the same measurement errors are better in the case of using thermocouples. On the other hand, it is difficult to obtain measured temperatures with such a low error level. In the case of infrared cameras, the phase change front location is reasonable in view of the costs of the experiment. Furthermore, measurements can easily be repeated as many times as required.

## 6. Conclusions

This paper presented an algorithm for solving inverse geometry problems in continuous casting. The usefulness of the application of cubic Bezier functions in modelling the phase change boundary has been shown. Using this approach, a significant reduction in the number of identified values and, consequently, the number of measurements have been achieved.

The dependence of the final results on the number, location and accuracy of measurements was investigated. Temperatures were assumed to be measured using thermocouples and/or infrared cameras. The results obtained with both methods were presented and compared.

Some modifications to the solution algorithm, providing faster convergence of the iteration process, have also been discussed. These modifications consist of guessing the initial phase change front position employing a lumping procedure. The paper also demonstrated the applicability of sensitivity analysis to phase change heat transfer processes.

## References

- Beck, J.V. and Blackwell, B. (1988), "Inverse problems", in Minkowycz, W.J., Sparrow, E.M., Schneider, G.E. and Pletcher, R.H. (Eds), *Handbook of Numerical Heat Transfer*, Wiley Interscience, New York.
- Bénard, C. and Afshari, A. (1992), "Inverse Stefan problem: tracking of the interface position from measurements on the solid phase", *International Journal for Numerical Methods in Engineering*, Vol. 35, pp. 835-51.
- Brebbia, C.A., Telles, J.C.F. and Wrobel, L.C. (1984), *Boundary Element Techniques – Theory and Applications in Engineering*, Springer-Verlag, Berlin.
- Crank, J. (1984), *Free and Moving Boundary Problems*, Clarendon Press, Oxford.
- Draus, A. and Mazur, T. (1991), *Corel DRAW Version 2.0 User Handbook*, PLJ Publishing House, Warsaw (in Polish).
- Goldman, N.L. (1997), *Inverse Stefan Problem*, Kluwer Academic Publishers, Dordrecht.
- Kang, S. and Zabaras, N. (1995), "Control of the freezing interface motion in two-dimensional solidification processes using the adjoint method", *International Journal for Numerical Methods in Engineering*, Vol. 38, pp. 63-80.

- Kurpisz, K. and Nowak, A.J. (1995), *Inverse Thermal Problems*, Computational Mechanics Publications, Southampton.
- Nowak, A.J. (1997), "BEM approach to inverse thermal problems", in Ingham, D.B. and Wrobel, L.C. (Eds), *Boundary Integral Formulations for Inverse Analysis*, Computational Mechanics Publications, Southampton.
- Nowak, I., Nowak, A.J. and Wrobel, L.C. (2000), "Tracking of phase change front for continuous casting – inverse BEM solution", in Tanaka, M. and Dulikravich, G.S. (Eds), *Inverse Problems in Engineering Mechanics II, Proceedings of ISIP2000*, Nagano, Japan, Elsevier, pp. 71-80.
- Nowak, I., Nowak, A.J. and Wrobel, L.C. (2001), "Solution of inverse geometry problems using Bezier splines and sensitivity coefficients", in Tanaka, M. and Dulikravich, G.S. (Eds), *Inverse Problems in Engineering Mechanics III, Proceedings of ISIP2001*, Nagano, Japan, Elsevier, pp. 87-97.
- Tanaka, M., Matsumoto, T. and Yano, T. (2000), "A combined use of experimental design and Kalman filter – BEM for identification of unknown boundary shape for axisymmetric bodies under steady-state heat conduction", in Tanaka, M. and Dulikravich, G.S. (Eds), *Inverse Problems in Engineering Mechanics II, Proceedings of ISIP2000*, Nagano, Japan, Elsevier, pp. 3-13.
- Wrobel, L.C. and Aliabadi, M.H. (2002), *The Boundary Element Method*, Wiley, Chichester.
- Zabaras, N. (1990), "Inverse finite element techniques for the analysis of solidification processes", *International Journal for Numerical Methods in Engineering*, Vol. 29, pp. 1569-87.
- Zabaras, N. and Ruan, Y. (1989), "A deforming finite element method analysis of inverse Stefan problems", *International Journal for Numerical Methods in Engineering*, Vol. 28, pp. 295-313.



# Optimization of a window frame by BEM and genetic algorithm

Optimization of a window frame

565

Małgorzata Król

*Department of Heat Supply, Ventilation and Dust Removal Technology,  
Silesian University of Technology, Gliwice, Poland*

Ryszard A. Bialecki

*Institute of Thermal Technology, Silesian University of Technology,  
Gliwice, Poland*

Received April 2002  
Revised September 2002  
Accepted January 2003

**Keywords** *Boundary elements, Genetic algorithms, Heat transfer, Windows*

**Abstract** *Genetic algorithms and boundary elements have been used to find an optimal design of a plastic window frame with air chambers and steel stiffeners. The objective function has been defined as minimum heat loss subject to a constraint of prescribed stiffness and weight of the steel insert.*

## 1. Introduction

### 1.1 Algorithms of shape optimization

Optimization of engineering objects is an inherent portion of the design process. Intuition and experience have been the only available techniques for performing this task for generations of engineers. Introduction of computer techniques opened the possibility of using a systematic approach to optimization. The iterative algorithms used in this process require the solution of a sequence of boundary value problems, typically in domains of varying geometry. As such, computations are numerically very intensive, and nontrivial optimization problems were beyond the reach of practicing engineers for a long time.

The potential economic gains of shape optimization attracted many researchers to this problem (Fox, 1971; Gallagher and Zienkiewicz, 1973; Haftka *et al.*, 1990). An important theoretical tool developed to deal with shape optimization is the sensitivity analysis. The outcome of this technique is a set of sensitivity coefficients defining the influence of the increments of the design parameters onto the variation of the objective function. This set, the gradient of the objective function, is instrumental in many optimization algorithms (conjugate gradient, variable metric, etc.) whose outcome is the optimal shape of the domain under consideration. Various aspects of the sensitivity analysis in the context of shape optimization and inverse analysis have been widely discussed in the literature. The first monograph on this subject seems to be



---

the book by Haung *et al.* (1986). Dems and Mróz (1998) present a state-of-the-art of sensitivity analysis in elasticity and thermoelasticity, and gives a comprehensive literature review of this topic.

The practical application of this technique is often cumbersome due to its mathematical complexity and inherent limitations. The latter situation results from the required properties of the objective function, which should be regular and should possess a positive definite Hessian. As a result, the case of discrete design parameters, specifically the variations in the topology of the domain (e.g. introduction of openings), is not straightforward. Another disadvantage of the standard optimization techniques is their tendency to stall at local optima of the objective function.

Genetic algorithms, whose principle mimics the natural selection process, offer an elegant way of circumventing these disadvantages. The algorithms do not require the calculation of the sensitivity coefficients and can readily be employed to problems with varying topology. Another advantage of genetic algorithms is their robustness in the presence of local optima. On the other hand, the computing time of genetic algorithms is much longer than the case of standard nonlinear programming. The recent reduction in computing costs along with the parallel computing options have made genetic algorithms competitive with standard optimization techniques.

Genetic algorithms (often referred to as evolutionary computations) have been introduced independently by two groups of researchers working in the USA (Fogel *et al.*, 1966; Holland, 1975) and one in Germany (Rechenberg, 1973). The monograph (Goldberg, 1989) presented an unified approach to the problem and is the most frequently cited book in genetic algorithms. Recently, a monograph on applications of evolutionary algorithms has been published in Poland (Arabas, 2001). The important question of parallelization of the genetic calculations is discussed in a review (Seredyński, 1998).

The evaluation of the objective function in the case of shape optimization is achieved by the solution of a boundary value problem in a region of complex shape. In nontrivial cases, this can be accomplished only by using the numerical techniques. This in turn requires the generation of a numerical grid. The finite element method, a domain discretization technique, entails a generation of the grid throughout the entire computational domain. This task, although conceptually trivial, is computationally fairly demanding.

Using the boundary element method (BEM), instead of the FEM, offers a significant advantage, as the discretization of the domain in most cases is restricted solely to the boundary. Thus, due to the reduction of the dimensionality, the automatic grid generation in BEM is much easier to implement than in FEM. Therefore, if the problem at hand can be reduced to a boundary only formulation, BEM is a preferred numerical technique in shape optimization.

---

Summing up this short review of the available shape optimization techniques, the combination of genetic algorithms and the BEM seem to be the most attractive technique for solving this class of problems, and this has been recognized by Kita and Tani (1997). A recent paper of Burczyński *et al.* (2002) discusses the application of BEM and evolutionary algorithms in optimization and identification.

### 1.2 Window frame optimization

The increasing energy costs and lower admissible CO<sub>2</sub> emission are the driving forces for the need to reduce heat losses from buildings. The building envelope elements exert a major influence on the energy consumption of buildings. In the early stage of the R&D process in this field, the main stress has been on increasing the thermal resistance of the walls. Progress in this area has been achieved mainly by the introduction of new materials and additional layers of thermal insulation. Because of the new regulations in national and international standards, the admissible value of the heat losses of the walls has been considerably reduced in the last few decades.

Another potential source for the reduction in heat losses from buildings is the optimization of the ventilation system. Research in this area concentrates on decreasing the amount of infiltrating air and introducing forced ventilation equipped with recuperating heat exchangers.

However, about 30 per cent of heat is lost through the windows in a building. Typical windows consist of double glazed panes and wooden, plastic or metal frames. Many efforts have therefore been made to reduce the transmissivity of the glazing system. The heat resistance of a double pane can be increased by selecting an optimal distance between the glass sheets and filling this gap with a low conductivity gas. Radiative heat losses through the glazing system are reduced by the introduction of thin coatings and by using glass of low emissivity. In contemporary designs, the total heat losses from panes are as low as 1.1 W/m<sup>2</sup>K. At the current energy price level, further insulation improvement does not seem to be economically justified.

Window frames have smaller surface area than window panes, thus, for a long time, the optimal thermal design of these elements has been of secondary importance. At current levels of glazing and wall insulation, the question of heat losses from window frames has become more important.

The present paper deals with the optimal design of a plastic window frame. This kind of frame has become very popular due to its low price, easy maintenance and reasonable insulation properties. To increase the thermal resistance of the frame and minimize its weight, the air cavities are introduced. However, as the plastic frames do not have the required stiffness, metal profiles are inserted in the frame and the presence of a high conducting metal increases the heat losses. The topic of the present study is the optimal placement of the stiffener and the air cavities in order to achieve minimum heat losses through

the frame while maintaining the required stiffness and using the same amount of metal.

## 2. Formulation of the problem

### 2.1 Heat transfer

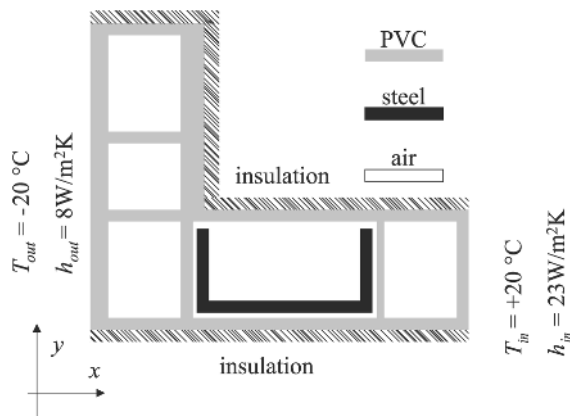
A 2D steady-state heat transfer problem is considered. The frame consists of three materials: PVC, air and steel. Constant material properties have been assumed. The values taken in the calculations are shown in Table I. For the temperature differences and geometrical dimensions occurring in the problem, both natural convection and radiation are of minor importance in the air filled enclosures. Thus, it is assumed that the heat in the cavities is transferred solely by conduction.

Prescribed boundary conditions are shown in Figure 1. On the portions of the contour exposed to the environment and in contact with the air in the room, Robin boundary conditions are prescribed. The values of the indoor and outdoor temperatures were set to +20 and  $-20^{\circ}\text{C}$ , which is in agreement with the Polish standards PN-82/B-02402 and PN-82/B-02403. The values of the indoor and outdoor heat transfer coefficients, 23 and  $8\text{ W/m}^2\text{K}$ , have been taken from another Polish standard PN-EN ISO 6946. Heat transfer through the remaining portions of the external surface of the frame has been neglected. On the interfaces between the different materials, ideal thermal contact,

**Table I.**  
Material properties  
used in the  
calculations

Material	Heat conductivity ( $\text{W/m}^2\text{K}$ )
PVC	0.163
Air	0.023
Steel	58.00

**Figure 1.**  
Geometry and prescribed  
boundary conditions  
for the window frame



i.e. continuity of both temperature and heat flux has been assumed. The geometry of the numerical examples investigated is a simplified version of a real frame taken from Technical approval ITB (1998). Optimization of a window frame

### 2.2 Formulation of the optimization problem

The objective of the optimization is to minimize the heat losses subjected to several constraints.

It is assumed that the element of the frame can be modeled as a beam. Additional stiffness resulting from the connections with other elements of the frame is neglected, which is a conservative assumption. The standard 1D beam equation used in the study is given by

$$EI \frac{d^4 u}{dx^4} = 0 \quad (1)$$

where  $u$  is the deflection of the axis of the beam,  $E$  and  $I$  are the Young's modulus and moment of inertia, respectively.

As the contribution of the plastic to the overall stiffness of the frame is negligible, the measure of the stiffness is the moment of inertia of the metal insert with respect to the vertical ( $y$ ) axis passing through the centre of gravity.

With this definition of stiffness, the following additional conditions should be fulfilled:

- minimum stiffness should be maintained,
- amount of metal should not exceed a prescribed value,
- stiffener is contained within air cavities (and not immersed in plastic),
- outer contour of the plastic frame is not changed by the algorithm,
- thickness of the plastic interior walls is 1 mm while that of the exterior is 3 mm, and
- geometry of the frame is approximated by a set of line segments.

The design variables are contractions, expansions and translations of the air cavities, and deformations of the steel insert. The location of the *characteristic points* of the boundary, i.e. the corner points of the air cavities and the stiffener, is expressed in terms of decision variables defined as the coordinates of some *control points*. In the developed algorithm, the coordinates of the characteristic points are defined as an arbitrary linear combination of the coordinates of the control points. This approach offers significant flexibility in defining the admissible variation of the geometry.

## 3. Numerical technique

### 3.1 Solution of the heat conduction problem

The heat losses from the frame have been computed using BETTI, a boundary element code (Bialecki and Kuhn, 1993). The details of the BEM technique are

available in Wrobel (2002). Only the basic steps of BEM are mentioned in the present paper.

The first step in the BEM is a transformation of the original boundary value problem in a homogeneous domain into an equivalent integral equation of the form (Wrobel, 2002)

$$c(\mathbf{p})T(\mathbf{p}) = \int_C [q(\mathbf{r})T^*(\mathbf{p}, \mathbf{r}) - T(\mathbf{r})q^*(\mathbf{p}, \mathbf{r})] dC(\mathbf{r}) \quad (2)$$

where  $\mathbf{r}$  and  $\mathbf{p}$  are vector coordinates of the current and observation points, respectively.  $T$  is the temperature and  $q$  the associated heat flux  $q = -k\nabla T \cdot \mathbf{n}$ , where  $k$  is the heat conductivity and  $\mathbf{n}$  is the outward unit normal vector of the contour,  $T^*$  is the fundamental solution of the Laplace equation and  $q^* = -k\nabla T^* \cdot \mathbf{n}$ .  $c(\mathbf{p})$  is a fraction of the angle with vertex at  $\mathbf{p}$  subtended in the domain.

The next step is the discretization of equation (2). The first stage of this procedure is the subdivision of the contour into a set of (boundary) elements. The geometry of every element is approximated using locally based shape functions, expressed in local coordinates. The same set of functions is used to approximate the variation of temperature and normal flux within elements. Introduction of these approximations into the original integral equation (2) produces residuals. The final set of equations is then generated by the nodal collocation, i.e. requiring that the residuals vanish a set of nodal points. The result reads

$$\mathbf{H}^i \mathbf{T}^i + \mathbf{G}^i \mathbf{q}^i = 0 \quad (3)$$

where  $\mathbf{H}$  and  $\mathbf{G}$  are the influence matrices and the vectors  $\mathbf{T}$  and  $\mathbf{q}$  are the values of temperature and heat fluxes at the boundary nodes. Superscript  $i$  refers to the subregion number.

The procedure is repeated in all subregions and the sets of linear equations corresponding to the subregions are linked by enforcing the continuity of temperature and heat flux on the interface between the adjacent subregions.

In the present study, the geometry as well as the distributions of both boundary temperature and heat flux have been approximated by isoparametric continuous quadratic elements. In the presence of corner points at the interface, this type of element fails to produce the sufficient number of equations (Bialecki *et al.*, 1993). To circumvent this problem, a pair of constant elements meeting at such points have been introduced.

### 3.2 Constraints

To check the satisfaction of the constraints, evaluation of the surface area, coordinates of the mass centre and the moment of inertia are required. All these quantities may be expressed in terms of the surface integrals, namely

$$A = \int_A dA \quad (4)$$

$$x_0 = \frac{\int_A x dA}{A} \quad (5)$$

$$I_{yy} = \int_A (x - x_0)^2 dA \quad (6)$$

where  $A$  is the surface area,  $x_0$  is the  $x$  coordinate of the mass centre and  $I_{yy}$  is the moment of inertia with respect to the  $y$  axis passing through the mass centre.

The evaluation of these surface integrals can be significantly simplified by converting them into the contour integrals. This has been accomplished by making use of the Stokes theorem

$$\oint_C \vec{w} \cdot d\vec{C} = \int_A \text{curl} \vec{w} \cdot d\vec{A} \quad (7)$$

where  $\vec{w}$  is an arbitrary vector and  $C$  is the contour of the surface  $A$ .

As the surface of integration lies in the  $xy$  plane, the normal infinitesimal surface vector is defined as  $d\vec{A} = [0, 0, dx dy]$  and the tangential contour line vector has the form of  $d\vec{C} = [dx, dy, 0]$

Denoting the vectors used to calculate the surface area, center of gravity and moment of inertia by  $w_A$ ,  $w_y$  and  $w_I$ , respectively, their curls are defined as

$$\text{curl} \vec{w}_A = [0, 0, 1] \quad (8)$$

$$\text{curl} \vec{w}_y = [0, 0, x] \quad (9)$$

$$\text{curl} \vec{w}_I = [0, 0, (x - x_0)^2] \quad (10)$$

It can be readily proved that the vectors  $\vec{w}$  should be defined as

$$\vec{w}_A = [0, x, 0] \quad (11)$$

$$\vec{w}_y = [-xy, 0, 0] \quad (12)$$

$$\vec{w}_I = [-y(x - x_0)^2, 0, 0] \quad (13)$$

The parametric equations of the line segments constituting the contour of the frames can be written as

$$x = x_b + (x_e - x_b)t \quad (14)$$

$$y = y_b + (y_e - y_b)t \quad (15)$$

where the indices  $b$  and  $e$  correspond to the start and end points of the segments, respectively, and  $t$  represents a parameter assuming values in the interval  $[0, 1]$ . Using the parametric representations (14) and (15), the infinitesimal tangential contour vector can be expressed as

$$d\vec{C} = [x_e - x_b, y_e - y_b, 0] dt \quad (16)$$

Using equations (7-16), the surface area, coordinates of the mass center and the moment of inertia can be written as a sum of definite integrals over  $[0, 1]$  intervals corresponding to the subsequent line segments constituting the contour of the frame.

### 3.3 Genetic algorithm

The evaluation of the optimal geometry of the frame, in the sense of minimum heat losses subject to the constraints defined in the previous section, has been accomplished using a standard genetic algorithm. The details of this technique have been described in Goldberg (1989).

The main features of the implemented version of the algorithm are given in the following description.

The procedure starts with the creation of an initial population consisting of  $N_G$  identical members. The fitness function used is expressed in terms of heat losses  $Q_L$  by relationship  $fitness = (Q_L)^{-p}$ , where  $p$  is a user defined constant.

In the subsequent steps of the procedure, new generations are created. The number of individuals in a generation does not change throughout the iterative process and the new generation is generated in three stages: selection, mutation and mating.

The probability of selecting candidates for the next generation is proportional to their fitness functions. The genes of the selected members undergo creeping mutation and the probability of this process is  $P_m$ . If after this operation the genes of the member fulfill the prescribed constraints, then the individual is included in the new generation, otherwise, the procedure of generating a new member is repeated.

Mating starts with the random selection of two members of the new population. The probability of selection is the same for all members. After a pair is selected, the crossover is triggered with a probability of  $P_c$ . In the process of procreation, the location of the chromosome interchange is selected at random. If the offspring fulfill the constraints, then they substitute the parents, otherwise, the parents remain in the population. The number of individuals selected for crossover is equal to the number of individuals in the generation. The version of the genetic algorithm used in this work uses the predefined number  $N_p$  of generations that have been created as the stopping

criterion. The termination condition can also be formulated in terms of the convergence defined as the improvement of the fitness in the best member of the subsequent generations.

The coordinates of the control points are coded as genes associated with a given member of the population. Gen is coded as a sequence of 32 bits. The smallest change of the displacement within the procedure is defined as 0.001 mm. This is much higher than the accuracy of frame manufacturing. From the practical point of view, the changes of the geometry can therefore be treated as continuous. The number of genes in a chromosome is equal to the number of degrees of freedom, i.e. admissible displacements of the control points.

#### 4. Numerical examples

Even in the very simplified geometry considered in this paper, the number of design parameters is very large. The present study is an introductory step to the optimization of a movable and fixed window framework taking into account their thermal interaction with the glass pane and the wall. The aim of the numerical examples discussed in this paper is to identify the crucial degrees of freedom whose change would significantly influence the objective function. Another purpose of this paper is to tune the genetic algorithm by finding out the values of its characteristic parameters controlling the convergence of the procedure. Because of the required CPU times, this kind of parametric study would be difficult to perform in the case of the target being a large computational domain.

##### 4.1 Example 1

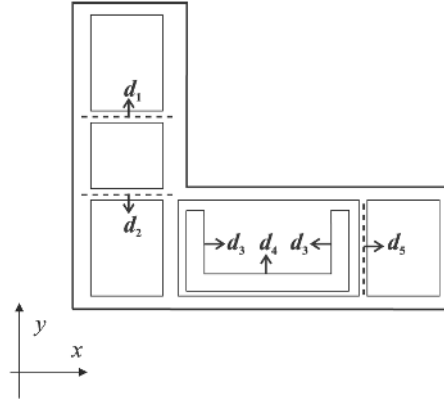
In this example, the initial moment of inertia of the metal insert has been chosen as  $2.12 \text{ cm}^4$ , i.e. it was larger than the minimum required value of  $1.3 \text{ cm}^4$ . The motivation for such a choice of the starting solution was to check whether the procedure will reduce, as the common sense suggests, the moment of inertia to the predefined minimum. The stiffener has been allowed to bend in the center of its segments. The surface area of the insert was constant throughout the optimization process, namely  $1.17 \text{ cm}^2$ . The design parameters used in this example are shown in Figure 2.

This example has been used to study the influence of the control parameters of the genetic algorithm on the convergence and numerical efficiency.

The efficiency and accuracy of the genetic algorithm depends on the values of a set of tuning parameters:

- number of individuals in the generation,  $N_g$ ;
- probability of mutation,  $P_m$ ;
- probability of crossover,  $P_c$ ;
- power used in the definition of the fitness function,  $p$ ;
- number of populations,  $N_p$ .

**Figure 2.**  
Design parameters  
used – example 1

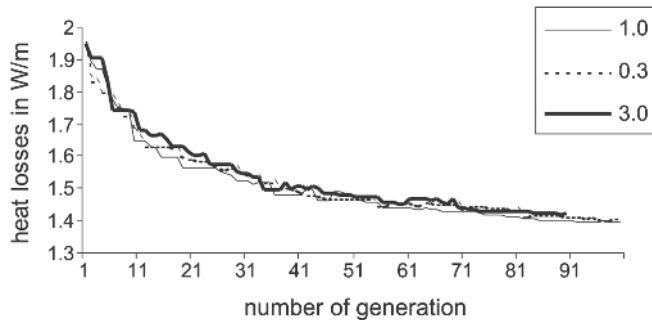


Only the last quantity can be adjusted during the computations by a simple check of the convergence. There is no sound theory on how the remaining parameters should be selected. Thus, it is a common practice to choose these values using heuristic reasoning. To gain some experience on how these parameters influence the convergence rate, several test runs have been made. The best set of parameters have been used in the next numerical examples.

The methodology used in these tests is simple: while keeping the values of all but one parameter at the same level, the parameter of interest was changed. The standard values of the parameters used in these tests were as follows: number of individuals in the generation  $N_g = 30$ , number of populations  $N_p = 100$ , probability of mutation  $P_m = 0.15$ , probability of crossover  $P_c = 0.5$  and power of the fitness function  $p = 1$ .

In the first set of calculations, the power used in the definition of the fitness function has been examined. The selected values were  $p = 0.3, 1$  and  $3$ . As can be seen in Figure 3, this parameter has practically no influence on both the convergence rate and the value of the optimum.

**Figure 3.**  
Plots of the lowest heat losses with a given population showing the influence of the power used in the fitness function. The parameter on the curves are the values of  $p$  in the definition fitness =  $1/Q_L^p$



In the second set of calculations, the number of individuals in the generation has been varied. The values used in calculations were  $N_g = 10, 20$  and  $30$ . Figure 4 shows that for  $N_g = 10$ , the convergence rate is much lower than the other values. Populations of  $20$  and  $30$  individuals produce almost the same results.

Similar tests have been conducted out for different values of the probability of mutation. Here, values of  $P_m = 0.05, 0.15$  and  $0.45$  have been selected. The results are shown in Figure 5. While  $P_m = 0.05$  result in a slow convergence, probabilities  $P_m = 0.15$  and  $0.45$  give practically the same results.

The final result of the optimization was a reduction in the heat losses from  $1.94$  to  $1.38$  W/m, i.e. about 30 per cent. At the optimal point, the moment of inertia has, as expected, reached the lowest admissible value of  $1.3$  cm<sup>4</sup>. These results have been obtained taking 100 generations with population of one generation equal to 30 and the probabilities of mutation  $P_m = 0.15$  and mating  $P_c = 0.5$ . Figure 6 shows the history of the reduction of the heat losses within the optimization process and Figures 7 and 8 show the initial and resulting geometries of the frame.

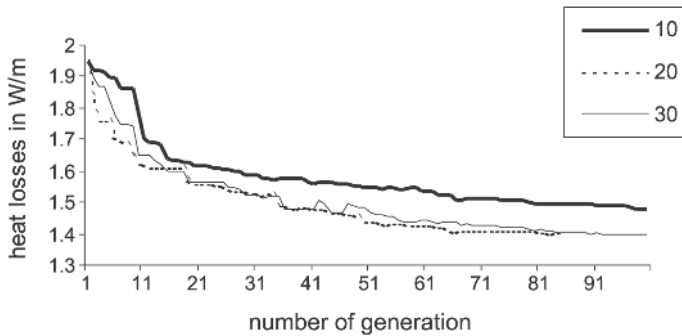


**Figure 4.** Plots of the lowest heat losses within a given generation showing the influence of the number of individuals in the population

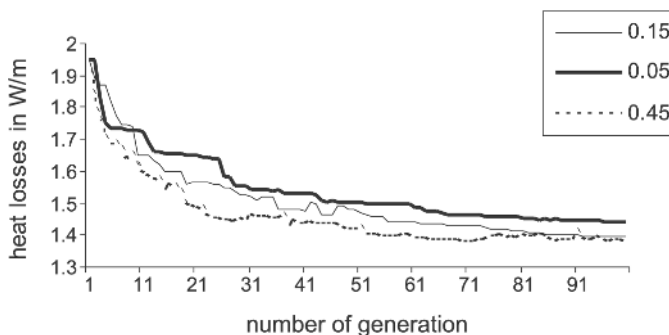


**Figure 5.** Plots of the lowest heat losses within a given generation showing the influence of the probability of mutation

Another outcome of these tests was the observation that the optimum can be achieved for two different configurations of walls separating the three leftmost cavities. Thus, more than one optimal configurations of the frame may exist.

4.2 Example 2

In this example, the starting configuration was the same as in the previous example. The moment of inertia has been kept constant at the level of  $2.12 \text{ cm}^4$ .

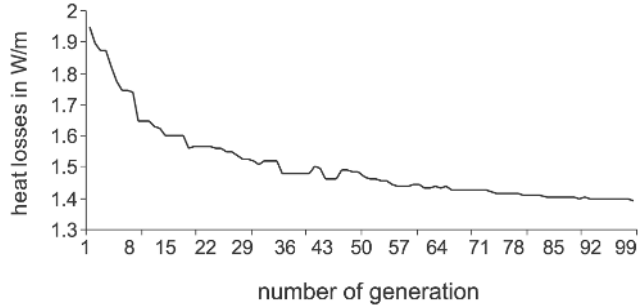


**Figure 6.**  
Plots of the lowest heat losses within a given generation showing the reduction of heat losses in the course of iterations

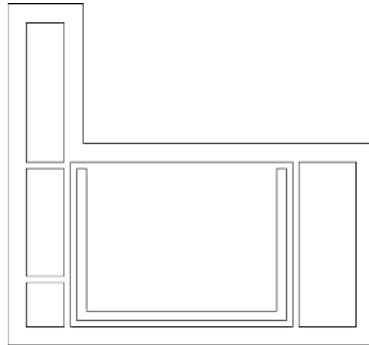


**Figure 7.**  
Starting configuration of the frame – example 1

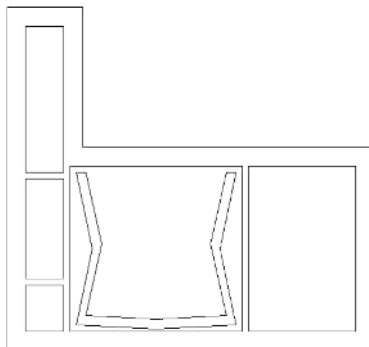


**Figure 8.**  
Resulting geometry of the frame after optimization – example 1

A constant value for the surface area has been taken as in the previous example, namely  $1.17\text{ cm}^2$ . The thickness and length of the horizontal and vertical arms of the stiffener were allowed to change independently and the initial value of the thickness was  $1.5\text{ mm}$ . The lowest admissible thickness was set to  $1\text{ mm}$ . This condition was introduced to prevent solutions with too slender profiles. The angle of inclination of the vertical arms were allowed to vary. The surface area of the insert was constant. The remaining parameters of the genetic algorithm were taken as in the previous example. A sketch of the degrees of freedom is shown in Figure 9.

The result of the optimization was a reduction in the heat losses from  $1.94$  to  $1.72\text{ W/m}$ , i.e. about  $13\text{ per cent}$ . These results have been obtained by taking  $250$  generations. Figures 10 and 11 show the initial and resulting geometries of the frame. The optimal values of the thicknesses were  $d_7 = 2.43\text{ mm}$ ,  $d_8 = 2.27\text{ mm}$  and  $d_9 = 1\text{ mm}$ . It should be noted that the latter value is the lowest admissible thickness of the profile.

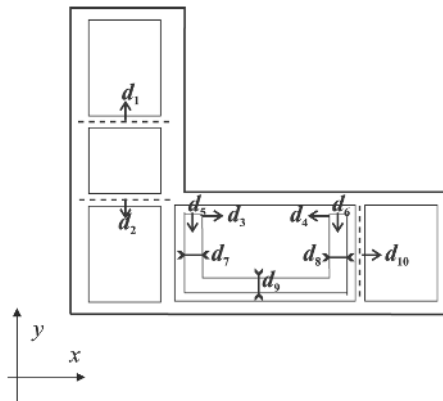


**Figure 9.**  
Design parameters used – example 2

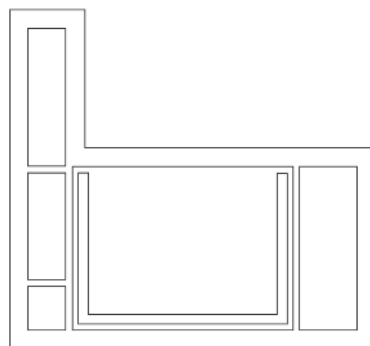


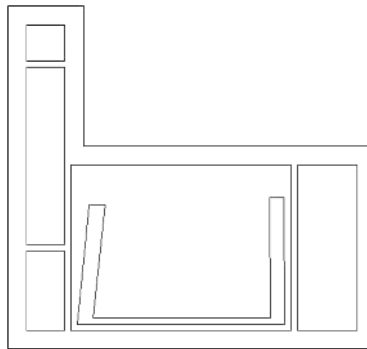
**Figure 10.**  
Starting configuration of the frame – example 2

4.3 Example 3

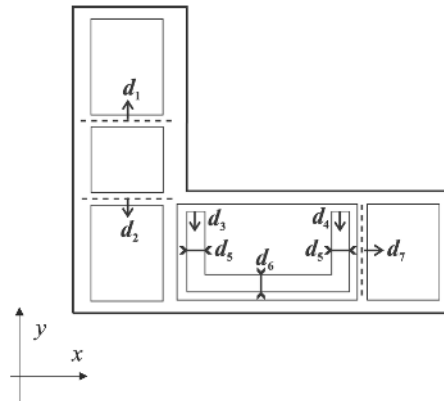
In this example, the initial moment of inertia has been kept constant at the level of the admissible value, i.e.  $1.3 \text{ cm}^4$ . The thickness and length of the horizontal and vertical arms of the stiffener were allowed to change. While the thickness of the left and right arm were the same, their lengths could vary independently. No constraint has been imposed on the minimum thickness of the profile and the surface area of the insert was constant. The remaining parameters of the genetic algorithm were taken as in the previous example. A sketch of the degrees of freedom is shown in Figure 12.

The final result of the optimization was a reduction in the heat losses from 1.66 to 1.44 W/m, i.e. about 12 per cent. These results have been obtained by taking 450 generations. Figures 13 and 14 show the initial and resulting geometries of the frame. The obtained thickness of the vertical arms was  $d_5 = 3.28 \text{ mm}$  while the thickness of the horizontal arm was  $d_6 = 0.87 \text{ mm}$ .

**Figure 11.**  
Resulting geometry of  
the frame after  
optimization – example 2



**Figure 12.**  
Design parameters used  
in example 3



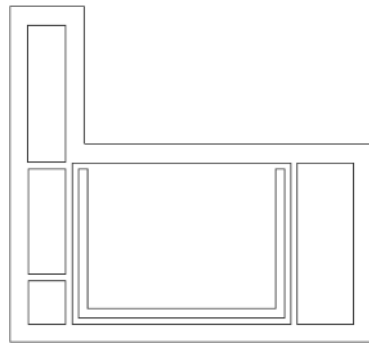


**Figure 13.**  
Starting configuration of  
the frame – example 3

---

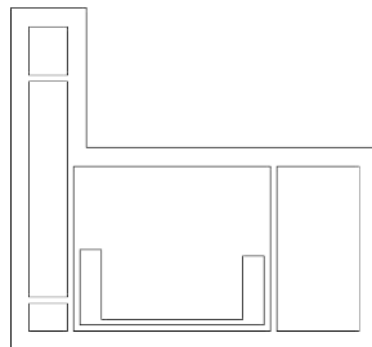


**Figure 14.**  
Resulting geometry of  
the frame after  
optimization – example 3

---

## 5. Conclusions

The application of genetic algorithms with fitness calculated by the BEM has proved to be a robust technique in dealing with the shape optimization problem, where heat transfer and elasticity interact. The calculations carried out show the possibility of a substantial reduction in the heat losses from a window frame. This can be achieved by a simple modification of the geometry of the plastic frame and the steel stiffener. In the final configuration, the heat losses may be reduced by as much as 30 per cent. The heat losses can be reduced by decreasing the length of the horizontal arm of the stiffener and its thickness, while increasing the thickness of the vertical arms and changing their inclination and shape.

Test runs have given some optimal values of the tuning parameters of the algorithm. This knowledge and the observations concerning the possible degrees of freedom will be used in the next stage of the research, when more complex configurations of the computational domain will be considered.

**References**

- Arabas, J. (2001), *Lectures on Evolutionary Algorithms*, Wydawnictwa Naukowo Techniczne, Warsaw.
- Bialecki, R.A. and Kuhn, G. (1993), *Upgrading BETTI: Introducing Nonlinear Material, Heat Radiation and Multiple Right Hand Sides Options*, Rept. No. 019 2 0199894 2 9 under contract with Mercedes Benz A.G., Lehrstuhl für Technische Mechanik, Universität Erlangen-Nürnberg, Erlangen, Germany.
- Bialecki, R.A., Dallner, R. and Kuhn, G. (1993), "New application of the hypersingular equations in the boundary element method", *Computer Methods in Applied Mechanics and Engineering*, Vol. 103, pp. 399-416.
- Burczyński, T., Beluch, W., Długosz, A., Kuś, W., Nowakowski, M. and Orantek, P. (2002), "Evolutionary computation in optimization and identification", *Computer Assisted Mechanics and Engineering Sciences*, Vol. 9, pp. 3-20.
- Dems, K. and Mróz, Z. (1998), "Methods of sensitivity analysis", in Kleiber, M. (Ed.), *Handbook of Computational Solid Mechanics*, Springer-Verlag, Berlin.
- Fogel, L., Owens, A. and Walsh, M. (1966), *Artificial Intelligence through Simulated Evolution*, Wiley, Chichester.
- Fox, R.L. (1971), *Optimization Methods for Engineering Design*, Addison-Wesley, Reading, MA.
- Gallagher, R.M. and Zienkiewicz, O.C. (Eds) (1973), *Optimum Structural Design: Theory and Applications*, Wiley, London.
- Goldberg, D.E. (1989), *Genetic Algorithms in Search, Optimization and Machine Learning*, Addison-Wesley, Reading, MA.
- Haftka, R.T., Gürdal, Z. and Kamat, M.P. (1990), *Elements of Structural Optimization*, Kluwer, Dordrecht.
- Haung, H.J., Choi, K.K. and Komkov, V. (1986), *Design Sensitivity Analysis of Structural Systems*, Academic Press, Orlando.
- Holland, J.H. (1975), *Adaptation in Natural and Artificial Systems*, University of Michigan Press, Ann Arbor.
- Kita, E. and Tani, H. (1997), "Shape optimization of continuum structures by genetic algorithm and boundary element method", *Engineering Analysis with Boundary Elements*, Vol. 19 No. 2, pp. 129-36.
- Polish Standard PN-82/B-02402 *Heating; Temperature for Heated Rooms in Building*.
- Polish Standard PN-82/B-02403 *Heating; Exterior Calculated Temperatures*.
- Polish Standard PN-EN ISO 6946 *Building Components and Building Elements. Heat Resistance and Thermal Transmittance – Calculation Methods*.
- Rechenberg, I. (1973), *Evolutionsstrategie: Optimierung technischer Systeme nach Prinzipien der biologischen Evolution*, Frohmann-Holzboog, Stuttgart.
- Seredyński, F. (1998), "New trends in parallel and distributed evolutionary computing", *Fundamenta Informaticae*, IOS Press, Vol. 35 Nos 1-4 pp. 211-30.
- Technical approval ITB AT-15-2045/98 (1998), *Windows and Balcony Doors of the KBE AD and KBE MD Systems of Plastified PVC Sections*, Institute of Building Technology, Warsaw.
- Wrobel, L.C. (2002), *The Boundary Element Method*, Wiley, Chichester, Vol. 1.



# BEM/FVM conjugate heat transfer analysis of a three-dimensional film cooled turbine blade

BEM/FVM  
conjugate heat  
transfer analysis

581

Received July 2002  
Revised January 2003  
Accepted January 2003

A. Kassab and E. Divo

*Mechanical, Materials, and Aerospace Engineering Department,  
University of Central Florida, Orlando, Florida, USA*

J. Heidmann

*James D. Heidmann, NASA Glenn Research Center, Cleveland,  
Ohio, USA*

E. Steinhörsson

*A&E Consulting, 27563 Hemlock Drive, Westlake, Ohio, USA*

F. Rodriguez

*Mechanical, Materials, and Aerospace Engineering Department,  
University of Central Florida, Orlando, Florida, USA*

**Keywords** Heat transfer, Coupled phenomena, Boundary elements, Finite volume

**Abstract** We report on the progress in the development and application of a coupled boundary element/finite volume method temperature-forward/flux-back algorithm developed to solve conjugate heat transfer arising in 3D film-cooled turbine blades. We adopt a loosely coupled strategy where each set of field equations is solved to provide boundary conditions for the other. Iteration is carried out until interfacial continuity of temperature and heat flux is enforced. The NASA-Glenn explicit finite volume Navier-Stokes code Glenn-HT is coupled to a 3D BEM steady-state heat conduction solver. Results from a CHT simulation of a 3D film-cooled blade section are compared with those obtained from the standard two temperature model, revealing that a significant difference in the level and distribution of metal temperatures is found between the two. Finally, current developments of an iterative strategy accommodating large numbers of unknowns by a domain decomposition approach is presented. An iterative scheme is developed along with a physically-based initial guess and a coarse grid solution to provide a good starting point for the iteration. Results from a 3D simulation show the process that converges efficiently and offers substantial computational and storage savings.

## 1. Introduction

Engineering analysis of complex mechanical devices such as turbomachines requires an ever-increasing fidelity in numerical models upon which designers

This research was carried out under the funding from an NRA grant NAG3-2311 from NASA Glenn Research Center. The authors are grateful to Dr Ali Ameri of AYT corporation for his helpful input and advice in the course of this study.

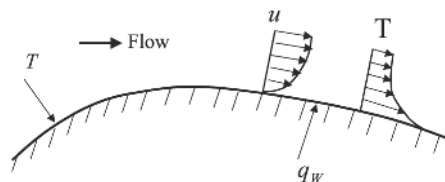


rely in their efforts to attain demanding specifications placed on the efficiency and durability of modern machinery. Consequently, the trend in computational mechanics is to adopt coupled-field analysis to obtain computational models, which attempt to better mimic the physics under consideration (Kassab and Aliabadi, 2001). The coupled-field problem, which we address in this paper is conjugate heat transfer (CHT), i.e. the coupling of convective heat transfer external to the solid body of a thermal component coupled to conduction heat transfer within the solid body of that component (Figure 1). CHT thus applies to any thermal system in which the multi-mode convective/conduction heat transfer is of particular importance to thermal design, and thus CHT in most instances arises naturally where the external and internal temperature fields are coupled.

Conjugacy is often ignored in most analytical solutions and numerical simulations. For instance, it is in common practice in the analysis of turbomachinery (Heidmann *et al.*, 2002) to carry out separate flow and heat conduction analyses. Heat transfer coefficient as well as film effectiveness values are predicted using two independent external flow solutions, each computed by imposing a different constant wall temperature at the surfaces of the turbine blade exposed to hot gases and film cooling air. The film effectiveness determines the reference temperature for the computed film coefficients. In turn, these values are used to impose convective boundary conditions to a conduction solver to obtain predicted metal temperatures. As shown in the example section of this paper, the shortcomings of this approach, which neglects the effects of the wall temperature distribution on the development of the thermal boundary layer are readily overcome by a CHT analysis, in which the coupled nature of the field problem is explicitly taken into account in the analysis.

There are two basic approaches to solve the coupled field problems. In the first approach, a direct coupling is implemented in which different fields are solved simultaneously in one large set of equations. Direct coupling is mostly applicable for problems where time accuracy is critical, for instance, in aero-elasticity applications where the timescale of the fluid motion is of the same order as the structural modal frequency. However, this approach suffers a major disadvantage due to mismatch in the structure of the coefficient matrices arising from boundary element method (BEM), finite element method (FEM) and/or finite volume method (FVM) solvers. That is, given the fully populated nature of the BEM coefficient matrix, the direct coupling approach would

**Figure 1.**  
CHT problem: external convective heat transfer coupled to heat conduction within the solid



---

severely degrade the numerical efficiency of the solution by directly incorporating the fully populated BEM equations into the sparsely banded FEM or FVM equations. A second approach which may be followed is a loose coupling strategy where each set of field equations is solved separately to produce boundary conditions for the other. The equations are solved in turn until an iterated convergence criterion, namely continuity of temperature and heat flux, is met at the fluid-solid interface. The loose coupling strategy is particularly attractive when coupling auxiliary field equations to computational fluid dynamics codes as the structure of neither solver interferes in the solution process.

Several approaches can be taken to solve the coupled field problems and are mostly based on either FEM or FVM or a combination of these two field solvers. Examples of such loosely coupled approaches applied to a variety of CHT problems ranging from engine block models to turbomachinery can be found in Bohn *et al.* (1997, 1999), Comini *et al.* (1993), Hahn *et al.* (2000), Kao and Liou (1997), Patankar (1978), Shyy and Burke (1994), and in Tayala *et al.* (2000) where multi-disciplinary optimization is considered for CHT modelled turbine airfoil designs. Hassan *et al.* (1998) developed a conjugate algorithm, which loosely couples a FVM-based hypersonic CFD code to an FEM heat conduction solver in an effort to predict ablation profiles in hypersonic re-entry vehicles. Here, the structured grid of the flow solver is interfaced with the unstructured grid of heat conduction solvers in a quasi-transient CHT solution tracing the re-entry vehicle trajectory. Issues in loosely coupled analysis of the elastic response of the solid structures perturbed by the external flowfields arising in aero-elastic problems can be found in Brown (1997) and Dowell and Hall (2001). In either case, the coupled field solution requires complete meshing of both fluid and solid regions while enforcing solid/fluid interface continuity of fluxes and temperatures, in the case of CHT analysis, or displacement and traction, in the case of aero-elasticity analysis.

A different approach was taken by Li and Kassab (1994a, b) and Ye *et al.* (1998), to develop a BEM-based CHT algorithm thereby avoiding meshing of the solid region for the conduction solution. The method couples the BEM to a FVM Navier-Stokes solver and was applied to solve the two-dimensional steady-state compressible subsonic CHT problems over the cooled and uncooled turbine blades. The conduction problem requires solution of the Laplace equation for the temperature (or the Kirchhoff transform in the case of temperature dependent conductivity), and, as such, only requires a boundary discretization thereby eliminating the onerous task of grid generation within the intricate regions of the solid. The boundary discretization utilized to generate the computational grid for the external flow-field can be considerably coarsened to provide the boundary discretization required for the BEM. Most modern grid generators used in the computational fluid dynamics, for instance, GridPro™ (Program Development Corporation, 1997), the topology-based

---

algebraic grid generator used in the examples presented in this paper, allow the multigrid option. Several levels of coarse discretization can thus be readily obtained. Furthermore, the BEM/FVM methods offer the additional advantage of providing heat flux values and this stems from the fact that nodal unknowns which appear in the BEM are the surface temperatures and heat fluxes. Consequently, solid/fluid interfacial heat fluxes that are required to enforce continuity in the CHT problems are naturally provided by the BEM conduction analysis. This is in sharp contrast to the domain meshing methods, such as FVM and FEM where heat fluxes are computed by the numerical differentiation in a post-processing stage. He *et al.* (1995a, b) adopted the BEM/FVM approach in the further studies of CHT in incompressible flow in ducts subjected to a constant wall temperature and constant heat flux boundary conditions. Kontinos (1997) also adopted the BEM/FVM coupling algorithm to solve the CHT over metallic thermal protection panels at the leading edge of the X-33 in a Mach 15 hypersonic flow regime. Rahaim *et al.* (1997, 2000) adopted a BEM/FVM strategy to solve the time-accurate CHT problems for supersonic compressible flow over a 2D wedged, and they present experimental validation of this CHT solver. In their studies, the dual reciprocity BEM (Partridge *et al.*, 1992) was used for transient heat conduction, while a cell-centered FVM was chosen to resolve the compressible turbulent Navier-Stokes equations.

In this paper, we report on the progress in the development and application of a BEM-based temperature forward/flux back (TFFB) coupling algorithm developed to solve the CHT arising in the 3D film-cooled turbine blades. The NASA-Glenn turbomachinery Navier-Stokes code Glenn-HT is coupled to a 3D BEM steady-state heat conduction solver. The steady-state solution is sought by marching in time until dependent variables reach their steady-state values, and, as such, intermediate temporal solutions are not physically meaningful. In this mode of solving the steady-state problem, time-marching can be viewed as a relaxation scheme, and local time-stepping and implicit residual smoothing are used to accelerate convergence. The steady heat conduction equation reduces to the Laplace equation, and it is solved using the BEM with isoparametric bilinear discontinuous elements. We chose to employ discontinuous elements as they provide high levels of accuracy in computed heat flux values especially at sharp corner regions where first kind boundary conditions are imposed without resorting to special treatment of corner points required by continuous elements in particular, when first kind boundary conditions are imposed (Kane, 1994; Kassab and Nordlund, 1994). In this application, sharp corners occur in many locations and first kind boundary conditions are imposed on all metal surfaces. Moreover, the use of discontinuous elements throughout the BEM model eliminates much of the overhead associated with continuous elements, in particular, there is no need to generate, store, or access a connectivity matrix when using the discontinuous elements.

In order to resolve the flow physics, the CFD grid must be clustered in many regions. The BEM grid does not require such fine clustering and consequently, the two grids are of quite different coarsenesses. The details of the interpolation used to exchange nodal temperature and flux information from the disparate CFD and BEM grids are presented. Results from a CHT numerical simulation of a 3D film-cooled blade section are presented and results are compared with those obtained from the standard approach of a two-temperature model. Significant difference in the level and distribution of the metal temperature is found between the two-temperature and CHT models. Finally, in order to address the large number of unknowns appearing in the 3D BEM model, current developments of a strategy of artificial subsectioning of the blade are presented. Here, the approach is to subsection the blade in the spanwise direction. A specially tailored iterative scheme is developed to solve the conduction problem with each subsection BEM problem solved using a direct LU solver. A physically based initial guess is used to provide a good starting point for the iterative algorithm. Results from the 2D and 3D simulations show the process converging efficiently and offers a substantial computational and storage savings.

## 2. Governing equations

We first present the governing equations for the coupled field problem under consideration. The CHT problems arising in turbomachinery involves external flow-fields that are generally compressible and turbulent, and these are governed by the compressible Navier-Stokes equations supplemented by a turbulence model. Heat transfer within the blade is governed by the heat conduction equation. Linear as well as non-linear options are considered. However, fluid flows within the internal structures to the blade, such as film cooling holes and channels, are usually of low-speed and are incompressible. Consequently, density-based compressible codes tend to experience numerical difficulties in modeling such flows, unless low Mach number pre-conditioning is implemented (Turkel, 1987, 1993). The Glenn-HT code is specialized to turbomachinery applications for which air is the working fluid and is modelled as an ideal gas.

### 2.1 Governing equations for the flow-field

The governing equations for the flow-field are the compressible Navier-Stokes equations, which describe the conservation of mass, momentum and energy. These can be written in integral form as

$$\int_{\Omega} \frac{\partial \mathcal{W}}{\partial t} d\Omega + \int_{\Gamma} (\mathcal{F} - \mathcal{T}) \cdot \hat{n} d\Gamma = \int_{\Omega} \mathcal{S} d\Omega \quad (1)$$

where  $\Omega$  denotes the volume,  $\Gamma$  denotes the surface bounded by the volume  $\Omega$ , and  $\hat{n}$  is the outward-drawn normal. The conserved variables are contained in the vector  $\underline{W} = (\rho, \rho u, \rho v, \rho w, \rho e, \rho k, \rho \omega)$ , where,  $\rho, u, v, w, e, k, \omega$  are the density, the velocity components in  $x, y,$  and  $z$ -directions, and the specific total energy. The kinetic energy of turbulent fluctuations is denoted by  $k$  and the specific dissipation rate is denoted by  $\omega$  and both appear in the two equation – Wilcox turbulence model (Wilcox, 1993, 1994) with modifications by Menter (1993) and Chima (1996) as implemented in Glenn-HT. The vectors  $\underline{F}$  and  $\underline{T}$  are convective and diffusive fluxes, respectively,  $\underline{S}$  is a vector containing all terms arising from the use of a non-inertial reference frame as well as in the production and dissipation of turbulent quantities. The working fluid is air, and it is modeled as an ideal gas. A rotating frame of reference can be adopted for the modeling of rotating flows. The effective viscosity is given by

$$\mu = \mu_l + \mu_t \tag{2}$$

where  $\mu_t = \rho k / \omega$ . The thermal conductivity of the fluid is then computed by a Prandtl number analogy where

$$k_f = \frac{\gamma}{\gamma - 1} \left[ \frac{\mu_l}{Pr_l} + \frac{\mu_t}{Pr_t} \right] \tag{3}$$

where  $Pr$  is the Prandtl number and  $\gamma$  is the specific heat ratio. The subscripts  $l$  and  $t$  refer to laminar and turbulent values, respectively.

### 2.2 The governing equations of the heat conduction field

In the steady-state CHT solutions obtained in this paper, the NS equations are solved to steady-state by a time marching scheme converging towards steady-state. A steady heat conduction analysis is carried out using the BEM at each time level chosen for the external flow-field and internal conduction field to interact in the iterative process. As such, the governing equation under consideration is

$$\nabla \cdot [k(T_s) \nabla T_s] = 0 \tag{4}$$

where  $T_s$  denotes the temperature of the solid, and  $k_s$  is the thermal conductivity of the solid material. If the thermal conductivity is taken as constant, then the above equation reduces to the Laplace equation for the temperature. When the thermal conductivity variation with temperature is an important concern, the nonlinearity in the steady-state heat conduction equation can readily be removed by introducing the classical Kirchoff transform,  $U(T)$  (Azevedo and Wrobel, 1988; Bialecki and Nhalik, 1989; Kassab and Wrobel, 2000), which is defined as

$$U(T) = \frac{1}{k_0} \int_{T_0}^T k_s(T) dT \tag{5}$$

where  $T_o$  is the reference temperature and  $k_o$  is the reference thermal conductivity. The transform and its inverse are readily evaluated, either analytically or numerically, and the heat conduction equation transforms to a Laplace equation for the transform parameter  $U(T)$ . The heat conduction equation thus reduces to the Laplace equation in any case, and this equation is readily solved by the BEM.

In the conjugate problem, continuity of temperature and heat flux at the blade surface,  $\Gamma$ , must be satisfied:

$$\begin{aligned} T_f &= T_s \\ k_f \frac{\partial T_f}{\partial n} &= -k_s \frac{\partial T_s}{\partial n} \end{aligned} \quad (6)$$

Here,  $T_f$  is the temperature computed from the N-S solution,  $T_s$  is the temperature within the solid which is computed from the BEM solution, and  $\partial/\partial n$  denotes the normal derivative. Both first kind and second kind boundary conditions transform linearly in the case of temperature-dependent conductivity. In such a case, the fluid temperature is used to evaluate the Kirchhoff transform and this used a boundary condition of the first kind for the BEM conduction solution in the solid. Subsequently, the computed heat flux, in terms of  $U$ , is scaled to provide the heat flux which is in turn used as an input boundary condition for the flow-field.

### 3. Field solver solution algorithms

A brief description of the Glenn-HT code is given in this section. Details of the code and its verification in turbomachinery application can be found in Ameri *et al.* (1997), Heidmann *et al.* (2002), Rigby *et al.* (1997), Steinhthorsson *et al.* (n.d., 1993). The heat conduction equation is solved using the BEM.

#### 3.1 Navier-Stokes solver

Glenn-HT uses a cell-centered FVM to discretize the NS equations. Equation (1), is integrated over a hexahedral computational cell with the nodal unknowns located at the cell center  $(i, j, k)$ . The convective flux vector is discretized by a central difference supplemented by artificial dissipation as described in Jameson *et al.* (1981). The artificial dissipation is a blend of first and third order differences with the third order term active everywhere except at shocks and locations of strong pressure gradients. The viscous terms are evaluated using central differences. The overall accuracy of the code is second order (Heidmann *et al.*, 2002). The resulting finite volume equations can be written at every computational node as

$$V_{i,j,k} \frac{d\bar{w}_{i,j,k}}{dt} + \underline{q}_{i,j,k} - \underline{q}_{i,j,k} = \underline{s}_{i,j,k} \quad (7)$$

where  $\bar{W}_{i,j,k}$  is the cell-volume averaged vector of conserved variables,  $q_{i,j,k}$  and  $\bar{d}_{i,j,k}$  are the net flux and dissipation for the finite volume obtained by the surface integration of equation (1), and  $\bar{s}_{i,j,k}$  is the net finite source term. The above is solved using a time marching scheme based on a fourth order explicit Runge-Kutta time-stepping algorithm. The steady-state solution is sought by marching in time until the dependent variables reach their steady-state values, and, as such, intermediate temporal solutions are not physically meaningful. In this mode of solving the steady-state problem, time-marching can be viewed as a relaxation scheme, and local time-stepping and implicit residual smoothing are used to accelerate convergence. A multigrid option is available in the code. The code also adopts a multi-block strategy to model complex geometries associated with the film-cooled blade problems. Here, locally structured grid blocks are generated into a globally unstructured assembly.

Glenn-HT adopts a  $k-\omega$  turbulence model, which integrates to the wall and does not require maintaining a specified distance from the wall, as no wall functions are used. The computational grid is sufficiently fine near the wall to yield a  $y^+$  value of less than 1.0 at the first grid point away from the wall. A constant value of 0.9 is taken for the turbulent Prandtl number in all heat transfer computations, while a constant value of 0.72 is used for the laminar Prandtl number. Moreover, the temperature variation of the laminar viscosity is taken as a 0.7 power law (Schlichting, 1979), and  $c_p$  is taken as constant.

### 3.2 Heat conduction boundary element solution

The heat conduction equation reduces to the same governing Laplace equation in the temperature or the Kirchhoff transform. In the boundary element method, this governing partial differential equation is converted into a boundary integral equation (BIE) (Banerjee, 1994; Brebbia and Dominguez, 1989; Brebbia *et al.*, 1984), as

$$C(\xi)T(\xi) + \oint_S T(x)q^*(x, \xi) dS(x) = \oint_S q(x)T^*(x, \xi) dS(x) \quad (8)$$

where  $S(x)$  is the surface bounding the domain of interest,  $\xi$  is the source point,  $x$  is the field point,  $q(x) = -k \partial T / \partial n$  is the heat flux,  $T^*(x, \xi)$  is the so-called fundamental solution, and  $q^*(x, \xi)$  is its normal derivative with  $\partial / \partial n$  denoting the normal derivative with respect to the outward-drawn normal. The fundamental solution (or Green free space solution) is the response of the adjoint governing differential operator at any field point  $x$  due to perturbation of a Dirac delta function acting at the source point  $\xi$ . In our case, since the steady-state heat conduction equation is self-adjoint, we have

$$k \nabla^2 T^*(x, \xi) = -\delta(x, \xi) \quad (9)$$

Solution to this equation can be found by several means, see for instance Kellogg (1953), Liggett and Liu (1983) and Morse and Feshbach (1953), as

$$T^*(x, \xi) = \frac{1}{4\pi kr(x, \xi)} \quad \text{in 3D} \quad (10)$$

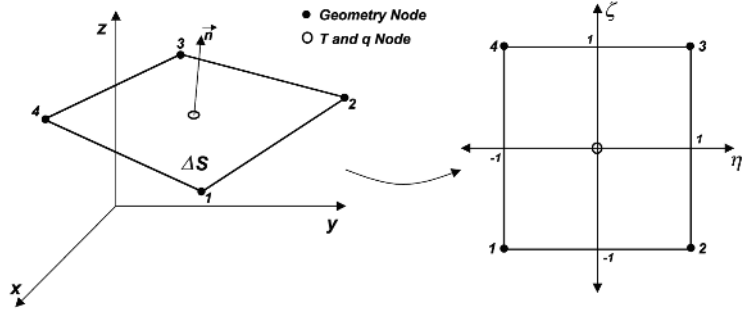
where  $r(x, \xi)$  is the Euclidean distance from the source point  $\xi$ . The free term  $C(\xi)$  can be shown analytically to be:

$$C(\xi) = \oint_{S(x)} -k \left[ \frac{\partial T^*(x, \xi)}{\partial n} \right] dS(x).$$

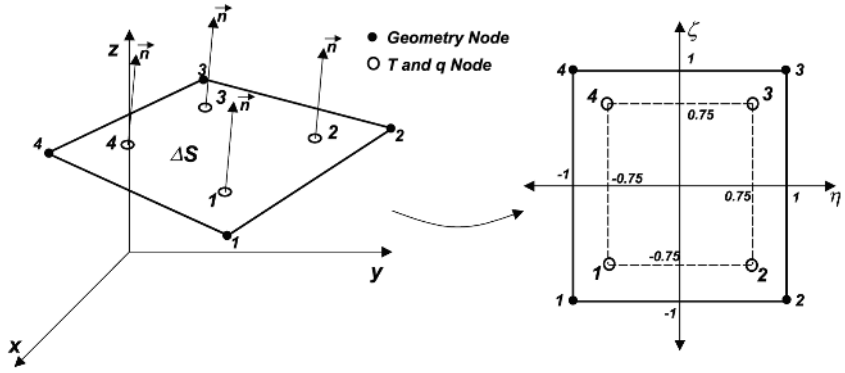
Moreover, introducing the definition of the fundamental solution in the above equation, it can be readily determined that, in 3D,  $C(\xi)$  is the internal angle (in steradians) subtended at source point divided by  $4\pi$  when the source point  $\xi$  is on the boundary and takes on a value of one when the source point  $\xi$  is at the interior.

In the standard BEM, the BIE is discretized using two levels of discretization: Firstly, the surface  $S$  is discretized into a series of  $j = 1, 2, \dots, N$  elements  $\Delta S_j$ , traditionally accomplished using polynomial interpolation, bilinear and biquadratic being the most common, and secondly, the distribution of the temperature and heat flux is modeled on the surface, and this is usually accomplished using the polynomial interpolation as well. It is noted that the order of discretization of the temperature and heat flux need not be same as that used for the geometry, leading to subparametric (lower order than that used for the geometry), isoparametric (same order than that used for the geometry), and superparametric (higher order than that used for the geometry) discretizations. Moreover, the temperature and heat flux are discretized using  $k = 1, 2, \dots, NPE$  number of nodal points per element whose location within the element  $j$  can be chosen to coincide with the location of the geometric nodes leading to continuous elements or to be located offset from the geometric nodes leading to discontinuous elements. We chose to employ the bilinear discontinuous isoparametric elements as they provide high levels of accuracy in computed heat flux values, especially at sharp corner regions where first kind boundary conditions are imposed without resorting to special treatment of corner points required by continuous elements (Kane, 1994; Kassab and Nordlund, 1994). In this type of boundary element, the field variables  $T$  and  $q$  are modeled with discontinuous bilinear shape functions across each element, while the geometry is represented locally as continuous bilinear surfaces. We also employed constant elements for the coarse grid solution as will be discussed later (Figure 2).

The discretized BIE is collocated at each of the boundary nodes  $\xi_i$  and there results



(a) Constant element used for coarse grid



(b) Discontinuous bi-linear element used in fine grid

**Figure 2.**  
Constant and bilinear  
isoparametric  
discontinuous boundary  
elements used in analysis

$$C(\xi_i)T(\xi_i) + \sum_{j=1}^N \sum_{k=1}^{NPE} H_{ij}^k T_j^k = \sum_{j=1}^N \sum_{k=1}^{NPE} G_{ij}^k q_j^k \quad (11)$$

where

$$H_{ij}^k = \oint_{\Delta S_j} q^*(x, \xi_i) M^k(\eta, \zeta) dS(x)$$

and

$$G_{ij}^k = \oint_{\Delta S_j} T^*(x, \xi_i) M^k(\eta, \zeta) dS(x)$$

are evaluated numerically via Gauss-Legendre quadratures with special adaption when evaluating the integrals on  $\Delta S_i$  and heuristic adaptive

quadratures for elements that are close to the node of interest, and  $M^k(\eta, \zeta)$  are the discontinuous shape functions used to model  $T$  and  $q$ , whose nodes located at an off-set position of 12.5 percent from the edges of the element. Upon assembly of the collocated BIEs, the following algebraic form is obtained:

$$[H]\{T_s\} = [G]\{q_s\} \quad (12)$$

Here the influence matrices  $[H]$  and  $[G]$  are evaluated numerically using quadratures. Once the boundary conditions are specified, the above is re-arranged in the standard form  $[A]\{x\} = \{b\}$ , and the ensuing equations are solved by direct or iterative methods. In a fully conjugate solution using the algorithm described in this paper, these BEM equations are solved subject to the following boundary condition at external and internal bounding walls, which are in contact with the fluid and denoted by  $\Gamma_{\text{conjugate}}$ :

$$T_s|_{\Gamma_{\text{conjugate}}} = T_f \quad (13)$$

In the reduced periodic 3D computational model to be discussed in the example section, adiabatic conditions are also imposed at the flowfield periodic surfaces in the spanwise direction, i.e. there

$$q_s = 0 \quad (14)$$

Once these equations are solved, the heat flux is known at all surface nodes. This is the sought-after quantity in the CHT algorithm to be shortly outlined. In the case, where the conduction problem is solved without further treatment, the basic BEM code had options of using an LU decomposition for small numbers of equations and a GMRES iterative solver with an incomplete LU (ILU) pre-conditioning for large numbers of equations. When the number of equations gets very large, storage becomes an important issue, as the coefficient matrix is fully-populated. We will discuss an effective treatment of such problems in a later section.

### 3.3 CHT algorithm

The Navier-Stokes equations for the external fluid flow and the heat conduction equation for heat conduction within the solid are interactively solved to steady-state through a time-marching algorithm. The surface temperature obtained from the solution of the Navier-Stokes equations is used as the boundary condition of the BEM for the calculation of heat flux through the solid surface. This heat flux is in turn used as a boundary condition for the Navier-Stokes equations in the next time-step. This procedure is repeated until a steady-state solution is obtained. In practice, the BEM is solved at every few cycles of the FVM to update the boundary conditions, as intermediate solutions are not physical in this scheme. In the calculations carried out in this study,

BEM solution was run for every ten cycles of the finite volume solver. This is referred to as the TFFB coupling algorithm as outlined below:

- (1) FVM Navier-Stokes solver:
  - begins with initial adiabatic boundary condition at solid surface;
  - solves compressible NS for fluid region;
  - provides temperature distribution to the BEM conduction solver after a number of iterations;
  - receives flux boundary condition from the BEM as input for next set of iterations.
- (2) BEM conduction solver:
  - receives temperature distribution from the FVM solver;
  - solves steady-state conduction problem;
  - provides flux distribution to the FVM solver.

The transfer of heat flux from the BEM to the FVM solver is accomplished as

$$q = \beta q_{\text{old}}^{\text{BEM}} + (1 - \beta) q_{\text{new}}^{\text{BEM}} \quad (15)$$

with an under-relaxation is used setting the parameter  $\beta$  as 0.2 in all reported calculations. The choice of the relaxation parameter is through trial and error. In certain cases, it has been our experience that a choice of larger relaxation parameter can lead to nonconvergent solutions (Bialecki *et al.*, 2001). The process is continued until the NS solver converges and wall temperatures and heat fluxes converge, i.e. until equation (6) is satisfied within a set tolerance

$$\begin{aligned} \|\tilde{T}_f - \tilde{T}_s\| &< \varepsilon_T \\ \|\tilde{q}_f - \tilde{q}_s\| &< \varepsilon_q \end{aligned} \quad (16)$$

where the tolerances  $\varepsilon_T$  and  $\varepsilon_q$  are taken as 0.001.

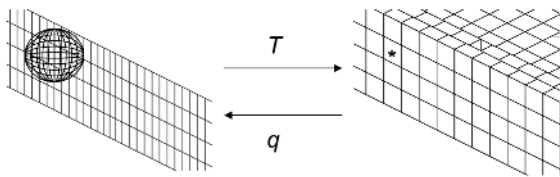
It should be noted that alternatively the flux could be specified as a boundary condition for the BEM code leading to a flux forward temperature back (FTTB) approach. However, when a fully conjugate solution is undertaken, this would amount to specify second kind boundary conditions completely around the surface of a domain governed by an elliptic equation, resulting in a nonunique solution. The TFFB algorithm avoids such a situation.

### 3.4 Interpolation between BEM and FVM grids

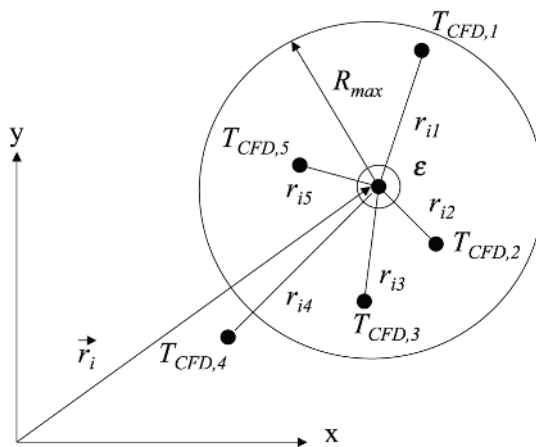
An issue arises in information transfer between the CFD and the BEM as there exists a significant difference in the levels of discretization between the two meshes in a typical CHT simulation. Accurate resolution of the boundary layer requires a FVM surface grid, which is much too fine to be used directly in the

BEM. A much coarser surface grid is typically generated for the BEM solution of the conduction problem. The disparity between the two grids requires a general interpolation of the surface temperature and heat flux between the two solvers as it is not possible in general to isolate a single BEM node and identify a set of nearest FVM nodes. Indeed in certain regions where the CFD mesh is very fine, a BEM node can readily be surrounded by ten or more FVM nodes.

A distance-weighted interpolation, reminiscent of radial basis function (RBF) interpolation (Partridge *et al.*, 1992), is adopted for the transfer of temperature and flux values between the BEM and the CFD grids. Consider Figure 3(a), where the location of a BEM node is identified on the right-hand side by a star-like symbol. Let us consider the problem of transferring the temperature from the FVM grid to the BEM grid. Let us denote the position of the BEM node of interest by  $\vec{r}_i$ , and the location of an FVM node by  $\vec{r}_j$ . The radial distance from every FVM node to the BEM node of interest is then  $r_{ij} = |\vec{r}_j - \vec{r}_i|$ . Let us suppose that the number of all FVM surface nodes lying within a ball of radius  $R_{max}$  centered about  $\vec{r}_i$  is  $N_{ball}$ . Moreover, let us denote two cases. In case I, all  $r_{ij} > \epsilon$  and in case II, there is an FVM node located at  $\vec{r}_{j,\epsilon}$



(a) Transfer of nodal temperatures and fluxes between CFD and BEM grids



(b) 2-D illustration of five CFD nodes nearest to a BEM node located at  $\vec{r}_i$

**Figure 3.**  
Transfer of nodal values  
from FVM and BEM  
(and back) independent  
surface meshes is  
performed with a  
distance weighted radial  
interpolation

such that  $r_{ij} \leq \varepsilon$ , where  $\varepsilon$  is a tolerance. Then, the value of the temperature at the BEM node  $\vec{r}_j$  is evaluated as

$$T_{\text{BEM}}(\vec{r}_i) = \frac{\sum_{j=1}^{N_{\text{ball}}} \frac{T_{\text{CFD}}(\vec{r}_j)}{r_{ij}}}{\sum_{j=1}^{N_{\text{ball}}} \frac{1}{r_{ij}}} \quad \text{for case I} \tag{17}$$

$$= T_{\text{CFD}}(\vec{r}_{j,\varepsilon}) \quad \text{for case II}$$

In all calculations, the maximum radius  $R_{\text{max}}$  of the sphere is set to 2.5 percent of the maximum distance within the solid region and  $\varepsilon$  is set to  $R_{\text{max}} \times 10^{-20}$ . These limits may be adjusted to suit the problems at hand.

#### 4. A domain decomposition strategy for BEM models of large-scale three-dimensional heat conduction problems

As mentioned, the BEM is ideally suited for the solution of linear and non-linear heat conduction problems and is particularly a advantageous numerical method due to its boundary-only feature, however, the coefficient matrix of the resulting system of algebraic equations is fully populated. For large-scale 3D problems, this poses very serious numerical challenges due to its large storage requirements and iterative solution of large sets of non-sparse equations. This problem has been approached in the BEM community by one of the two approaches: one is the artificial subsectioning of the 3D model into a multi-region model in conjunction with block-solvers reminiscent of the FEM frontal solvers (Bialecki *et al.*, 1996; Kane *et al.*, 1990) and (2) the adoption of multipole methods in conjunction with the GMRES nonsymmetric iterative solver (Greengard and Strain, 1990; Hackbush and Nowak, 1989). The first approach of domain decomposition (or subsectioning) produces a sparse block coefficient matrix that is efficiently stored and has been successfully implemented in commercial codes such as BETTI and GPBEST in the context of continuous boundary elements. However, the method requires generation of complex data-structures identifying connecting regions and interfaces prior to analysis. The second approach is very efficient, however, it requires complete re-writing of the BEM code to adopt multipole formulation. Recently, a novel technique using wavelet decomposition has been proposed to reduce matrix storage requirements without a need for major alteration of traditional BEM codes (Bucher and Wrobel, 2000).

We propose to adopt the first approach, however, we do not use a block solver but rather a region-by-region iterative solver. Although, it was reported in the literature that this process sometimes has difficulty in converging the non-linear problems (Chima, 1996; Azevedo and Wrobel, 1988), it is shown that

the process converges very efficiently in the linear case and can offer very substantial savings in memory. Moreover, the technique does not require any complex data-structure preparation. Indeed, the approach is somewhat transparent to the user, a significant advantage in coupling the BEM to other field solvers. It should be noted that this subsectioning method is under current development and has not yet been integrated into the CHT solver at the point of writing this paper, and thus the technique along with an example of 3D conduction solution is presented herein with this explicit caveat.

In the standard BEM, if  $N$  is the number of boundary nodes used to discretize the problem, the number of floating point operations (FLOPS) required to arrive at the algebraic system is proportional to  $N^2$  as well as direct memory allocation also is proportional to  $N^2$ . Enforcing imposed boundary conditions, yields

$$[H]\{T\} = [G]\{q\} \Rightarrow [A]\{x\} = \{b\} \quad (18)$$

where  $\{x\}$  contains nodal unknowns  $T$  or  $q$ , whichever is not specified in the boundary conditions. The solution of the algebraic system for the boundary unknowns can be performed using a direct solution method such as LU decomposition, requiring proportional to  $N^3$  FLOPS or iterative methods such as bi-conjugate gradient or general minimization of residuals that, in general, require FLOPS proportional to  $N^2$  to achieve convergence. In 3D problems of any appreciable size this approach is computationally prohibitive and leads to enormous memory demands.

If a domain decomposition solution process is adopted instead, the domain is decomposed into  $K$  subdomains and each one is independently discretized and solved by the standard BEM while enforcing continuity of temperature and heat flux at the interfaces. It is worth mentioning that discretization of neighboring subdomains does not have to be coincident, this is, at the connecting interface, boundary elements and nodes from the two adjoining sub-domains are not required to be structured following a sequence or particular position. The only requirement at the connecting interface is that it forms a closed boundary with the same path on both sides. The information between the neighboring sub-domains separated by an interface can be passed through an interpolation.

The process is shown in two-dimension in Figure 4, with a decomposition four ( $K = 4$ ) subdomains. The boundary value problem is solved independently over each subdomain where initially, a guessed boundary condition is imposed over the interfaces in order to ensure the well-posedness of each subproblem. The problem in subdomain  $\Omega_1$  is transformed into

$$\nabla^2 T_{\Omega_1}(x, y) = 0 \Rightarrow [H_{\Omega_1}]\{T_{\Omega_1}\} = [G_{\Omega_1}]\{q_{\Omega_1}\} \quad (19)$$

The composition of this algebraic system requires  $(n^2)$  FLOPS where  $n$  is the number of boundary nodes in the subdomain as well as  $(n^2)$  for direct memory

allocation. This new proportionality number  $n$  is roughly equivalent to  $n \approx 2N/K + 1$ , as long as the discretization along the interfaces has the same level of resolution as the discretization along the boundaries. Direct memory allocation requirement for later algebraic manipulation is now reduced to a proportion of  $n^2$  as the influence coefficient matrices can easily be stored in ROM memory for later use after the boundary value problems on remaining subdomains have been effectively solved. For the example shown here, where the number of subdomains is  $K = 4$ , the new proportionality value  $n$  is approximately equal to  $n \approx 2N/5$ . This simple multi-region example reduces the memory requirements to about  $n^2/N^2 = (4/25) = 16$  percent of the standard BEM approach.

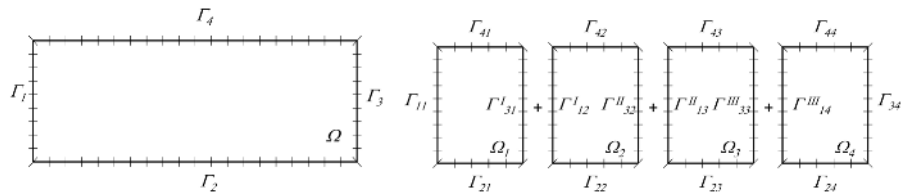
The algebraic system for subdomain  $\Omega_1$  is re-arranged, with the aid of given and guessed boundary conditions, as:

$$[H_{\Omega_1}]\{T_{\Omega_1}\} = [G_{\Omega_1}]\{q_{\Omega_1}\} \Rightarrow [A_{\Omega_1}]\{x_{\Omega_1}\} = \{b_{\Omega_1}\} \quad (20)$$

Now, the solution of the new algebraic system of subdomain  $\Omega_1$  requires a number FLOPS proportional to  $n^3/N^3 = (8/125) = 6.4$  percent of the standard BEM approach if a direct algebraic solution method is employed, or a number of FLOPS proportional to  $n^2/N^2 = (4/25) = 16$  percent of the standard BEM approach if an indirect algebraic solution method is employed. For both, FLOPS count and direct memory requirement, the reduction is dramatic. However, as the first set of solutions for the subdomains were obtained using guessed boundary conditions along the interfaces, the global solution needs to follow an iteration process and satisfy a convergence criteria.

Globally, the FLOPS count for the formation of the algebraic setup for all  $K$  subdomains must be multiplied by  $K$ , therefore, the total operation count for the coefficient matrices computation is given by:  $Kn^2/N^2 \approx 4K/(K + 1)^2$ . For this particular case with  $K = 4$ ,  $Kn^2/N^2 = 16/25 = 64$  percent of the standard BEM approach. Moreover, the more significant reduction is revealed in the RAM memory requirements as only the memory needs for one of the subdomains must be allocated at a time. The rest of the coefficient matrices for the remaining subdomains can be temporarily stored in ROM memory until access and manipulation is required or if a parallel strategy is adopted the matrices for each subdomain are stored by its assigned processor. Therefore, for this case of  $K = 4$ , the true memory reduction is  $n^2/N^2 = 4/25 = 16$  percent of the standard BEM.

**Figure 4.**  
BEM single region  
discretization and four  
domain BEM  
decomposition



With respect to the algebraic solution of the system of equation (20), if a direct approach as the LU factorization is employed for all subdomains, the LU factors of the coefficient matrices for all subdomains can be computed only once at the first iteration step and stored in ROM memory, or on disc, for later use during the iteration process for which only a forward and a backward substitution will be required. This feature allows a significant reduction in the operational count through the iteration process until convergence is achieved, as only a number of floating point operations proportional to  $n$  as opposed to  $n^3$  is required at each iteration step. To this computation time the access to ROM memory is added at each iteration step, which is usually larger than access to RAM. Alternatively, if the overall convergence of the problem requires few iterations, iterative solvers such as GMRES offer an efficient alternative.

Providing a good initial guess is crucial to the success of any iteration. To this end, first we typically solve the problem using a coarse grid constant model (Figure 2) obtained by collapsing the nodes of the discontinuous bilinear element to the centroid, and supply that model with a physically-based initial guess for interface temperatures. An efficient initial guess can be made using a physically based 1D heat conduction argument for every node on the external surfaces to every node at the interface. The initial guess for any interfacial node is provided algebraically as:

$$T_i = \frac{\sum_{j=1}^{N_T} B_{ij} T_j - \sum_{j=1}^{N_q} B_{ij} R_{ij} q_j + \sum_{j=1}^{N_h} \frac{B_{ij} H_{ij} T_{\infty j}}{H_{ij} + 1}}{S_i - \sum_{j=1}^{N_T} B_{ij} + \sum_{j=1}^{N_h} \frac{B_{ij} H_{ij}}{H_{ij} + 1}} \quad (21)$$

where  $N_T$ ,  $N_q$ , and  $N_h$  are the number of first, second, and third kind boundary conditions specified at the external (non-interfacial) surfaces and

$$B_{ij} = \frac{A_j}{|r_{ij}|}, \quad R_{ij} = \frac{\vec{r}_{ij} \cdot \hat{n}_j}{k}, \quad H_{ij} = \frac{h_j}{k} (\vec{r}_{ij} \cdot \hat{n}_j), \quad S_i = \sum_{j=1}^N \frac{A_j}{|r_{ij}|} \quad (22)$$

with  $N = N_T + N_q + N_h$ , the thermal conductivity of the medium is  $k$ , the film coefficient at the  $j$ -th convective surface is  $h_j$ , the outward-drawn normal to any surface is  $\hat{n}_j$ , the position vector from the interfacial node  $i$  to the external surface node  $j$  is  $\vec{r}_{ij}$  and its magnitude is  $r_{ij} = |\vec{r}_{ij}|$ , while the area of element  $j$  denoted is readily computed as:

$$A_j = \oint_{\Gamma_j} d\Gamma(x, y, z) = \int_{-1}^{+1} \int_{-1}^{+1} |J_j(\eta, \zeta)| d\eta d\zeta.$$

Once the initial temperatures are imposed as boundary conditions at the interfaces, a resulting set of normal heat fluxes along the interfaces will be computed. These are then non-symmetrically averaged in an effort to match the heat flux from neighboring subdomains. Considering a two-domain substructure, the non-symmetric averaging at the interface is explicitly given as,

$$q_{\Omega_1}^I = q_{\Omega_1}^I - \frac{q_{\Omega_1}^I + q_{\Omega_2}^I}{2} \quad \text{and} \quad q_{\Omega_2}^I = q_{\Omega_2}^I - \frac{q_{\Omega_2}^I + q_{\Omega_1}^I}{2} \quad (23)$$

to ensure the flux continuity condition  $q_{\Omega_1}^I = -q_{\Omega_2}^I$  after averaging. Compactly supported radial basis interpolation can be employed for the flux average to account for the unstructured grids along the interface from neighboring subdomains.

Using these fluxes, the BEM equations are again solved leading to mismatched temperatures along the interfaces for neighboring subdomains. These temperatures are interpolated, if necessary, from one side of the interface to the other side using a compactly supported radial basis functions to account for the possibility of interface mismatch between the adjoining substructure grids. Once this is accomplished, the temperature is averaged out at each interface. Illustrating this for a two-domain substructure, again we have for regions 1 and 2 interfaces,

$$T_{\Omega_1}^I = \frac{T_{\Omega_1}^I + T_{\Omega_2}^I}{2} + R'' q_{\Omega_1}^I \quad \text{and} \quad T_{\Omega_2}^I = \frac{T_{\Omega_1}^I + T_{\Omega_2}^I}{2} + R'' q_{\Omega_2}^I \quad (24)$$

in general, to account for a case where a physical interface exists and a thermal contact resistance is present between the connecting subdomains, where  $R''$  is the thermal contact resistance imposing a jump on the interface temperature values. These now matched temperatures along the interfaces are used as the next set of boundary conditions.

The iteration process is continued until a convergence criterion is satisfied. A measure of convergence may be defined as the  $L_2$  norm of mismatched temperatures along all interfaces as:

$$L_2 = \sqrt{\frac{1}{K \cdot N^I} \sum_{k=1}^K \sum_{i=1}^{N^I} (T^I - T_u^I)^2} \quad (25)$$

This norm measures the standard deviation of BEM computed interface temperatures  $T^I$  and averaged-out updated interface temperatures  $T_u^I$ . The iteration routine can be stopped once this standard deviation reaches a small fraction  $\varepsilon$  of  $\Delta T_{\max}$ , where  $\Delta T_{\max}$  is the maximum temperature span of the global field. It is noted, that we refer to an iteration as the process by which an iterative sweep is carried out to update both the interfacial fluxes and

---

temperatures such that the above norm may be computed. We set  $\varepsilon = 5 \times 10^{-3}$  in our computations.

## 5. Numerical results and discussion

We now present results of a full conjugate solution of a film-cooled blade under operating conditions, which match a planned experiment at NASA Glenn Research center and assumes periodicity in the spanwise direction for one pitch of film-cooling hole patterns. We compare results of this simulation to those obtained from the standard two temperature method. This simulation uses the standard BEM approach to heat conduction. We also present results from a heat conduction simulation for a cooled turbine vane using the subsectioning method described in this paper.

### 5.1 CHT simulation of a 3D film-cooled turbine blade

Film cooling is commonly used in turbine designs to produce a buffer layer of relatively cool air between the turbine blade and the hot freestream gas in the first and second rows of blades and vanes. The CHT computation is carried out on a computational model of a realistic film-cooled turbine vane according to the three-dimensional vane geometry including plena and film holes and is based on a Honeywell film-cooled engine design, (Heidmann *et al.*, 2002). The geometry of this test vane is based on the engine vane midspan coordinates, and is scaled up by a factor of 2.943 to allow matching of engine exit Mach number (0.876) and exit Reynolds number ( $2.9 \times 10^6$  based on true chord) with atmospheric inlet conditions. The test vane has a true chord of 0.206 m. Since the test vane is of constant cross-section, only one spanwise pitch of the film hole pattern was discretized, with periodicity of the flow-field enforced at each end. This simplification assumes no effect of endwalls, but greatly reduces the number of grid points required to model the vane. However, the thermal boundary conditions enforced at these ends in the conduction analysis were adiabatic. The vane has two plena, which feed 12 rows of film cooling holes as well as trailing-edge ejection slots, (Figure 5). Trailing edge ejection is blocked in the computation as the planned experiment has no slot cooling. Detailed geometrical data for each row of film holes as well as hole distribution are provided in Heidmann *et al.* (2002). A multi-block grid approach is adopted to model this complex geometry and generated the FVM grid using the topology-based algebraic grid-generation program GridPro™ (Program Development Corporation, 1997) with the final grid consisting of 140 blocks and a total of  $1.2 \times 10^6$  finite volume computational cells. The FVM grid consists of 20 cells across both the inlet and outlet boundaries, 60 cells on the periodic boundary, over 200 cells around the vane, and 44 cells from the vane to the periodic boundary.

A blade-to-blade view of the FVM grid is shown in Figure 6. Figure 7 shows the FVM grid in the leading edge region of the vane.

HF  
13,5

600

---

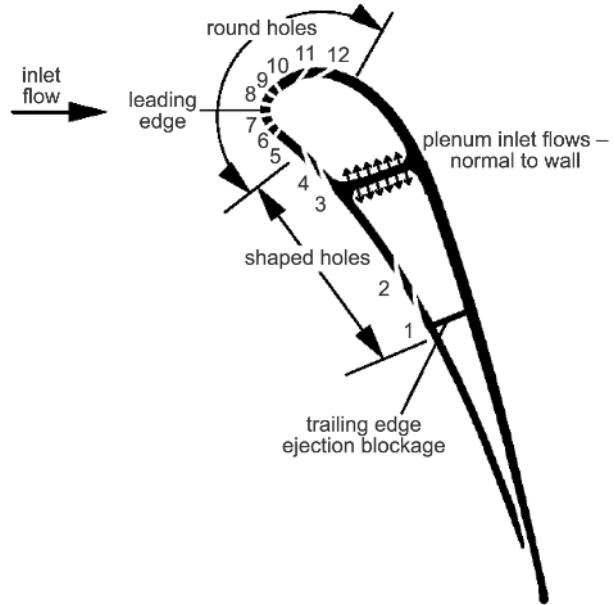


**Figure 5.**  
Film-cooled blade profile  
used in the CHT  
simulation

---

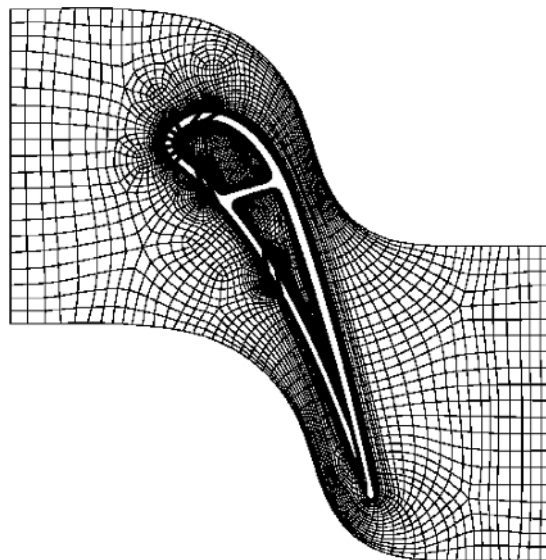


**Figure 6.**  
Blade-to-blade  
computational grid  
cross-section

---

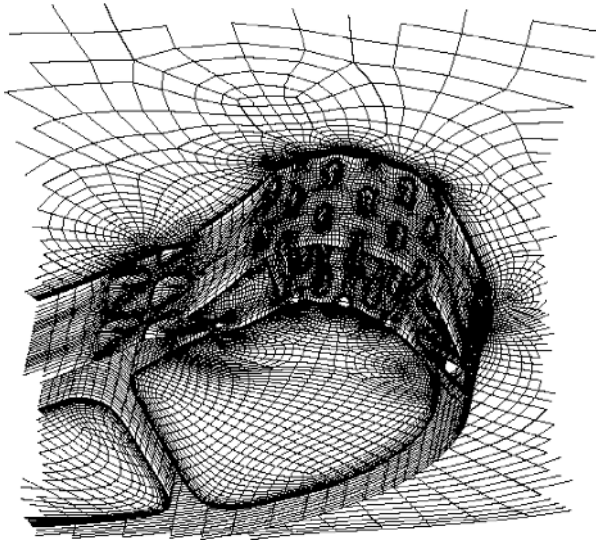


**Figure 7.**  
FVM grid in the leading  
edge region of the blade

---

The flow conditions for all simulations use a free-stream inlet flow to the vane at an angle of  $0^\circ$  to the axial direction, with all temperatures and pressures normalized by the inlet stagnation values of 3,109 R and 10 atmospheres, respectively. The inlet turbulence intensity is set at 8.0 percent and the turbulence scale is 15.0 percent of vane true chord. Other inflow quantities are set by means of the upstream-running Riemann invariant. The vane downstream exit flow is defined by imposing a constant normalized static pressure of 0.576, which was empirically determined to yield a desired exit Mach number of 0.876. Periodicity was enforced in both the blade-to-blade and spanwise directions based on vane and film hole pitches, respectively. Moreover, in order to maintain a true periodic solution, inflow to the plena was provided by defining a region of each plenum wall as an inlet and introducing uniform flow normal to the wall. In Figure 6, these regions are shown to lie on either side of the internal wall that separates the two plena. In practice, there will be spanwise flow in the plenum, but bleed of the plenum flow into the film holes results in a spanwise-varying mass flow rate and static pressure, which would violate spanwise periodicity imposed in this particular reduced computational model. The non-dimensionalized inflow stagnation temperature to the plena was 0.5, corresponding to a coolant temperature of 1554.5 R. The velocity was fixed to the constant value required to provide the design mass flow rate to each plenum, and static pressure was extrapolated from the interior. The inflow patch for each plenum was defined to be sufficiently large to yield very low inlet velocities (Mach number  $< 0.05$ ), allowing each plenum to approximate an ideal plenum. All solid walls were imposed with a no-slip

boundary condition. The blade metal material is taken as Inconel with a conductivity of  $k_{\text{blade}} = 1.34 \text{ Btu/h}$  in R taken at 2174.9 R which is estimated to be the average blade temperature.

The FVM metal surface grid consists of 38,000 cells at the 4th level of multi-grid. The grid was coarsened to generate a BEM grid of 13,000 bilinear cells with 52,000 nodal unknowns. Two cases are computed in the numerical simulation in order to obtain the metal temperature:

(1) The traditional two-temperature approach, whereby two different isothermal wall boundary conditions extended to all wall surfaces, including the film hole surfaces and plenum surfaces. Two solutions were generated with constant wall temperatures  $T_w$  of  $T_{w,1} = 2174.9 \text{ R}$  and  $T_{w,2} = 2485.6 \text{ R}$  imposed on all blade surfaces. The flow-field was computed from the plenum through the cooling holes and over the blade. The predicted wall heat fluxes at each node  $q_w''$  computed from each of these isothermal solutions were used to simultaneously solve adiabatic wall temperature,  $T_{aw}$ , and heat transfer coefficient,  $h$ , referenced to the computed adiabatic wall temperature, under the assumption that  $T_{aw}$  and  $h$  are independent of the wall temperature. That is at each node we have

$$\begin{aligned} q_w'' &= h(T_{w,1} - T_{aw}) \\ q_w'' &= h(T_{w,2} - T_{aw}) \end{aligned} \tag{26}$$

In turn, these film coefficient and associated adiabatic wall distributions were used in the BEM to compute metal temperatures.

(2) A full CHT solution was carried out using the same grids and boundary conditions as above except at the blade surface where conjugate conditions were imposed. The conjugate solutions converged in 1,000 iterations with a BEM conduction calculation performed each ten FVM iterations. The BEM code was written as a subroutine to the Glenn-HT code and subroutines were coded to exchange information between the two codes in terms of the FVM and BEM grids as well as boundary condition information. The Glenn-HT code was modified to allow non-isothermal boundary condition specification.

All computations were performed at NASA Glenn Research Center on an SGI Origin 2000 cluster with 32 processors. Flow computations were carried out and considered converged when residuals were driven below  $10^{-5}$ . Results of the blade surface temperatures predicted by the simulations are shown in Figure 8 for the CHT solution and in Figure 9 for the two constant temperature approaches. The two temperature distributions are markedly different with a temperature span of  $\Delta T = 1720 - 2420 \text{ R}$  across the surface of the blade while the CHT solution predicted a temperature span of  $\Delta T = 1620 - 2620 \text{ R}$  across the blade. In addition to CHT computations predicting lower minimum (100 R colder) and higher maximum temperatures (200 R hotter), the distribution of cold and hot regions are quite different as is evident from the surface plots.

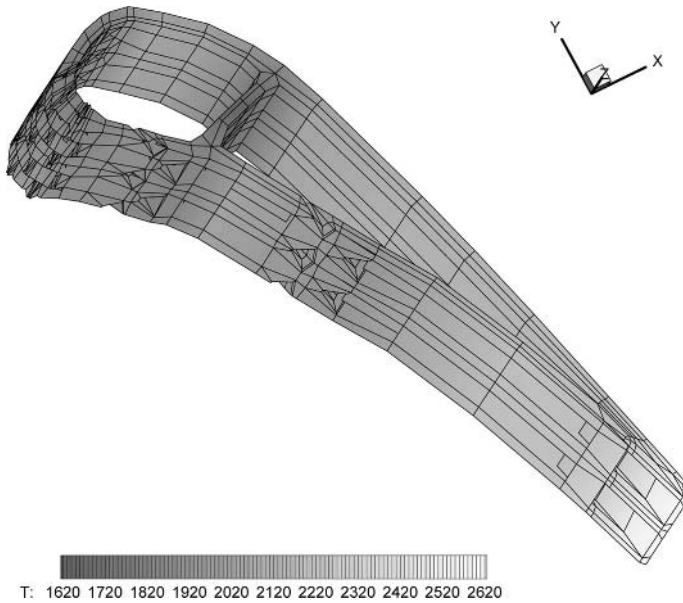


**Figure 8.**  
Blade surface  
temperature predicted by  
the CHT solution

---

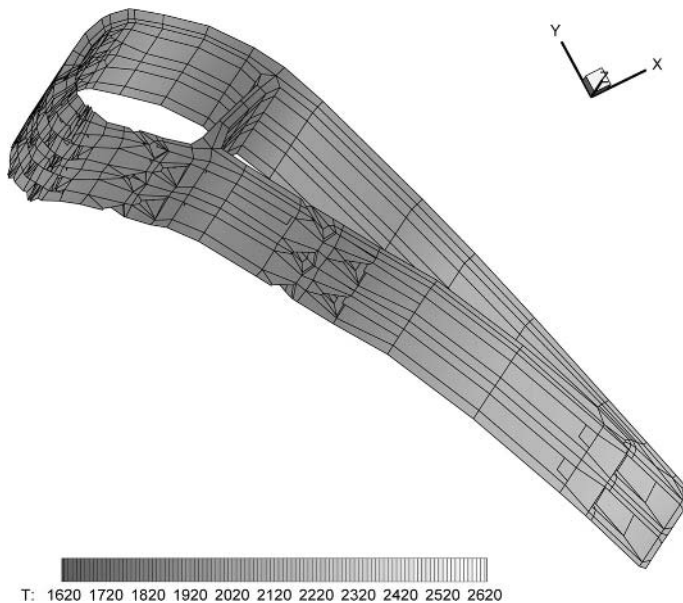


**Figure 9.**  
Blade surface  
temperature predicted by  
the BEM using  $h$  and  
 $T_{aw}$  provided from the  
two-temperature  
approach

---

For instance, with conduction taken into consideration in the CHT simulation, the thin trailing regions are seen to reach higher temperatures than predicted by the isothermal approach, while the forward plenum region is seen to be effectively cooler. This has severe implications in materials design and subsequent thermal stress analysis of the blade carried out using these metal temperatures.

Results are now presented for a simulation using the subsectioning iterative method for a pure heat conduction problem. Here, a blade with a 10 cm chord and 14 cm in the spanwise direction is taken. The blade is cooled by two plena (Figure 10). The blade is discretized using GridPro™ (Program Development Corporation, 1997) into six subsections with a surface grid of a total of nearly 6,000 bilinear elements or nearly 24,000 degrees of freedom (Figure 11). Each block is kept at a discretization level nearer to 1,000 bilinear boundary elements. Adiabatic conditions are imposed on the top and bottom surfaces of the blade. Convective boundary conditions are imposed on all other surfaces. The film coefficient on the outer surface of the blade is taken as  $h = 1,000 \text{ W/m}^2\text{K}$  with the reference temperature taken as 1,000 K, while the cooling plena are both imposed with film coefficients  $h = 500 \text{ W/m}^2\text{K}$  with the reference temperature taken as linearly varying from 300 K to 400 K in the increasing  $z$ -direction of the cooling plenum closest to the leading edge, while

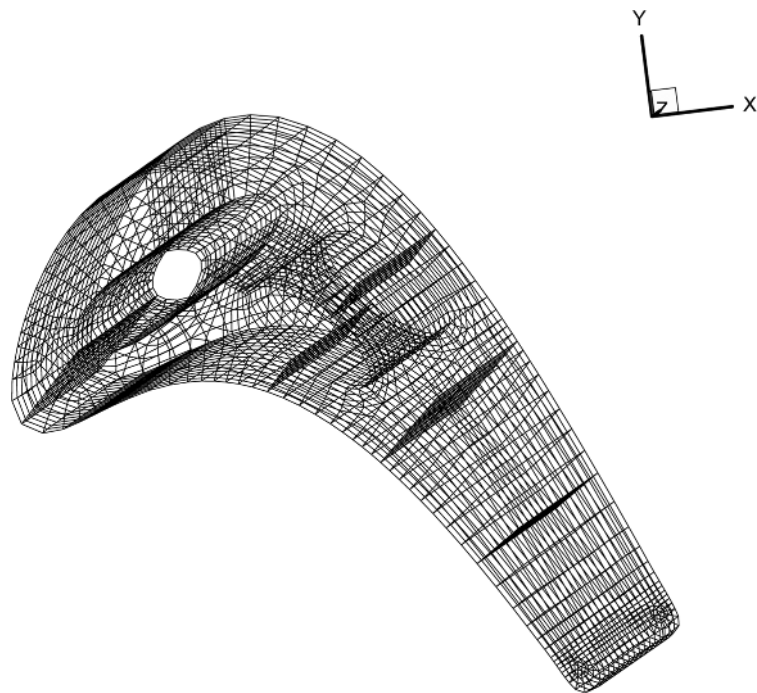


**Figure 10.**  
BEM grid for 3D cooled  
blade

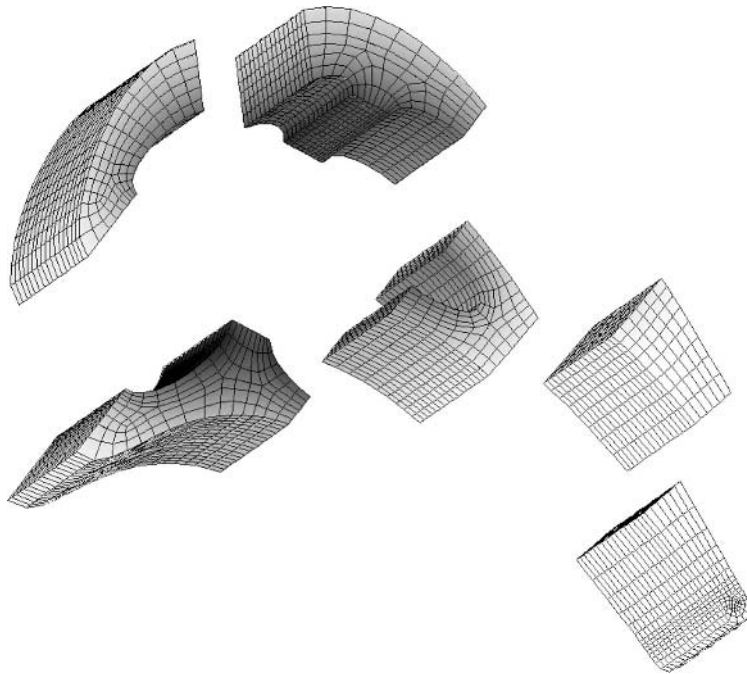


**Figure 11.**  
Domain decomposition  
of a 3D plenum-cooled  
turbine blade

---

linearly varying from 500 K to 400 K in the decreasing  $z$ -direction of the cooling plenum closest to the trailing edge.

All computations were performed on a Pentium 4, 1.8 GHz PC with 512 MB 800 MHz RDRAM. The initial guess using equation (21) alone without the coarse grid model provided an excellent starting point for the iteration, which converged on 8 steps to provide an  $L_2$  iterative norm, defined in equation (25), of 0.00011698. It took 34,905 s to set up the matrices, obtain and store their LU factors, and 813 s to solve the problem iteratively. The resulting temperature plots shown in Figures 11 and 12 reveal a very smooth distribution across all blocks. The resulting surface heat fluxes are presented in Figure 13 revealing a very smooth distribution from a minimum of  $-180,000 \text{ W/m}^2\text{K}$  to a maximum of  $230,000 \text{ W/m}^2\text{K}$ . It should be noted that the subsectioning approach is ideally suited for parallel implementation. The authors are pursuing this avenue prior to integration of the algorithm with the CHT solver. This concludes the example section.

## 6. Conclusions

A combined BEM/FVM approach using the TFFB conjugate method has been implemented in a 3D context to model CHT in cooled turbine blades. As a

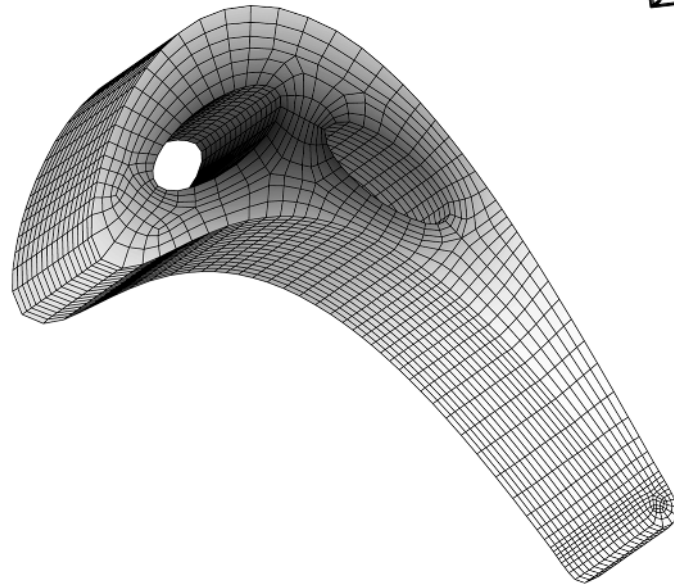
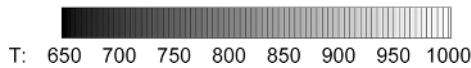
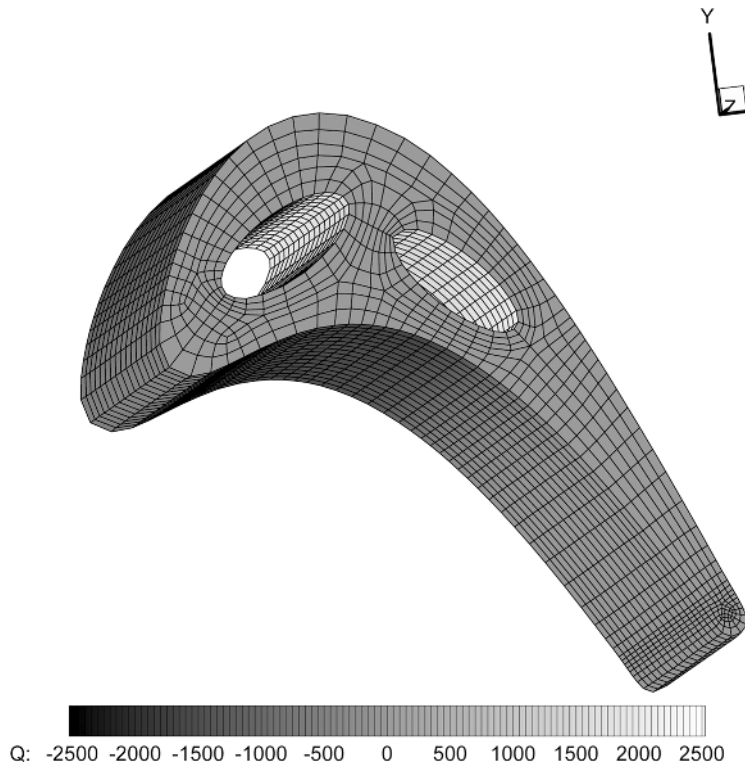


**Figure 12.**  
Converged surface  
temperature  
distribution (K)

---



boundary-only grid is used by the BEM, the computational time for the heat conduction analysis is insignificant compared to the time used for the NS analysis. The proposed method produces realistic results without using arbitrary assumptions for the thermal condition at the conductor surface. Results from a CHT numerical simulation of a 3D film-cooled blade section are presented and are compared with those obtained from the standard approach of a two temperature model. A significant difference in the level and distribution of the metal temperatures is found between the two models. These differences have severe implications in materials design and subsequent thermal stress analysis of the blade carried out using these metal temperatures. In practice, turbomachinery components such as modern cooled turbine blades often contain several hundred film cooling holes and intricate internal serpentine cooling passages with complex convective enhancement configurations such as turbulating trip strips. This poses a real computational challenge to BEM modeling. The subsectioning iterative approach outlined in this paper offers promising technique to address this problem. It is proposed to extend the current work by implementing the parallel implementation of iterative domain



---

**Figure 13.**  
Converged surface heat  
flux distribution  
( $1/100 \text{ W/m}^2\text{K}$ )

---

decomposition approach for the BEM in order to address large-scale CHT problems and results of such simulations will soon be reported elsewhere (Divo *et al.*, 2003; Heidmann *et al.*, 2003).

### References

- Ameri, A.A., Steinthorsson, E. and Rigby, D.L. (1997), "Effect of squealer tip on rotor heat transfer and efficiency", *ASME Paper 97-GT-128*.
- Azevedo, J.P.S. and Wrobel, L.C. (1988), "Non-linear heat conduction in composite bodies: a boundary element formulation", *International Journal for Numerical Methods in Engineering*, Vol. 26, pp. 19-38.
- Banerjee, P.K. (1994), *Boundary Element Method*, McGraw-Hill, NY, USA.
- Bialecki, R. and Nhalik, R. (1989), "Solving nonlinear steady state potential problems in inhomogeneous bodies using the boundary element method", *Numerical Heat Transfer, Part B*, Vol. 15, pp. 79-96.
- Bialecki, R.A., Merkel, M., Mews, H. and Kuhn, G. (1996), "In-and out-of-core BEM equation solver with parallel and nonlinear options", *International Journal for numerical Methods in Engineering*, Vol. 39, pp. 4215-42.

- Bialecki, R., Ostrowski, Z., Kassab, A., Qi, Y. and Sciubba, E. (2001), "Coupling finite element and boundary element solutions", *Proc. of the 2001 European Conference on Computational Mechanics*, 26-29 June, 2001, Cracow, Poland.
- Bohn, D.E., Becker, V.J. and Rungen, A.U. (1997), "Experimental and numerical conjugate flow and heat transfer investigation of a shower-head cooled turbine guide vane", *ASME Paper 97-GT-15*.
- Bohn, D., Becker, V., Kusterer, K., Otsuki, Y., Sugimoto, T. and Tanaka, R. (1999), "3-D internal conjugate calculations of a convectively cooled turbine blade with serpentine-shaped ribbed channels", *IGTI Paper 99-GT-220*.
- Brebbia, C.A. and Dominguez, J. (1989), *Boundary Elements: An Introductory Course*, Computational Mechanics Pub., Southampton and McGraw-Hill, NY, USA.
- Brebbia, C.A., Telles, J.C.F. and Wrobel, L.C. (1984), *Boundary Element Techniques*, Springer-Verlag, Berlin.
- Brown, S.A. (1997), "Displacement extrapolations for CFD+CSM aeroelastic analysis", *AIAA Paper 97-1090*
- Bucher, H. and Wrobel, L.C. (2000), "A novel approach to applying wavelet transforms in boundary element method", in Denda, M., Aliabadi, M.H. and Charafi, A. (Eds), *Advances in Boundary Element Techniques, II*, Hogaar Press, Switzerland, pp. 3-11.
- Chima, R.V. (1996), "A  $k-\omega$  turbulence model for quasi-dimensional turbomachinery flows", *NASA TM-107051*.
- Comini, G., Saro, O. and Manzan, M. (1993), "A physical approach to finite element modeling of coupled conduction and convection", *Numerical Heat Transfer, Part B*, Vol. 24, pp. 243-61.
- Divo, E.A., Kassab, A.J. and Rodriguez, F. (2003), "Domain decomposition for 3D boundary elements in non-linear heat conduction", *ASME Paper HT2003-40553*.
- Dowell, E. and Hall, K.C. (2001), "Modeling of fluid structure interaction", *Annual Review of Fluid Mechanics*, Vol. 33, pp. 445-90.
- Greengard, L. and Strain, J. (1990), "A fast algorithm for the evaluation of heat potentials", *Communications in Pure and Applied Mathematics*, Vol. 43, pp. 949-63.
- Hackbush, W. and Nowak, Z.P. (1989), "On the fast multiplication in the boundary element method by panel clustering", *Numerische Mathematik*, Vol. 54, pp. 463-91.
- Hahn, Z., Dennis, B. and Dulikravich, G. (2000), "Simultaneous prediction of external flow-field and temperature in internally cooled 3-D turbine blade material", *IGTI Paper 2000-GT-253*.
- Hassan, B., Kuntz, D. and Potter, D.L. (1998), "Coupled fluid/thermal prediction of ablating hypersonic vehicles", *AIAA Paper 98-0168*.
- He, M., Bishop, P., Kassab, A.J. and Minardi, A. (1995a), "A coupled FDM/BEM solution for the conjugate heat transfer problem", *Numerical Heat Transfer, Part B: Fundamentals*, Vol. 28 No. 2, pp. 139-54.
- He, M., Kassab, A.J., Bishop, P.J. and Minardi, A. (1995b), "A coupled FDM/BEM iterative solution for the conjugate heat transfer problem in thick-walled channels: constant temperature imposed at the outer channel wall", *Engineering Analysis*, Vol. 15 No. 1, pp. 43-50.
- Heidmann, J., Rigby, D. and Ameri, A. (2002), "A three-dimensional coupled external/internal simulation of a film-cooled turbine vane", *ASME Journal of Turbomachinery*, Vol. 122, pp. 348-59.

- 
- Heidmann, J.D., Kassab, A.J., Divo, E.A., Rodriguez, F. and Steinhilber, E. (2003), "Conjugate heat transfer effects on a realistic film-cooled turbine vane", *ASME Paper GT2003-G38553*.
- Jameson, A., Schmidt, W. and Turkel, E. (1981), "Numerical simulation of the Euler equations by the finite volume methods using Runge-Kutta time stepping schemes", *AIAA Paper 81-1259*.
- Kane, J. (1994), *Boundary Element Analysis in Engineering and Continuum Mechanics*, Prentice-Hall, Englewood Cliffs, New Jersey.
- Kane, J.H., Kashava-Kumar, B.L. and Saigal, S. (1990), "An arbitrary condensing, noncondensing strategy for large scale, multi-zone boundary element analysis", *Computer Methods in Applied Mechanics and Engineering*, Vol. 79, pp. 219-44.
- Kao, K.H. and Liou, M.S. (1997), "Application of chimera/unstructured hybrid grids for conjugate heat transfer", *AIAA Journal*, Vol. 35 No. 9, pp. 1472-8.
- Kassab, A.J. and Aliabadi, M.H. (Eds) (2001), *Advances in Boundary Elements: Coupled Field Problems*, Computational Mechanics, Boston.
- Kassab, A.J. and Nordlund, R.S. (1994), "Addressing the corner problem in the BEM solution of heat conduction problems", *Communications in Numerical Methods in Engineering*, Vol. 10, pp. 385-92.
- Kassab, A.J. and Wrobel, L.C. (2000), "Boundary element methods in heat conduction", in Minowycz, W.J. and Sparrow, E.M. (Eds), *Recent Advances in Numerical Heat Transfer*, Chapter 5, Taylor and Francis, New York, Vol. 2, pp. 143-88.
- Kellogg, O.D. (1953), *Foundations of Potential Theory*, Dover, New York.
- Kontinos, D. (1997), "Coupled thermal analysis method with application to metallic thermal protection panels", *AIAA Journal of Thermophysics and Heat Transfer*, Vol. 11 No. 2, pp. 173-81.
- Li, H. and Kassab, A.J. (1994a), "Numerical prediction of fluid flow and heat transfer in turbine blades with internal cooling", *AIAA/ASME Paper 94-2933*.
- Li, H. and Kassab, A.J. (1994b), "A coupled FVM/BEM solution to conjugate heat transfer in turbine blades", *AIAA Paper 94-1981*.
- Liggett, J.A. and Liu, P.L.-F. (1983), *The Boundary Integral Equation Method for Porous Media Flow*, Allen and Unwin, Boston.
- Menter, F.R. (1993), "Zonal two-equation  $k-\omega$  turbulence models for aerodynamic flows", *AIAA Paper 93-2906*.
- Morse, P.M. and Feshbach, H. (1953), *Methods of Theoretical Physics*, McGraw-Hill, NY, USA.
- Partridge, P.W., Brebbia, C.A. and Wrobel, L.C. (1992), *The Dual Reciprocity Boundary Element Method*, Computational Mechanics Publications, Southampton.
- Patankar, S.V. (1978), "A numerical method for conduction in composite materials, flow in irregular geometries and conjugate heat transfer", *Proc. 6th. Int. Heat Transfer Conf.*, NRC Canada, and Hemisphere Pub. Co., New York, Vol. 3, pp. 297-302
- Program Development Corporation (1997), *GridPro™/az3000-User's guide and reference manual*, White Plains, New York.
- Rahaim, C., Cavalleri, R.J. and Kassab, A.J. (1997), "Computational code for conjugate heat transfer problems an experimental validation effort", *AIAA Paper 97-2487*.
- Rahaim, C.P., Kassab, A.J. and Cavalleri, R. (2000), "A coupled dual reciprocity boundary element/finite volume method for transient conjugate heat transfer", *AIAA Journal of Thermophysics and Heat Transfer*, Vol. 14 No. 1, pp. 27-38.

- Rigby, D.L., Ameri, A.A. and Steinthorsson, E. (1997), "Numerical prediction of heat transfer in a channel with ribs and bleed", *ASME Paper 97-GT-431*.
- Schlichting, H. (1979), *Boundary Layer Theory*, 7th edition, McGraw-Hill, NY, USA, pp. 312-13.
- Shyy, W. and Burke, J. (1994), "Study of iterative characteristics of convective diffusive and conjugate heat transfer problems", *Numerical Heat Transfer, Part B*, Vol. 26, pp. 21-37.
- Steinthorsson, E., Ameri, A. and Rigby, D. (n.d.), *LeRC-HT-The NASA Lewis Research Center General Multi-Block Navier-Stokes Convective Heat Transfer Code*, (unpublished).
- Steinthorsson, E., Liou, M.-S. and Povinelli L.A. (1993), "Development of an explicit multi-block/multigrid flow solver for viscous flows in complex geometries", *AIAA Paper 93-2380*.
- Tayala, S.S., Rajadas, J.N. and Chattopadhyay, A. (2000), "Multidisciplinary optimization for gas turbine airfoil design", *Inverse Problems in Engineering*, Vol. 8 No. 3, pp. 283-307.
- Turkel, E. (1987), "Preconditioned methods for solving the incompressible and low-speed compressible equations", *Journal of Computational Physics*, Vol. 72 No. 2, pp. 277-98.
- Turkel, E. (1993), "Review of preconditioning methods for fluid dynamics", *Applied Numerical Mathematics*, Vol. 12, pp. 257-84.
- Wilcox, D.C. (1993), *Turbulence Modeling for CFD*, DCW Industries, La Canada, California.
- Wilcox, D.C. (1994), "Simulation of transition with a two-equation turbulence model", *AIAA Journal*, Vol. 32 No. 2, pp. 247-55.
- Ye, R., Kassab, A.J. and Li, H.J. (1998), "FVM/BEM approach for the solution of nonlinear conjugate heat transfer problems", in Kassab, A.J., Brebbia, C.A. and Chopra, M.B. (Eds) *Proc. BEM 20*, 19-21 August, Orlando, Florida, pp. 679-89.

**Further reading**

- Abramowitz, M. and Stegun, I. (1965), *Handbook of Mathematical Functions*, Dover Publications, New York.
- Divo, E., Rodriguez, F. and Kassab, A.J. (n.d.), "A strategy for linear and nonlinear three dimensional BEM heat conduction models", *Numerical Heat Transfer* (in review).
- Ralston, A. and Rabinowitz, P. (1978), *A First Course in Numerical Analysis*, McGraw-Hill, NY, USA.



# RBF interpolation of boundary values in the BEM for heat transfer problems

RBF  
interpolation of  
boundary values

611

Nam Mai-Duy and Thanh Tran-Cong

Faculty of Engineering and Surveying, University of Southern  
Queensland, Toowoomba, Australia

Received February 2002  
Revised September 2002  
Accepted January 2003

**Keywords** Boundary element method, Boundary integral equation, Heat transfer

**Abstract** This paper is concerned with the application of radial basis function networks (RBFNs) as interpolation functions for all boundary values in the boundary element method (BEM) for the numerical solution of heat transfer problems. The quality of the estimate of boundary integrals is greatly affected by the type of functions used to interpolate the temperature, its normal derivative and the geometry along the boundary from the nodal values. In this paper, instead of conventional Lagrange polynomials, interpolation functions representing these variables are based on the "universal approximator" RBFNs, resulting in much better estimates. The proposed method is verified on problems with different variations of temperature on the boundary from linear level to higher orders. Numerical results obtained show that the BEM with indirect RBFN (IRBFN) interpolation performs much better than the one with linear or quadratic elements in terms of accuracy and convergence rate. For example, for the solution of Laplace's equation in 2D, the BEM can achieve the norm of error of the boundary solution of  $O(10^{-5})$  by using IRBFN interpolation while quadratic BEM can achieve a norm only of  $O(10^{-2})$  with the same boundary points employed. The IRBFN-BEM also appears to have achieved a higher efficiency. Furthermore, the convergence rates are of  $O(h^{1.38})$  and  $O(h^{4.78})$  for the quadratic BEM and the IRBFN-based BEM, respectively, where  $h$  is the nodal spacing.

## 1. Introduction

Boundary element methods (BEMs) have become one of the popular techniques for solving boundary value problems in continuum mechanics. For linear homogeneous problems, the solution procedure of BEM consists of two main stages:

- (1) estimate the boundary solution by solving boundary integral equations (BIEs), and
- (2) estimate the internal solution by calculating the boundary integrals (BIs) using the results obtained from the stage (1).

Invited paper for the special issue of the *International Journal of Numerical Methods for Heat & Fluid Flow* on the BEM.

This work is supported by a Special USQ Research Grant (Grant No. 179-310) to Thanh Tran-Cong. This support is gratefully acknowledged. The authors would like to thank the referees for their helpful comments.



The first stage plays an important role, because the solution obtained here provides sources to compute the internal solution. However, it can be seen that both stages involve the evaluation of BIs, of which any improvements achieved result in the betterment of the overall solution to the problem. In the evaluation of BIs, the two main topics of interest are how to represent the variables along the boundary adequately and how to evaluate the integrals accurately, especially in the cases where the moving field point coincides with the source point (singular integrals). In the standard BEM (Banerjee and Butterfield, 1981; Brebbia *et al.*, 1984), the boundary of the domain of analysis is divided into a number of small segments (elements). The geometry of an element and the variation of temperature and temperature gradient over such an element are usually represented by Lagrange polynomials, of which the constant, linear and quadratic types are the most widely applied. With regard to the evaluation of integrals, including weakly and strongly singular integrals, considerable achievements have been reported by Sladek and Sladek (1998). It is observed that the accuracy of solution by the standard BEM greatly depends on the type of elements used. On the other hand, neural networks (NN) which deal with interpolation and approximation of functions, have been developed recently and become one of the main fields of research in numerical analysis (Haykin, 1999). It has been proved that the NNs are capable of universal approximation (Cybenko, 1989; Girosi and Poggio, 1990). Interest in the application of NNs (especially the multiquadric (MQ) radial basis function networks (RBFNs)) for numerical solution of PDEs has been increasing (Kansa, 1990; Mai-Duy and Tran-Cong, 2001a, b, 2002; Sharan *et al.*, 1997; Zerroukat *et al.*, 1998). In this study, “universal approximator” RBFNs are introduced into the BEM scheme to represent the variables along the boundary. Although RBFNs have an ability to represent any continuous function to a prescribed degree of accuracy, practical means to acquire sufficient approximation accuracy still remain an open problem. Indirect RBFNs (IRBFNs) which perform better than direct RBFNs in terms of accuracy and convergence rate (Mai-Duy and Tran-Cong, 2001a, 2002) are utilised in this work. Due to the presence of NNs in BIs, the treatment of the singularity in CPV integrals requires some modification in comparison with the standard BEM. The paper is organised as follows. In Section 2, the IRBFN interpolation of functions is presented and its performance is then compared with linear and quadratic element results via a numerical example. Section 3 is to introduce the IRBFN interpolation into the BEM scheme to represent the variable in BIEs. In Section 4, some 2D heat transfer problems governed by Laplace’s or Poisson’s equations are simulated to validate the proposed method. Section 5 gives some concluding remarks.

## 2. Interpolation with IRBFN

The task of interpolation problems is to estimate a function  $y(s)$  for arbitrary  $s$  from the known value of  $y(s)$  at a set of points  $s^{(1)}, s^{(2)}, \dots, s^{(n)}$  and therefore,

the interpolation must model the function by some plausible functional form. The form is expected to be sufficiently general in order to describe large classes of functions which might arise in practice. By far the most common functional forms used are based on polynomials (Press *et al.*, 1988). Generally, for problems of interpolation, universal approximators are highly desired in order to handle large classes of functions. It has been proved that RBFNs, which can be considered as approximation schemes, are able to approximate arbitrarily well continuous functions (Girosi and Poggio, 1990). The function  $y$  to be interpolated/approximated is decomposed into radial basis functions as

$$y(x) \approx f(x) = \sum_{i=1}^m w^{(i)} g^{(i)}(x), \quad (1)$$

where  $m$  is the number of radial basis functions,  $\{g^{(i)}\}_{i=1}^m$  is the set of chosen radial basis functions and  $\{w^{(i)}\}_{i=1}^m$  is the set of weights to be found. Theoretically, the larger the number of radial basis functions used, the more accurate the approximation will be as, stated in Cover's theorem (Haykin, 1999). However, the difficulty here is how to choose the network's parameters such as RBF widths properly. IRBFNs were found to be more accurate than direct RBFNs with relatively easier choice of RBF widths (Mai-Duy and Tran-Cong, 2001a, 2002) and will be employed in the present work. In this paper, only the problems in 2D are discussed. In view of the fact that the interpolation IRBFN method will be coupled later with the BEM where the problem dimensionality is reduced by one, only the MQ-IRBFN for function and its derivatives (e.g. up to the second order) in 1D needs to be employed here and its formulation is briefly recaptured as follows:

$$y''(s) \approx f''(s) = \sum_{i=1}^m w^{(i)} g^{(i)}(s), \quad (2)$$

$$y'(s) \approx f'(s) = \sum_{i=1}^m w^{(i)} H^{(i)}(s) + C_1, \quad (3)$$

$$y(s) \approx f(s) = \sum_{i=1}^m w^{(i)} \bar{H}^{(i)}(s) + C_1 s + C_2, \quad (4)$$

where  $s$  is the curvilinear coordinate (arclength),  $C_1$  and  $C_2$  are constants of integration and

$$g^{(i)}(s) = ((s - c^{(i)})^2 + a^{(i)2})^{1/2}, \quad (5)$$

$$H^{(i)}(s) = \int g^{(i)}(s) ds = \frac{(s - c^{(i)})(s - c^{(i)})^2 + a^{(i)2})^{1/2}}{2} + \frac{a^{(i)2}}{2} \ln((s - c^{(i)}) + ((s - c^{(i)})^2 + a^{(i)2})^{1/2}), \quad (6)$$

$$\begin{aligned} \bar{H}^{(i)}(s) = \int H^{(i)}(s) ds &= \frac{((s - c^{(i)})^2 + a^{(i)2})^{3/2}}{6} \\ &+ \frac{a^{(i)2}}{2} (s - c^{(i)}) \ln((s - c^{(i)}) + ((s - c^{(i)})^2 + a^{(i)2})^{1/2}) \\ &- \frac{a^{(i)2}}{2} ((s - c^{(i)})^2 + a^{(i)2})^{1/2}, \end{aligned} \quad (7)$$

in which  $\{c^{(i)}\}_{i=1}^m$  is the set of centres and  $\{a^{(i)}\}_{i=1}^m$  is the set of RBF widths. The RBF width is chosen based on the following simple relation

$$a^{(i)} = \beta d^{(i)},$$

where  $\beta$  is a factor and  $d^{(i)}$  is the minimum arclength between the  $i$ th centre and its neighbouring centres. Since  $C_1$  and  $C_2$  are to be found, it is convenient to let  $w^{(m+1)} = C_1$ ,  $w^{(m+2)} = C_2$ ,  $\bar{H}^{(m+1)} = s$  and  $\bar{H}^{(m+2)} = 1$  in equation (4), which becomes

$$y(s) \approx f(s) = \sum_{i=1}^{m+2} w^{(i)} \bar{H}^{(i)}(s), \quad (8)$$

$$\bar{H}^{(i)} = \text{RHS of equation (7)}, \quad i = 1, \dots, m, \quad (9)$$

$$\bar{H}^{(m+1)} = s, \quad (10)$$

$$\bar{H}^{(m+2)} = 1. \quad (11)$$

The detailed implementation and accuracy of the IRBFN method were reported previously (Mai-Duy and Tran-Cong, 2002). In all the numerical examples carried out in this paper, the value of  $\beta$  is simply chosen to be in the range of 7-10. Before introducing the IRBFN interpolation into the BEM scheme, the performance of the IRBFN and element-based method are compared using the interpolation of the following function

$y = 0.02(12 + 3s - 3.5s^2 + 7.2s^3)(1 + \cos 4\pi s)(1 + 0.8 \sin 3\pi s)$ ,  
 where  $0 \leq s \leq 1$  (Figure 1). The accuracy achieved by each technique is evaluated via the norm of relative error of the solution  $N_e$  defined by

$$N_e = \left( \frac{\sum_{i=1}^q (y(s^{(i)}) - f(s^{(i)}))^2}{\sum_{i=1}^q y(s^{(i)})^2} \right)^{1/2}, \tag{12}$$

where  $y(s^{(i)})$  and  $f(s^{(i)})$  are the exact and approximate solutions at the point  $i$ , respectively, and  $q$  is the number of test points. The performance of linear, quadratic and IRBFN interpolations are assessed using four data sets of 13, 15, 17 and 19 known points. For each data set, the function  $y$  is estimated at 500 test points. Note that the known and test points here are uniformly distributed. The results obtained using  $\beta = 10$  are displayed in Figure 2 showing that the IRBFN method achieves superior accuracy and convergence rate to the element-based method. The solution converges apparently as  $O(h^{1.95})$ ,  $O(h^{1.98})$  and  $O(h^{9.47})$  for linear, quadratic and IRBFN interpolations, respectively, where  $h$  is the grid point spacing. At  $h = 0.06$ , which corresponds to a set of 19 grid

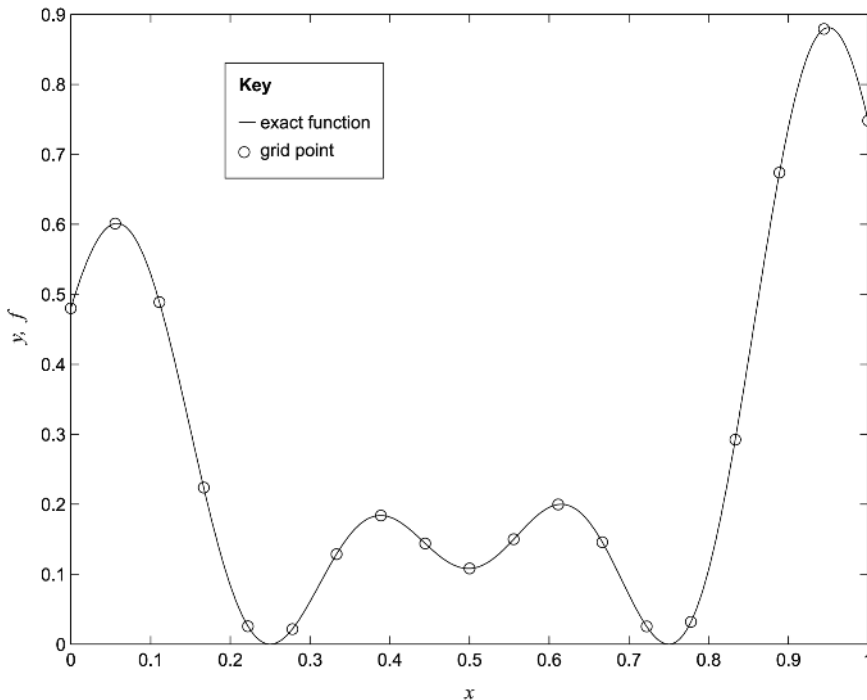
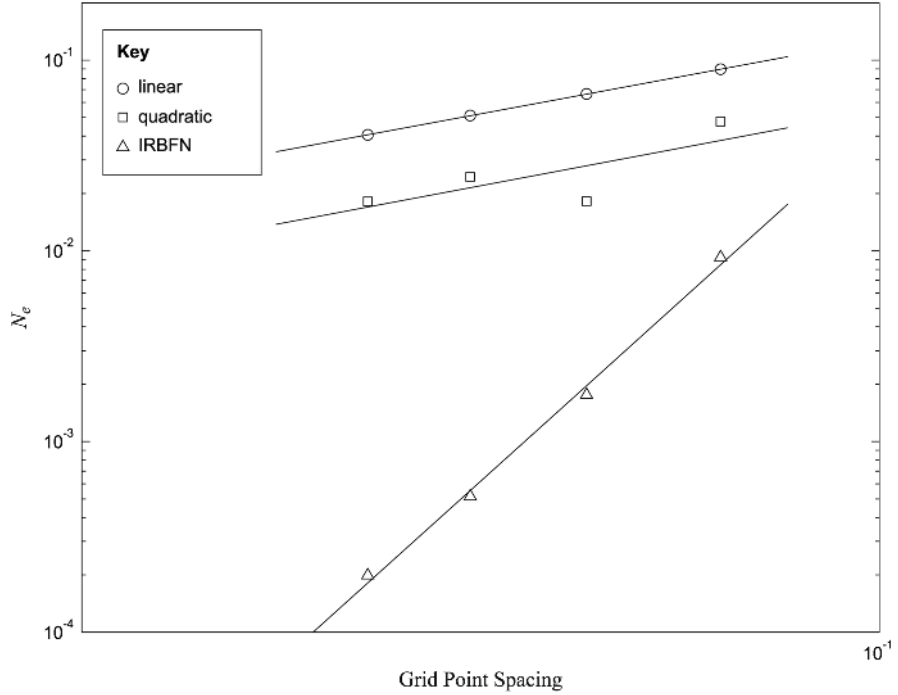


**Figure 1.**  
 Interpolation of function  
 $y = 0.02(12 + 3x$   
 $- 3.5x^2 + 7.2x^3)$   
 $(1 + \cos 4\pi x)$   
 $(1 + 0.8 \sin 3\pi x)$   
 from  
 a set of grid points

**Figure 2.** Interpolation of function  $y = 0.02(12 + 3x - 3.5x^2 + 7.2x^3)(1 + \cos 4\pi x)(1 + 0.8 \sin 3\pi x)$ . The rate of convergence with grid point spacing refinement. The solution converges apparently as  $O(h^{1.95})$ ,  $O(h^{1.98})$  and  $O(h^{9.47})$  for linear, quadratic and IRBFN interpolations, respectively, where  $h$  is the grid point spacing



points, the error norms obtained are  $4.06e - 2$ ,  $1.81e - 2$  and  $1.98e - 4$  for linear, quadratic and IRBFN schemes, respectively.

### 3. A new interpolation method for the evaluation of BIs

For heat transfer problems, the governing equations take the form

$$\nabla^2 u = b, \quad \mathbf{x} \in \Omega, \quad (13)$$

$$u = \bar{u}, \quad \mathbf{x} \in \Gamma_u, \quad (14)$$

$$q \equiv \frac{\partial u}{\partial n} = \bar{q}, \quad \mathbf{x} \in \Gamma_q, \quad (15)$$

where  $u$  is the temperature,  $q$  is the temperature gradient across the surface,  $\mathbf{n}$  is the unit outward normal vector,  $\bar{u}$  and  $\bar{q}$  are the prescribed boundary conditions,  $b$  is a known function of position and  $\Gamma = \Gamma_u + \Gamma_q$  is the boundary of the domain  $\Omega$ .

Integral equation (IE) formulations for heat transfer problems are well documented in a number of texts (Banerjee and Butterfield, 1981; Brebbia *et al.*, 1984). Equations (13)-(15) can be reformulated in terms of the IEs for a given spatial point  $\xi$  as follows

$$\begin{aligned}
 c(\xi)u(\xi) + \int_{\Gamma} q^*(\xi, x)u(x) \, d\Gamma + \int_{\Omega} b(x)u^*(\xi, x) \, d\Omega \\
 = \int_{\Gamma} u^*(\xi, x)q(x) \, d\Gamma, \quad (16)
 \end{aligned}$$

where  $u^*$  is the fundamental solution to the Laplace equation, e.g. for a 2D isotropic domain  $u^* = (1/2\pi)\ln(1/r)$  in which  $r$  is the distance from the point  $\xi$  to the current point of integration  $x$ ,  $q^* = \partial u^*/\partial n$ ,  $c(\xi) = \theta/2\pi$  with  $\theta$  being the internal angle of the corner in radians, if  $\xi$  is a boundary point and  $c(\xi) = 1$ , if  $\xi$  is an internal point. Note that the volume integral here does not introduce any unknowns because the function  $b$  is given and furthermore, it can be reduced to the BIs by using the particular solution (PS) techniques (Zheng *et al.*, 1991) or the dual reciprocity method (DRM) (Partridge *et al.*, 1992). Without loss of generality, the following discussions are based on equation (16) with  $b = 0$  (Laplace's equation).

For the standard BEM, the numerical procedure for equation (16) involves a subdivision of the boundary  $\Gamma$  into a number of small elements. On each element, the geometry and the variation of  $u$  and  $q$  are assumed to have a certain shape such as linear and quadratic ones. The study on the interpolation of function in Section 2 shows that the IRBFN interpolation achieves an accuracy and convergence rate superior to the linear and quadratic element-based interpolations. The question here is whether the employment of IRBFN interpolation in the BEM scheme can improve the solution in terms of accuracy and convergence rate as in the case of function approximation. The answer is positive and substantiated in the remainder of this paper.

The first issue to be considered is about the implementation of singular integrals when IRBFNs are present within integrands. The difference between the IRBFN and the Lagrange-type interpolation is that in the present IRBFN interpolation, none of the basis functions are null at the singular point (the point where the field point  $x$  and the source point  $\xi$  coincide) and hence the corresponding integrands obtained are not regular. Consequently, at the singular point all CPV integrals associated with the IRBFN weights are singular and cannot be evaluated by using the hypothesis of constant potential directly over the whole domain as in the case of the standard BEM. To overcome this difficulty, the treatment of singular CPV integrals needs to be slightly modified. The BIEs can be written in the following form (Hwang *et al.*, 2002; Tanaka *et al.*, 1994)

$$u(\xi) \int_{\Gamma_{\varepsilon, \varepsilon \rightarrow 0}} q^*(\xi, x) \, d\Gamma + \text{CPV} \int_{\Gamma} q^*(\xi, x)u(x) \, d\Gamma = \int_{\Gamma} u^*(\xi, x)q(x) \, d\Gamma, \quad (17)$$

where  $\Gamma_{\varepsilon}$  is part of a circle that excludes its origin (or the singular point) from the domain of analysis. Assume that the temperature  $u(x)$  is a constant unit on

the whole domain, i.e.  $u(\xi) = u(x) = 1$ , and hence the gradient  $q(x)$  is everywhere zero. Equation (17) then simplifies to

$$\int_{\Gamma_{\varepsilon, \varepsilon \rightarrow 0}} q^*(\xi, x) d\Gamma = -\text{CPV} \int_{\Gamma} q^*(\xi, x) d\Gamma. \quad (18)$$

Substitution of equation (18) into equation (17) yields

$$\text{CPV} \int_{\Gamma} q^*(\xi, x)(u(x) - u(\xi)) d\Gamma = \int_{\Gamma} u^*(\xi, x)q(x) d\Gamma. \quad (19)$$

The CPV integral is now written in the non-singular form, where the standard Gaussian quadrature can be applied. For weakly singular integrals, some well-known treatments such as logarithmic Gaussian quadrature and Telles' transformation technique (Telles, 1987) can be applied directly as in the case of the standard BEM.

The second issue is concerned with the employment of the IRBFNs in the BEM scheme to represent the variables in the BIs. In the present method, the boundary  $\Gamma$  of the domain of analysis is also divided into a number of segments  $N_s$ , i.e.

$$\Gamma = \sum_{j=1}^{N_s} \Gamma_j,$$

which are 1D domains to be represented by networks. Note that the size of the segment  $\Gamma_j$  can be much larger than the size of elements in the standard BEM provided that the associated boundary is smooth and the prescribed boundary conditions are of the same type. Equation (19) can be written in the discretised form as

$$\sum_{j=1}^{N_s} \int_{\Gamma_j} q^*(\xi, x)(u_j(x) - u_l(\xi)) d\Gamma_j = \sum_{j=1}^{N_s} \int_{\Gamma_j} u^*(\xi, x)q_j(x) d\Gamma_j, \quad (20)$$

where the subscript  $j$  denotes the general segments and the subscript  $l$  indicates the segment containing the source point  $\xi$ . The variation of temperature  $u$  and gradient  $q$  on the segment  $\Gamma_j$  is now represented by the IRBFNs in terms of the curvilinear coordinate  $s$  as (equation (9))

$$u_j = \sum_{i=1}^{mj+2} w_{uj}^{(i)} \bar{H}_j^{(i)}(s), \quad (21)$$

$$q_j = \sum_{i=1}^{mj+2} w_{qj}^{(i)} \bar{H}_j^{(i)}(s), \quad (22)$$

where  $s \in \Gamma_j$ ,  $m_j + 2$  is the number of IRBFN weights,  $\{w_{uj}^{(i)}\}_{i=1}^{mj+2}$  and  $\{w_{qj}^{(i)}\}_{i=1}^{mj+2}$  are the sets of weights of networks for the temperature  $u$  and temperature gradient  $q$ , respectively. Similarly, the geometry can be interpolated from the nodal value by using the IRBFNs as

$$x_{1j} = \sum_{i=1}^{mj+2} w_{x1j}^{(i)} \bar{H}_j^{(i)}(s), \quad (23)$$

$$x_{2j} = \sum_{i=1}^{mj+2} w_{x2j}^{(i)} \bar{H}_j^{(i)}(s). \quad (24)$$

Substitution of equations (21) and (22) into equation (20) yields

$$\begin{aligned} & \sum_{j=1}^{N_s} \int_{\Gamma_j} q^*(\xi, s) \left( \sum_{i=1}^{mj+2} w_{qj}^{(i)} \bar{H}_j^{(i)}(s) - \sum_{i=1}^{ml+2} w_{ul}^{(i)} \bar{H}_l^{(i)}(\xi) \right) d\Gamma_j \\ & = \sum_{j=1}^{N_s} \int_{\Gamma_j} u^*(\xi, s) \left( \sum_{i=1}^{mj+2} w_{qj}^{(i)} \bar{H}_j^{(i)}(s) \right) d\Gamma_j, \end{aligned} \quad (25)$$

or,

$$\begin{aligned} & \sum_{j=1}^{N_s} \left\{ \sum_{i=1}^{mj+2} w_{qj}^{(i)} \left( \int_{\Gamma_j} q^*(\xi, s) \bar{H}_j^{(i)}(s) d\Gamma_j \right) - \sum_{i=1}^{ml+2} w_{ul}^{(i)} \left( \int_{\Gamma_j} q^*(\xi, s) \bar{H}_l^{(i)}(s) d\Gamma_j \right) \right\} \\ & = \sum_{j=1}^{N_s} \sum_{i=1}^{mj+2} w_{qj}^{(i)} \left( \int_{\Gamma_j} u^*(\xi, s) \bar{H}_j^{(i)}(s) d\Gamma_j \right), \end{aligned} \quad (26)$$

where  $m_j$  is the number of training points on the segment  $j$ , which can vary from segment to segment. Equation (26) is formulated in terms of the IRBFN weights of networks for  $u$  and  $q$  rather than the nodal values of  $u$  and  $q$  as in the case of the standard BEM. Locating the source point  $\xi$  at the boundary training points results in the underdetermined system of algebraic equations with the unknown being the IRBFN weights. Thus, the system of equations obtained, which can have many solutions, needs to be solved in the general least squares sense. The preferred solution is the one whose values are smallest in the least squares sense (i.e. the norm of components is minimum). This can be achieved by using singular value decomposition technique (SVD). The procedural flow chart can be briefly summarised as follows:

- (1) divide the boundary into a number of segments over each of which the boundary is smooth and the prescribed boundary conditions are of the same type;
- (2) apply the IRBFN for approximation of the prescribed physical boundary conditions in order to obtain the IRBFN weights which are the boundary conditions in the weight space;
- (3) form the system matrices associated with the IRBFN weights  $w_u$  and  $w_q$ ;
- (4) impose the boundary conditions obtained from the step 2 and then solve the system for IRBFN weights by the SVD technique;
- (5) compute the boundary solution by using the IRBFN interpolation;
- (6) evaluate the temperature and its derivatives at selected internal points;
- (7) output the results.

Note that for the numerical solution of Poisson's equations using the BEM-PS approach, the PS is first found by expressing the known function  $b$  as a linear combination of radial basis functions and the volume integral is then transformed into the BIs (Zheng *et al.*, 1991). However, the first stage of this process produces a certain error which is separate from the error in the evaluation of the BIs. In order to confine the error of solution only to the evaluation of BIs, the following numerical examples of heat transfer problems governed by the Laplace's equations or Poisson's equations are chosen where the associated analytical PSs exist for the latter.

#### 4. Numerical examples

In this section, the proposed method is verified and compared with the standard BEM on heat transfer problems governed by the Laplace's or Poisson's equations. In order to make the BEM programs general in the sense that they can deal with any types of boundary conditions at the corners, all BEM codes with linear, quadratic and IRBFN interpolations employ discontinuous elements at the corner. The extreme boundary point at the corner is shifted into the element by one-fourth of the length of the element. Integrals are evaluated by using the standard Gaussian quadrature for regular cases and logarithmic Gaussian quadrature or Telles' quadratic transformation (Telles, 1987) for weakly singular cases with nine integration points. For the purpose of error estimation and convergence study, the error norm defined in equation (12) will be utilised here with the function  $y$  being the temperature  $u$  and its normal derivative  $q$  in the case of the boundary solution or the temperature  $u$  in the case of the internal solution.

##### 4.1 Boundary geometry with straight lines

It can be seen that the linear interpolation is able to represent exactly the geometry for a straight line and hence on the straight line segment the IRBFN

interpolation needs only to be used for representing the variation of temperature and gradient.

*4.1.1 Example 1.* Consider a square closed domain whose dimensions are taken to be 6 by 6 units as shown in Figure 3. The temperature on the left and right edges is maintained at 300 and 0, respectively, while the homogeneous Neumann conditions  $q = 0$  are imposed on the other edges. Inside the square, the steady-state temperature satisfies the Laplace's equation. The analytical solution is

$$u(x_1, x_2) = 300 - 50x_1.$$

This is a simple problem where the variation of temperature is linear. It can be seen that the use of linear interpolation is the best choice for this problem. Both linear and IRBFN ( $\beta = 10$ ) interpolations are employed and the corresponding BEM results on the boundary and at some internal points are displayed in Table I showing that the proposed method as well as the linear-BEM works. Significantly, the IRBFN-BEM works increasingly better than the linear-BEM as the number of boundary points increases, which seems to indicate that the IRBFN-BEM does not suffer numerical ill-conditioning as in the case of the standard BEM. Note that in the case of the IRBFN interpolation, each edge of the square domain and the boundary points on it become the domain and training points of the network associated with the edge, respectively. It is expected that the IRBFN-BEM approach performs better in dealing with higher order variations of temperature, which is verified in the following examples.

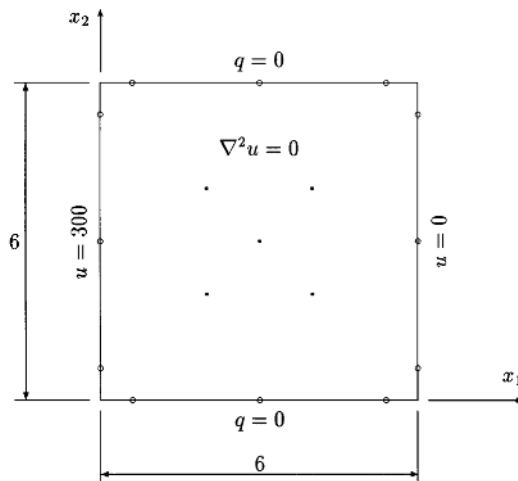


**Figure 3.**  
Example 1 – geometry,  
boundary conditions,  
boundary points and  
internal points

4.1.2 Example 2. The problem is to find the temperature field such that

$$\nabla^2 u = 0 \quad \text{inside the square } 0 \leq x_1 \leq \pi, \quad 0 \leq x_2 \leq \pi, \quad (27)$$

$$u(x_1, \pi) = \sin(x_1) \quad \text{on the top edge } (0 \leq x_1 \leq \pi), \quad (28)$$

$$u(x_1, x_2) = 0 \quad \text{on the other three sides.} \quad (29)$$

The exact solution of this problem is given by Snider (1999)

$$u(x_1, x_2) = \frac{1}{\sinh(\pi)} \sin(x_1) \sinh(x_2).$$

This is a Dirichlet problem for which the essential boundary condition is imposed along the boundary. Using discontinuous boundary elements at the corner for the case of the standard BEM or shifting the training points at the corner into the adjacent segments for the case of the IRBFN-BEM allows the correct description of multi-valued gradient  $q$  at the corner. In the case of IRBFN interpolation, each side of the square domain becomes the domain of network and the boundary points on it are utilised as training points. To study the convergence of the present method, four boundary point densities, namely  $5 \times 4$ ,  $7 \times 4$ ,  $9 \times 4$  and  $11 \times 4$ , and  $\beta = 7$  are employed. Some internal points are selected at  $(\pi/3, \pi/3)$ ,  $(\pi/3, 2\pi/3)$ ,  $(\pi/2, \pi/2)$ ,  $(2\pi/3, \pi/3)$  and  $(2\pi/3, 2\pi/3)$ . The performance of the BEM with linear, quadratic and IRBFN interpolations is assessed using the error norms of the boundary and internal solution. The boundary solution is displayed in Figure 4 showing that the proposed method is the most accurate one with higher convergence rate achieved. With these given boundary point densities, the solution converges as  $O(h^{2.24})$ ,  $O(h^{2.04})$  and  $O(h^{3.83})$  for linear, quadratic and IRBFN interpolations, respectively. At  $h = 0.31$ , which corresponds to the boundary point density of  $11 \times 4$ , error norms obtained are  $1.27e - 2$ ,  $1.17e - 2$

Boundary points	$3 \times 4$	$4 \times 4$	$5 \times 4$	$6 \times 4$
Linear elements	8	12	16	20
Error norm of the boundary solution				
Linear-BEM	$3.01e - 7$	$3.08e - 7$	$3.72e - 7$	$4.30e - 7$
IRBFN-BEM	$7.22e - 6$	$1.17e - 6$	$4.33e - 7$	$1.60e - 7$
Error norm of the internal solution				
Linear-BEM	$1.86e - 7$	$1.43e - 7$	$1.22e - 7$	$1.07e - 7$
IRBFN-BEM	$3.97e - 6$	$4.07e - 7$	$1.57e - 7$	$5.17e - 8$

**Note:** The selected internal points are (2, 2), (2, 4), (3, 3), (4, 2) and (4, 4). In the first row,  $n \times m$  means  $n$  boundary points per segment and  $m$  segments. The number of boundary elements in each case results in the same total number of boundary points

**Table I.**  
Example 1 – error norms  $N_s$  of the IRBFN-BEM and linear-BEM solutions

and  $2.80e - 5$  for linear, quadratic and IRBFN interpolations, respectively. The internal results are recorded in Table II showing that the IRBFN-BEM achieves a solution accuracy better than the linear/quadratic-BEM results by several orders of magnitude.

4.1.3 Example 3. The problem is to find the temperature field such that

$$\nabla^2 u = 0 \quad \text{inside the square } 0 \leq x_1 \leq \pi, 0 \leq x_2 \leq \pi, \quad (30)$$

$$u(\pi, x_2) = \sin^3(x_2) \quad \text{on the right edge } (0 \leq x_2 \leq \pi), \quad (31)$$

$$u(x_1, x_2) = 0 \quad \text{on the other three sides.} \quad (32)$$

The analytical solution of this problem (Snider, 1999) is

$$u(x_1, x_2) = \frac{3}{4 \sinh(\pi)} \sin(x_2) \sinh(x_1) - \frac{1}{4 \sinh(3\pi)} \sin(3x_2) \sinh(3x_1).$$

The shape of this solution is more complicated than the one in the previous example and provides a good test for the present method. The boundary point

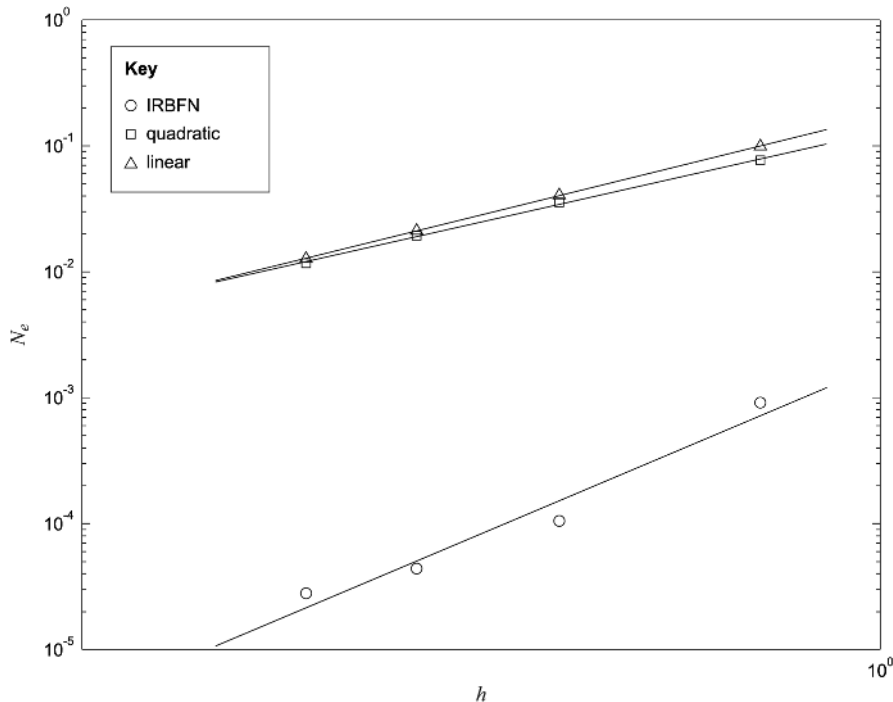


**Figure 4.**  
Example 2 – error norm  $N_e$  of the boundary solution versus boundary point spacing  $h$  obtained by the BEM with different interpolation techniques

**Note:** With the given boundary point densities of  $5 \times 4$ ,  $7 \times 4$ ,  $9 \times 4$  and  $11 \times 4$ , the rate of convergence appears to be  $O(h^{2.24})$ ,  $O(h^{2.04})$  and  $O(h^{3.83})$  for linear, quadratic and IRBFN interpolations, respectively, as depicted by solid lines. The proposed method achieves accuracy and convergence rate superior to the element-based method

densities are chosen to be  $9 \times 4$ ,  $11 \times 4$ ,  $13 \times 4$  and  $15 \times 4$ . The selected internal points are  $(\pi/3, \pi/3)$ ,  $(\pi/3, 2\pi/3)$ ,  $(\pi/2, \pi/2)$ ,  $(2\pi/3, \pi/3)$  and  $(2\pi/3, 2\pi/3)$ . The proposed method also performs much better than the standard BEM and similar remarks as mentioned in Example 2 apply. With  $\beta = 7$ , the error norms of the boundary solution and the internal solution are displayed in Figure 5 and Table III, respectively. The rates of convergence of the boundary solution are of  $O(h^{2.14})$ ,  $O(h^{1.38})$  and  $O(h^{4.78})$  for linear, quadratic and IRBFN interpolations,

**Table II.**  
Example 2 – error norms  $N_e$ s of the internal solution obtained by the BEM with different interpolation techniques

Boundary points	$5 \times 4$	$7 \times 4$	$9 \times 4$	$11 \times 4$
Linear	$2.96e - 2$	$1.25e - 2$	$6.90e - 3$	$4.30e - 3$
Quadratic	$2.80e - 3$	$5.90e - 4$	$1.82e - 4$	$7.66e - 5$
IRBFN	$1.27e - 5$	$4.79e - 7$	$1.49e - 7$	$3.40e - 8$

**Note:** The IRBFN-BEM yields a solution more accurate than the linear/ quadratic-BEM by several orders of magnitude

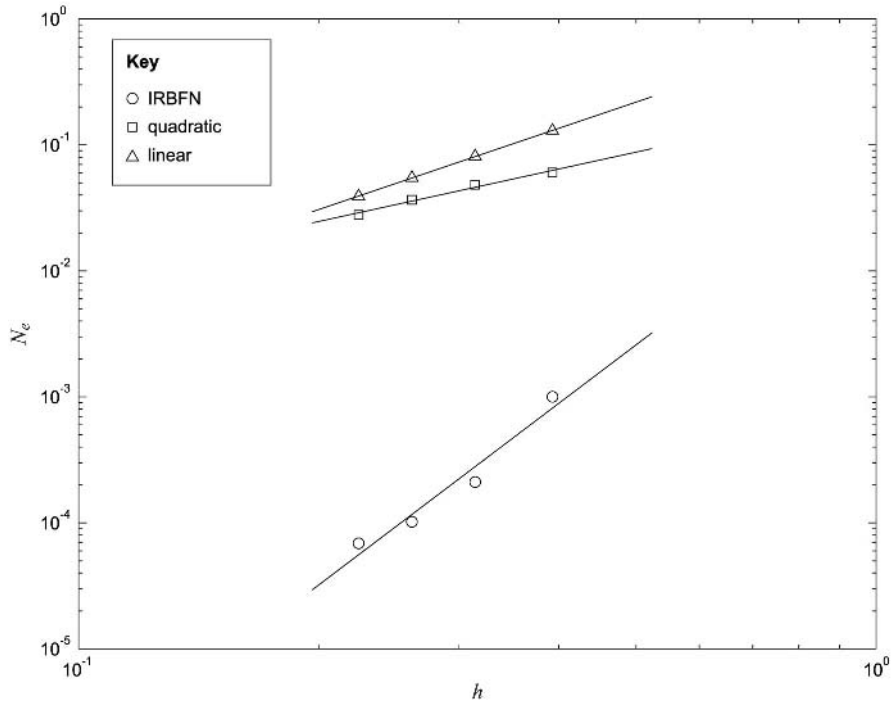


**Figure 5.**  
Example 3 – error norm  $N_e$  of the boundary solution versus boundary point spacing  $h$  obtained from the BEM with different interpolation techniques

**Note:** With the given boundary point densities of  $9 \times 4$ ,  $11 \times 4$ ,  $13 \times 4$  and  $15 \times 4$ , the rate of convergence appears to be  $O(h^{2.14})$ ,  $O(h^{1.38})$  and  $O(h^{4.78})$  for linear, quadratic and IRBFN interpolations, respectively, as depicted by solid lines. The proposed method achieves accuracy and convergence rate superior to the element-based method

respectively. At  $h = 0.07$ , which corresponds to the boundary point density of  $15 \times 4$ , the achieved error norms are  $3.91e - 2$ ,  $2.79e - 2$  and  $6.88e - 5$  for linear, quadratic and IRBFN interpolations, respectively. The accuracy of the internal solution by the present method is also better, by several orders of magnitude, than the ones by linear and quadratic BEMs. Furthermore, the CPU time requirements for the two methods are compared in Table IV. The structures of the MATLAB codes are the same and therefore it is believed that the higher efficiency achieved by the IRBFN-BEM is due to the fact that the number of segments (elements) used in the IRBFN-BEM is significantly less than that used in the standard BEM, resulting in a better vectorised computation for the former (MATLAB's internal vectorisation).

4.2 Boundary geometry with curved and straight segments

NNs are employed to interpolate not only the variables  $u$  and  $q$  by using equations (21) and (22), but also the geometry of the curved segments by using equations (23) and (24). All quantities in the BIs such as  $u$ ,  $q$  and  $d\Gamma$  are represented by IRBFNs necessarily in terms of the curvilinear coordinate (arclength)  $s$ . Special attention is given to the transformation of the quantity  $d\Gamma$  from rectangular to curvilinear coordinates where the use of a Jacobian is required as follows

$$d\Gamma = \left( \left( \frac{\partial x_1}{\partial s} \right)^2 + \left( \frac{\partial x_2}{\partial s} \right)^2 \right)^{1/2} ds, \tag{33}$$

in which the derivatives of  $x_1$  and  $x_2$  on the segment  $\Gamma_j$  can be expressed in terms of the basis function  $H$  (equation (6)) as

Boundary points	$9 \times 4$	$11 \times 4$	$13 \times 4$	$15 \times 4$
Linear	$6.60e - 3$	$4.20e - 3$	$2.90e - 3$	$2.20e - 3$
Quadratic	$3.25e - 4$	$1.74e - 4$	$7.84e - 5$	$4.09e - 5$
IRBFN	$2.79e - 6$	$1.91e - 6$	$7.97e - 7$	$9.64e - 7$

**Note:** The IRBFN-BEM yields a solution more accurate than the linear/quadratic-BEM by several orders of magnitude

**Table III.**  
Example 3 – error norms  $N_{e,s}$  of the internal solution obtained by the BEM with different interpolation techniques

Mesh	Linear-BEM		IRBFN-BEM	
	Boundary solution	Total solution	Boundary solution	Total solution
$9 \times 9$	1.98	4.57	2.07	2.19
$11 \times 11$	3.02	8.39	3.08	3.27
$13 \times 13$	4.29	13.88	4.27	4.63
$15 \times 15$	5.78	21.56	5.70	6.33

**Note:** The code is written in the MATLAB language (version R11.1 by The MathWorks, Inc.), which is run on a 548 MHz Pentium PC. Note that MATLAB language is interpretative

**Table IV.**  
Example 3 – CPU times (s) used to obtain the boundary solution and the total solution by the linear-BEM and IRBFN-BEM

$$\frac{\partial x_{1j}}{\partial s} = \sum_{i=1}^{mj+2} w_{x_{1j}}^{(i)} H_j^{(i)}(s), \tag{34}$$

$$\frac{\partial x_{2j}}{\partial s} = \sum_{i=1}^{mj+2} w_{x_{2j}}^{(i)} H_j^{(i)}(s). \tag{35}$$

Clearly, these derivatives can be calculated straightforwardly, once the interpolation of the function is done after solving equations (23) and (24). For more details covering the calculation of derivative functions by IRBFNs, the reader is referred to Mai-Duy and Tran-Cong (2002). Normally, the orders of IRBFN approximation for the boundary geometry and the variation of  $u$  and  $q$  are chosen to be the same. However, they can be different and are discussed shortly.

4.2.1 *Example 4.* Consider the boundary value problem governed by the Laplace equation

$$\nabla^2 u = 0$$

as shown in Figure 6. The domain of analysis is one quarter of the ellipse and the boundary conditions are

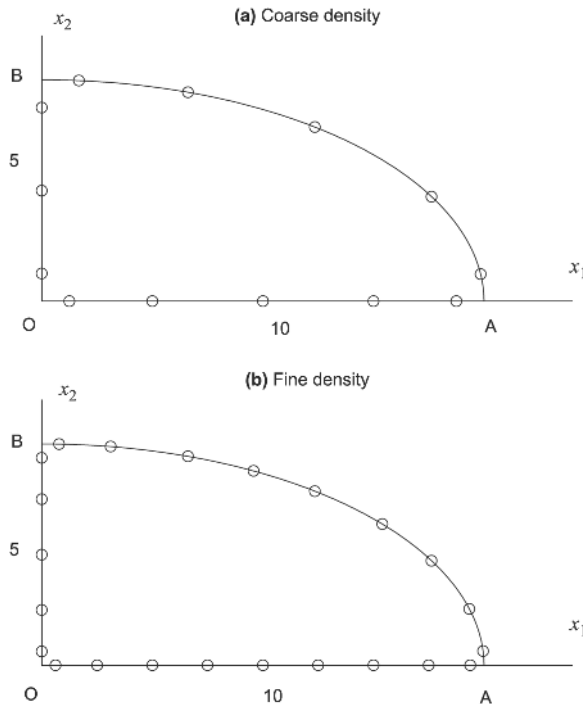


**Figure 6.**  
Example 4 – geometry definition and training points

on OA and BO and

$$u = 0,$$

RBF  
interpolation of  
boundary values

$$\frac{\partial u}{\partial n} = -\frac{a^2 - b^2}{(a^4x_2^2 + b^4x_1^2)^{1/2}}x_1x_2,$$

627

on AB with  $a$  and  $b$  being the half lengths of the major and minor axes, respectively. This problem with  $a = 10$  and  $b = 5$  was solved by quadratic BEM (Brebbia and Dominguez, 1992) using five and ten quadratic elements with two selected internal points (2, 2) and (4, 3.5). For the present method, the boundary is divided into three segments (two straight lines and one curve) and the training points are taken to be the same as the boundary nodes used in the case of the quadratic BEM. Thus, the densities are 5, 5 and 3 on segments OA, AB and BO, respectively, which corresponds to the case of five quadratic elements and densities 9, 9 and 5 corresponding to the case of ten quadratic elements. In order to compare the present results with the results obtained by quadratic BEM (Brebbia and Dominguez, 1992) and the exact solution, some values of the function  $u$  are extracted and the errors obtained by the two methods are displayed in Tables V and VI, which show that the present method yields better accuracy. For example, with four digit scaled fixed point, for the coarse density the range of the error is (0.02-0.2 per cent) and (0.84-2.32 per cent) for IRBFN-BEM and quadratic BEM, respectively, while for the fine density the error range is (0.00-0.02 per cent) and (0.02-0.14 per cent) for IRBFN-BEM and quadratic BEM, respectively.

4.2.2 *Example 5.* The distribution of the function  $u$  in an ellipse with a semi-major axis  $a = 2$  and a semi-minor axis  $b = 1$  is described by

$$\nabla^2 u = -2, \tag{36}$$

subject to the condition  $u = 0$  along the boundary  $\Gamma$ . The exact solution is

$$u(x_1, x_2) = -0.8\left(\frac{x_1^2}{a^2} + \frac{x_2^2}{b^2} - 1\right).$$

$x_1$	$x_2$	Exact	IRBFN-BEM		Quadratic BEM	
		$u$	$u$	Error (per cent)	$u$	Error (per cent)
8.814	2.362	-12.489	-12.514	0.20	-12.779	2.32
6.174	3.933	-14.570	-14.579	0.06	-14.839	1.85
3.304	4.719	-9.356	-9.354	0.02	-9.435	0.84
2.000	2.000	-2.400	-2.404	0.17	-2.431	1.29
4.000	3.500	-8.400	-8.413	0.15	-8.472	0.86

**Note:** Comparison of the error obtained by the present IRBFN-BEM ( $\beta = 7$ ) and the quadratic BEM using the same boundary nodes (five quadratic elements)

**Table V.**  
Example 4 –  
comparison (five  
quadratic elements)

This problem is governed by the Poisson's equation and hence the BEM with PS can be applied here for obtaining the numerical solution. The solution  $u$  can be decomposed into a homogeneous part  $u^H$  and a PS part  $u^P$  as

$$u = u^H + u^P.$$

The PS to equation (36) can be verified to be

$$u^P = -\frac{x_1^2 + x_2^2}{2}$$

while the complementary one satisfies the Laplace's equation  $\nabla^2 u^H = 0$  with the boundary condition  $u^H = -u^P$  on  $\Gamma$ . The latter is to be solved by BEM. Partridge *et al.* (1992) used this approach to solve the problem in which 16 linear boundary elements are employed and the solution obtained was displayed at seven internal points. In the present method, the boundary  $\Gamma$  is divided into two segments as shown in Figure 7. Four data densities, namely  $9 \times 2$ ,  $11 \times 2$ ,  $13 \times 2$  and  $15 \times 2$ , and  $\beta = 8$  are employed to simulate the problem. Error norms of the boundary solution obtained are 0.0105, 0.0037,  $9.4436e - 4$  and  $5.8135e - 4$  for the four densities, respectively, with the convergence rate achieved being  $O(N^{(-5.9289)})$ , where  $N$  is the number of the training boundary points employed (Figure 8). In order to compare with the linear BEM (Partridge *et al.*, 1992), the solution at seven internal points is also computed by the present method and the corresponding error norms obtained are 0.0063, 0.0026,  $8.0387e - 4$  and  $3.4900e - 5$  for the four densities, respectively. Hence with the coarse density of  $9 \times 2$  that corresponds to 16 linear boundary elements, the present method achieves the error norm of 0.0063, while the linear BEM achieves only  $N_e = 0.0109$ . The latter number is calculated by the present authors using the table shown in Partridge *et al.* (1992). Numerical result for the finest density is displayed in Table VII.

4.2.3 *Interpolation for geometry and boundary variables.* In the last two examples, the IRBFN interpolations for the geometry and the variables  $u$  and  $q$

$x_1$	$x_2$	Exact		IRBFN-BEM		Quadratic BEM	
		$u$	$u$	Error (per cent)	$u$	Error (per cent)	
8.814	2.362	-12.489	-12.487	0.02	-12.506	0.14	
6.174	3.933	-14.570	-14.568	0.01	-14.576	0.04	
3.304	4.719	-9.356	-9.355	0.01	-9.363	0.07	
2.000	2.000	-2.400	-2.400	0.00	-2.399	0.04	
4.000	3.500	-8.400	-8.400	0.00	-8.402	0.02	

**Table VI.**  
Example 4 –  
comparison (ten  
quadratic elements)

**Note:** Comparison of the error obtained by the present IRBFN-BEM ( $\beta = 7$ ) and the quadratic BEM using the same boundary nodes (ten quadratic elements)

have the same order, i.e. the training points used are same for both the cases. However, the order of IRBFN interpolation can be chosen differently for the geometry and the variables  $u$  and  $q$  in order to obtain high quality solutions with low cost as possible. The geometry is usually known and hence the

RBF interpolation of boundary values

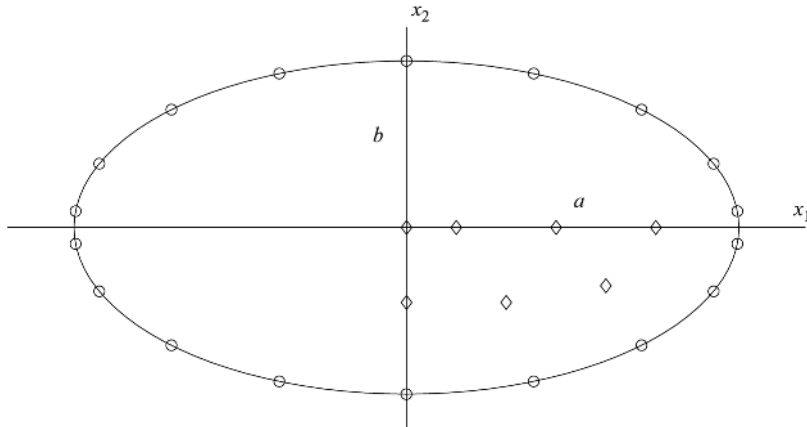


**Figure 7.** Example 5 – geometry definition, boundary training points and internal points. The boundary is divided into two segments  $(-a \leq x_1 \leq a, x_2 \geq 0)$  and  $(-a \leq x_1 \leq a, x_2 \leq 0)$

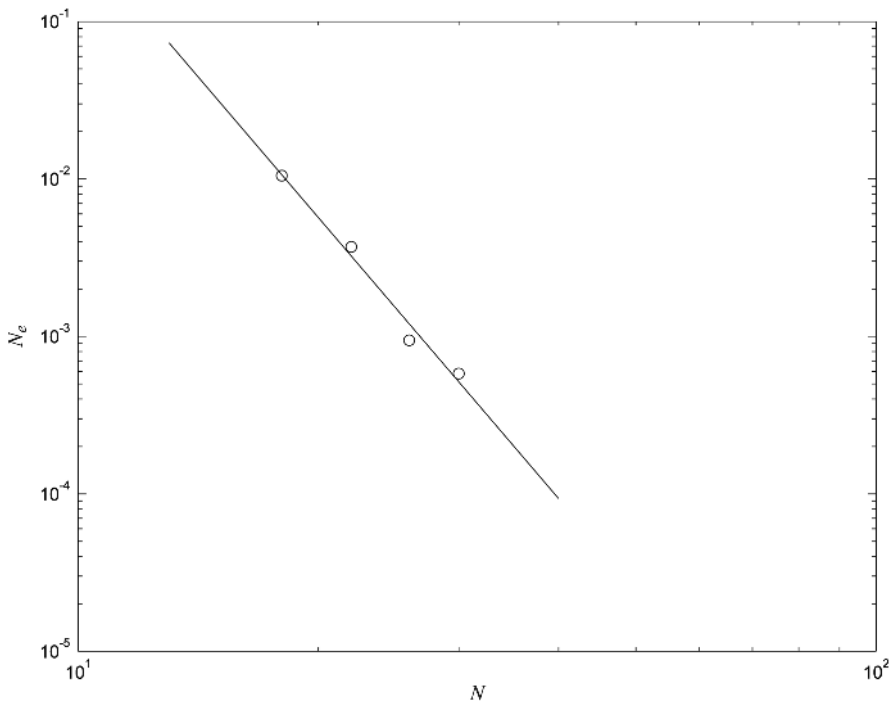


**Figure 8.** Example 5 – error norm  $N_e$  of the boundary solution versus the number of boundary points  $N$  by the present IRBFN-BEM. With the given boundary point densities of  $9 \times 2$ ,  $11 \times 2$ ,  $13 \times 2$  and  $15 \times 2$ , the rate of convergence appears as  $O(N^{-5.9289})$ , where  $N$  is the number of the boundary points employed

number of training points for the geometry interpolation can be estimated. It is emphasised that the size of the final system of equations only depends on the order of IRBFN interpolation for the variables  $u$  and  $q$  and hence in the case of highly curved boundary, it is recommended that the order of IRBFN interpolation can be chosen higher for the geometry than for the variables  $u$  and  $q$ . The problem in the last example is solved again with the increasing number of training points for the geometry interpolation. The density of training points employed is  $9 \times 2$  for the variables  $u$  and  $q$  while they are  $12 \times 2$  and  $14 \times 2$  for the geometry. The solution is improved as shown in Table VIII. For example, the error norm of the boundary solution decreases from 0.0105 for the normal case (the same order) to  $9.5093e - 4$  and  $8.2902e - 4$  for the increasing order of geometry interpolation.

**5. Concluding remarks**

In this paper, the introduction of IRBFN interpolation into the BEM scheme to represent the variables in BIEs for numerical solution of heat transfer problems is implemented and verified successfully. Numerical examples show that the proposed method considerably improves the estimate of the BIs resulting in

**Table VII.**  
Example 5 – the boundary solution obtained by the present IRBFN-BEM using the density of  $15 \times 2$

Coordinates		Exact Gradient $q$	Computed Gradient $q$
$x_1$	$x_2$		
1.997	0.056	-0.804	-0.802
1.950	0.223	-0.857	-0.859
1.802	0.434	-1.001	-1.000
1.564	0.623	-1.177	-1.178
1.247	0.782	-1.347	-1.347
0.868	0.901	-1.483	-1.483
0.445	0.975	-1.570	-1.570
0.000	1.000	-1.600	-1.600

**Note:** Although no symmetry condition was imposed in the numerical model, the results obtained are accurately symmetrical. Owing to symmetry, the displayed results corresponds to only a quarter of the elliptical domain

**Table VIII.**  
Example 5 – error norms obtained by the present method with increasing order of the IRBFN interpolation for the geometry

$N_e$	$9 \times 2$	$12 \times 2$	$14 \times 2$
Boundary solution	0.0105	$9.5093e - 4$	$8.2902e - 4$
Internal solution	0.0063	$1.5961e - 4$	$9.8966e - 5$

**Note:** The densities of IRBFN interpolation are  $9 \times 2$  for the boundary variables and  $9 \times 2$ ,  $12 \times 2$  and  $14 \times 2$  for the geometry

---

better solutions not only in terms of the accuracy but also in terms of the rate of convergence. The CPV integral is written in the non-singular form where the standard Gaussian quadrature can be applied while the weakly singular integrals are evaluated by using the well-known numerical techniques as in the case of the standard BEM. The method can be extended to problems of viscous flows which will be carried out in future work.

## References

- Banerjee, P.K. and Butterfield, R. (1981), *Boundary Element Methods in Engineering Science*, McGraw-Hill, London.
- Brebbia, C.A. and Dominguez, J. (1992), *Boundary Elements: An Introductory Course*, Computational Mechanics Publications, Southampton.
- Brebbia, C.A., Telles, J.C.F. and Wrobel, L.C. (1984), *Boundary Element Techniques: Theory and Applications in Engineering*, Springer-Verlag, Berlin.
- Cybenko, G. (1989), "Approximation by superpositions of sigmoidal functions", *Mathematics of Control Signals and Systems*, Vol. 2, pp. 303-14.
- Girosi, F. and Poggio, T. (1990), "Networks and the best approximation property", *Biological Cybernetics*, Vol. 63, pp. 169-76.
- Haykin, S. (1999), *Neural Networks: A Comprehensive Foundation*, Prentice-Hall, NJ.
- Hwang, W.S., Hung, L.P. and Ko, C.H. (2002), "Non-singular boundary integral formulations for plane interior potential problems", *International Journal for Numerical Methods in Engineering*, Vol. 53 No. 7, pp. 1751-62.
- Kansa, E.J. (1990), "Multiquadrics – a scattered data approximation scheme with applications to computational fluid-dynamics – II. Solutions to parabolic, hyperbolic and elliptic partial differential equations", *Computers and Mathematics with Applications*, Vol. 19 Nos 8/9, pp. 147-61.
- Mai-Duy, N. and Tran-Cong, T. (2001a), "Numerical solution of differential equations using multiquadric radial basis function networks", *Neural Networks*, Vol. 14 No. 2, pp. 185-99.
- Mai-Duy, N. and Tran-Cong, T. (2001b), "Numerical solution of Navier-Stokes equations using multiquadric radial basis function networks", *International Journal for Numerical Methods in Fluids*, Vol. 37, pp. 65-86.
- Mai-Duy, N. and Tran-Cong, T. (2002), "Mesh-free radial basis function network methods with domain decomposition for approximation of functions and numerical solution of Poisson's equations", *Engineering Analysis with Boundary Elements*, Vol. 26 No. 2, pp. 133-56.
- Partridge, P.W., Brebbia, C.A. and Wrobel, L.C. (1992), *The Dual Reciprocity Boundary Element Method*, Computational Mechanics Publications, Southampton.
- Press, W.H., Flannery, B.P., Teukolsky, S.A. and Vetterling, W.T. (1988), *Numerical Recipes in C: The Art of Scientific Computing*, Cambridge University Press, Cambridge.
- Sharan, M., Kansa, E.J. and Gupta, S. (1997), "Application of the multiquadric method for numerical solution of elliptic partial differential equations", *Journal of Applied Science and Computation*, Vol. 84, pp. 275-302.
- Sladek, V. and Sladek, J. (1998), *Singular Integrals in Boundary Element Methods*, Computational Mechanics Publications, Southampton.
- Snider, A.D. (1999), *Partial Differential Equations: Sources and Solutions*, Prentice-Hall, NJ.

---

HF  
13,5

Tanaka, M., Sladek, V. and Sladek, J. (1994), "Regularization techniques applied to boundary element methods", *Applied Mechanics Reviews*, Vol. 47, pp. 457-99.

Telles, J.C.F. (1987), "A self-adaptive co-ordinate transformation for efficient numerical evaluation of general boundary element integrals", *International Journal for Numerical Methods in Engineering*, Vol. 24, pp. 959-73.

**632**

---

Zerroukat, M., Power, H. and Chen, C.S. (1998), "A numerical method for heat transfer problems using collocation and radial basis functions", *International Journal for Numerical Methods in Engineering*, Vol. 42, pp. 1263-78.

Zheng, R., Coleman, C.J. and Phan-Thien, N. (1991), "A boundary element approach for non-homogeneous potential problems", *Computational Mechanics*, Vol. 7, pp. 279-88.



# Dual reciprocity boundary element analysis of transient advection-diffusion

Dual reciprocity

633

Krishna M. Singh

*Department of Engineering, Queen Mary, University of London,  
London, UK*

Masataka Tanaka

*Department of Mechanical Systems Engineering, Shinshu University,  
Nagano, Japan*

Received March 2002  
Revised August 2002  
Accepted January 2003

**Keywords** *Boundary element method, Plates, Approximation concepts*

**Abstract** *This paper presents an application of the dual reciprocity boundary element method (DRBEM) to transient advection-diffusion problems. Radial basis functions and augmented thin plate splines (TPS) have been used as coordinate functions in DRBEM approximation in addition to the ones previously used in the literature. Linear multistep methods have been used for time integration of differential algebraic boundary element system. Numerical results are presented for the standard test problem of advection-diffusion of a sharp front. Use of TPS yields the most accurate results. Further, considerable damping is seen in the results with one step backward difference method, whereas higher order methods produce perceptible numerical dispersion for advection-dominated problems.*

## 1. Introduction

The phenomenon of advection-diffusion is observed in many physical situations involving transport of energy and chemical species. Some of the examples are the transport of pollutants – thermal, chemical or radioactive – in the environment, flow in porous media, impurity redistribution in semiconductors, travelling magnetic field etc. The governing equation for advection-diffusion is usually characterized by a dimensionless parameter, called Peclet number,  $Pe$ , which is defined as

$$Pe = |v| \frac{L}{D}, \quad (1)$$

where  $v$  is the advective velocity,  $L$  is the characteristic length and  $D$  is the diffusivity associated with the transport process. When  $Pe$  is small, diffusion



The first author gratefully acknowledges the financial support provided by the Japan Society for Promotion of Science (JSPS). Partial financial support provided by the Monbusho Grant-in-Aid, and computational and logistic support provided by the CAE Systems Laboratory, Shinshu University are gratefully acknowledged.

International Journal of Numerical  
Methods for Heat & Fluid Flow  
Vol. 13 No. 5, 2003  
pp. 633-646  
© MCB UP Limited  
0961-5539  
DOI 10.1108/09615530310482481

dominates and the advection-diffusion equation is nearly parabolic. On the other hand, if  $Pe$  is large, then advection dominates and the governing equation becomes hyperbolic. Accurate numerical solution of the advection-diffusion equation becomes increasingly difficult as the  $Pe$  increases due to the onset of spurious oscillations or excessive numerical damping, if standard finite difference or finite element formulations are used. To deal with such advection dominated problems, numerous innovative algorithms have been suggested based on the local analytical solution of the advection-diffusion equation in the finite difference and finite element literature (Carey and Jiang, 1988; Celia *et al.*, 1989; Chen and Chen, 1984; Demkowicz and Oden, 1986; Ding and Liu, 1989; Donea *et al.*, 1984; Hughes and Brooks, 1982; Li *et al.*, 1992; Park and Liggett, 1990; Raithby and Torrance, 1974; Spalding, 1972; Westerink and Shea, 1989; Yu and Heinrich, 1986).

The reduction in the effective dimensionality of a problem offered by the boundary element method has attracted its application to the advection-diffusion problem as well, and it has been observed that the BEM solutions seem to be *relatively free* from spurious oscillations or excessive numerical damping (vis-à-vis finite element or finite difference solutions). The basic reason being the correct amount of upwinding provided by the fundamental solution in the BEM. Various formulations have been proposed for the transient advection-diffusion problems. Boundary element formulations based on time-dependent fundamental solutions have been suggested by Brebbia and Skerget (1984) and Ikeuchi and Onishi (1983). Ikeuchi and Onishi (1983) derived time-dependent fundamental solution to the advection-diffusion equation in  $\mathbf{R}^n$ , and proved that the boundary element solution is stable for large diffusion number and Courant number. This formulation is used by Ikeuchi and Tanaka (1985) for the solution of magnetic field problems. Tanaka *et al.* (1987) used the same formulation with mixed boundary elements and studied the dependence of the relative error on space and time discretization. On the other hand, Brebbia and Skerget (1984) used the fundamental solution of diffusion equation and treated the convective terms as a pseudo source term. Okamoto (1989, 1991) used Laplace transforms in conjunction with combined boundary and finite element methods for the solution of transient advection-diffusion problem on an unbounded domain.

Another class of boundary element formulations use the fundamental solution of a related steady-state operator and treat the time derivative and any other remaining terms as a pseudo source term. These formulations result in a system of differential-algebraic equations in time which can be solved using a suitable time integration algorithm. Taigbenu and Liggett (1986) proposed one such formulation. They use the fundamental solution of Laplace equation and treat the time derivative and convective terms as source terms which are incorporated in the boundary element formulation by domain discretization. Single step time-differencing scheme is used for time marching and solutions

are presented for a wide range of  $Pe$  – from very low (diffusion-dominated problems) to infinite (pure advection problems). Aral and Tang (1989) also used the fundamental solution of the Laplace equation, but made use of a secondary reduction process, called SR-BEM (Aral and Tang, 1988), to arrive at a boundary-only formulation. They present the results of the advection-diffusion problems with or without first order chemical reaction for low to moderate  $Pe$ . Two other formulations in this category are based on the dual reciprocity boundary element method (DRBEM) (Partridge *et al.*, 1991). The first one employs the fundamental solution to Laplace equation and applies the dual reciprocity treatment to time derivative and convective terms. The second one uses the fundamental solution to the steady-state advection-diffusion equation and transforms the domain integral arising from the time derivative term using a set of coordinate functions and particular solutions which satisfy the associated nonhomogeneous steady-state advection-diffusion equation (DeFigueiredo and Wrobel, 1990). In both these formulations, the resulting differential-algebraic equation is solved using one step  $\theta$ -method. Partridge *et al.* (1991) used  $\theta = 0.5$  in computations with first formulation and  $\theta = 1.0$ , with the second one, and observed that the accuracy of both the dual reciprocity formulations is very good for all problems considered, with no oscillations and only a minor damping of the wave front. They further indicate that the second formulation is more accurate than the first one. However, all the DRBEM applications have considered only the problems involving low values of  $Pe$ .

In this work, we concentrate on the application of the DRBEM based on the fundamental solution to the steady-state advection-diffusion equation to obtain a clear picture of its performance for advection-diffusion problems involving moderate to high  $Pe$ , since advection-dominated problems have received little attention in DRBEM literature. Further, only a simple set of radial basis functions has been previously used in this formulation. We consider two other sets of coordinate functions – complete radial basis functions and augmented thin plate splines (TPS), and analyse their performance in conjunction with higher order time integration algorithms for advection-dominated problems. We start with a brief review of the governing equations and the boundary element formulation, give the description of the coordinate functions and time integration schemes and present numerical results for a standard test problem of advection-diffusion of a sharp front.

## 2. Advection-diffusion equation

Let us consider a homogeneous isotropic region  $\Omega \subset \mathbf{R}^2$  bounded by a piece-wise smooth boundary  $\Gamma$ . Let  $\phi$  be the transported quantity, and  $(0, T] \subset \mathbf{R}$  be the time interval of interest. Let  $x$  represent the spatial coordinate, and  $t$  the time. The transport of  $\phi$  in the presence of a first order reaction is governed by the equation

$$\left(\frac{\partial}{\partial t} + v \cdot \nabla + k - D\nabla^2\right)\phi(x, t) = 0 \quad \text{in } \Omega \times (0, T], \quad (2)$$

with the initial condition

$$\phi(x, 0) = \phi_0(x) \quad \text{on } \bar{\Omega}, \quad (3)$$

and the boundary conditions

$$\phi(x, t) = \bar{\phi}(x, t) \quad \text{on } \Gamma_\phi \times (0, T], \quad (4)$$

$$q(x, t) = \bar{q}(x, t) \quad \text{on } \Gamma_q \times (0, T], \quad (5)$$

$$q(x, t) = h(x, t)\{\phi_r(x, t) - \phi(x, t)\} \quad \text{on } \Gamma_r \times (0, T], \quad (6)$$

where  $v$  denotes the velocity field,  $D$  is the diffusivity and  $k$  is the reaction rate.  $\phi_0$ ,  $\bar{\phi}$ ,  $\bar{q}$ ,  $\phi_r$  and  $h$  are known functions and  $q = \partial\phi/\partial n$ ,  $\mathbf{n}$  being the unit outward normal. Further,  $\Gamma_\phi$ ,  $\Gamma_q$  and  $\Gamma_r$  denote the disjoint segments (some of which may be empty) of the boundary such that  $\bar{\Gamma}_\phi \cup \bar{\Gamma}_q \cup \bar{\Gamma}_r = \Gamma$ . In this work, we assume that the advective velocity  $v$  and diffusivity  $D$  remain constant.

### 3. Boundary element formulation

This section presents a brief review of the dual reciprocity boundary element formulation for transient advection-diffusion based on the fundamental solution of the steady-state advection-diffusion equation. Further details are given in DeFigueiredo and Wrobel (1990) and Partridge *et al.* (1991).

To transform the advection-diffusion equation (2) into an equivalent boundary integral equation, we start with the weighted residual statement

$$\int_{\Omega} \left(\frac{\partial \phi}{\partial t} + v \cdot \nabla \phi + k\phi - D\nabla^2 \phi\right) \phi^* \, d\Omega = 0, \quad (7)$$

where  $\phi^*$  is the fundamental solution of the steady-state advection-diffusion equation, i.e. the solution of

$$D\nabla^2 \phi^* + v \cdot \nabla \phi^* - k\phi^* + \delta(\xi, x) = 0. \quad (8)$$

In the preceding equation,  $\delta$  is the Dirac delta function, and  $\xi$  and  $x$  denote the source and field points, respectively. For two-dimensional problems,  $\phi^*$  is given by (Partridge *et al.*, 1991)

$$\phi^* = \frac{1}{2\pi D} \exp\left(-\frac{v \cdot r}{2D}\right) K_0(\mu r), \quad (9)$$

where

$$\mu = \left[ \left( \frac{|v|}{2D} \right)^2 + \frac{k}{D} \right]^{1/2}, \quad (10)$$

and  $K_0$  is the Bessel function of the second kind of order zero. Application of Green's second identity and relation (8) to the statement (7) yields

$$c_i \phi_i + D \int_{\Gamma} \left[ \left( q^* + \frac{v_n}{D} \phi^* \right) \phi - \phi^* q \right] d\Gamma = - \int_{\Omega} \frac{\partial \phi}{\partial t} \phi^* d\Omega, \quad (11)$$

where the index  $i$  stands for the source point  $\xi$ ,  $q^* = \partial \phi^* / \partial n$ ,  $v_n = v \cdot \mathbf{n}$  and

$$c_i = \int_{\Omega} \delta(\xi, x) d\Omega.$$

To transform the domain integral in equation (11), the time derivative is approximated by

$$\dot{\phi} = \sum_{j=1}^{NP} f^j(x) \alpha^j(t), \quad (12)$$

where the dot  $\dot{\phi}$  on denotes the temporal derivative,  $\alpha^j$  are unknown functions of time and  $f^j$  are known coordinate functions. Further, it is assumed that for each function  $f^j$ , there exists a function  $\psi^j$  which is a particular integral of the equation

$$D \nabla^2 \psi - v \cdot \nabla \psi - k \psi = f. \quad (13)$$

Introducing approximation (12) into equation (11) and applying integration by parts, we obtain the following boundary integral equation:

$$\begin{aligned} c_i \phi_i + D \int_{\Gamma} \left[ \left( q^* + \frac{v_n}{D} \phi^* \right) \phi - \phi^* q \right] d\Gamma \\ = \sum_{j=1}^{NP} \alpha^j \left\{ c_i \psi_i^j + D \int_{\Gamma} \left[ \left( q^* + \frac{v_n}{D} \phi^* \right) \psi^j - \phi^* \eta^j \right] d\Gamma \right\}, \end{aligned} \quad (14)$$

where  $\eta^j = \partial \psi^j / \partial n$ .

Application of the standard boundary element discretization procedure and approximation of  $\phi$ ,  $q$ ,  $\psi$ , and  $\eta$  by the same set of interpolation functions within each boundary element followed by the collocation of the discretized boundary integral equation at all the freedom nodes (boundary plus internal) results in the system of equations

$$\mathbf{H}\boldsymbol{\phi} - \mathbf{G}\mathbf{q} = (\mathbf{H}\boldsymbol{\Psi} - \mathbf{G}\mathbf{E})\boldsymbol{\alpha}, \quad (15)$$

where  $\mathbf{H}$  and  $\mathbf{G}$  are the global matrices of the boundary integrals with kernels  $(q^* + v_n \phi^*/D)$  and  $\phi^*$ , respectively;  $\mathbf{\Psi}$  and  $\mathbf{E}$  are the coordinate function matrices of functions  $\psi$  and  $\eta$ , respectively; and  $\mathbf{\alpha}$ ,  $\mathbf{\phi}$  and  $\mathbf{q}$  denote global nodal vectors of respective functions. Equation (12) can be used to eliminate  $\mathbf{\alpha}$  from the preceding equation and thus, obtain the differential algebraic system

$$\mathbf{C}\mathbf{\phi} + \mathbf{H}\mathbf{\phi} - \mathbf{G}\mathbf{q} = 0, \tag{16}$$

where  $\mathbf{C} = (\mathbf{G}\mathbf{E} - \mathbf{H}\mathbf{\Psi})\mathbf{F}^{-1}$ ,  $\mathbf{F}$  being the coordinate function matrix of the functions  $f^j$ .

#### 4. Coordinate functions

Various sets of coordinate functions have been used in the dual reciprocity method for different class of problems. These include radial basis functions, TPS, multiquadrics etc. (Goldberg *et al.*, 1996, 1998). However, in the case of the dual reciprocity formulation for the advection-diffusion problems based on the fundamental solution of the steady-state advection-diffusion equation, the situation is quite different, probably due to the difficulty in obtaining closed form particular solutions to equation (13) for a given choice of  $f^j$ . Only the following set of coordinate functions has been used so far (DeFigueiredo and Wrobel, 1990):

$$\psi = r^3, \quad \eta = 3r \mathbf{r} \cdot \mathbf{n}, \quad f = 9Dr - 3r \mathbf{r} \cdot v - kr^3. \tag{17}$$

To obtain the preceding set, DeFigueiredo and Wrobel (1990) choose function  $\psi$  and obtained  $\eta$  and  $f$  by substituting directly into equation (13). This set would be referred to as RBF1 hereafter. This choice of the particular solution  $\psi$  essentially corresponds to the choice of  $f = 9r$  for the Poisson's equation. We can follow the same approach to obtain the other sets of coordinate functions. We consider two more alternative sets corresponding to  $f = 1 + r$  and augmented TPS for the Poisson's equation, both of which are known to possess better interpolation properties (Goldberg *et al.*, 1998), and thus are likely to yield more accurate results in the present context as well. If we choose  $\psi = r^2/4 + r^3/9$ , corresponding to the choice of  $f = 1 + r$  for Poisson's equation, we can obtain the following set (which would be referred to as RBF2):

$$\begin{aligned} \psi &= r^2/4 + r^3/9, \\ \eta &= (1/2 + r/3)\mathbf{r} \cdot \mathbf{n}, \\ f &= D(1 + r) - (1/2 + r/3)\mathbf{r} \cdot v - k(9r^2 + 4r^3)/36. \end{aligned} \tag{18}$$

Further, if we choose  $\psi$  corresponding to augmented TPS for the Poisson's equation, we obtain the following set:

$$\psi = r^4(2 \log r - 1)/32 + r^2/4 + r^3/9,$$

$$\eta = (12r^2 \log r - 3r^2 + 16r + 24) \mathbf{r} \cdot \mathbf{n}/48, \quad (19)$$

$$f = D(1 + r + r^2 \log r) - (12r^2 \log r - 3r^2 + 16r + 24) \mathbf{r} \cdot \mathbf{v}/48 - k\psi.$$

## 5. Temporal discretization

The differential algebraic system (16) has a form similar to the one obtained using the finite element method and hence, can be solved by any standard time integration scheme by incorporating suitable modifications to account for its *mixed-nature*. Based on our previous experience (Singh and Kalra, 1996; Singh and Tanaka, 1998), we opt for one and multistep  $\theta$ -methods of SS $p$ 1 family (Wood, 1990) in this work. Further details on the temporal discretization aspects are available in Singh and Kalra (1996) and Singh and Tanaka (1998).

The general form of a  $p$ -step algorithm of SS $p$ 1 family (Zienkiewicz *et al.*, 1984) for the differential-algebraic boundary element system (16) can be expressed as

$$\sum_{j=0}^p \{(\gamma_j \mathbf{C} + \beta_j \Delta t \mathbf{H}) \phi_{\alpha_j} - \beta_j \Delta t \mathbf{G} \mathbf{q}_{\alpha_j}\} = 0, \quad (20)$$

where  $\alpha_j = n + j + 1 - p$ , and  $\gamma_j, \beta_j$  are scalar coefficients which can be expressed as functions of  $p$   $\theta$ -parameters (Wood, 1990). Table I lists some schemes of this family and related parameters. The choice of the schemes has been made keeping in view the stringent stability requirements of a differential algebraic system. Of these algorithms, one step backward difference scheme is the most stable, but the least accurate. The Crank-Nicolson scheme is supposed to be the most accurate amongst the linear multistep methods, but is only marginally stable and prone to oscillations. Two and three step backward difference methods are likely to provide a compromise on accuracy and algorithmic damping.

Algorithm	Abbreviations	Parameters
Crank-Nicolson method	SS1C	$\theta = 1/2$
One step backward difference	SS1B	$\theta = 1$
Two step backward difference	SS2B	$\theta_1 = 1.5, \theta_2 = 2$
Three step backward difference	SS3B	$\theta_1 = 2, \theta_2 = 11/3, \theta_3 = 6$

**Table I.**  
Time integration algorithms from SS $p$ 1 family for advection-diffusion problem

Let us note that the multistep methods require additional starting values. Use of a higher order single step scheme such as the Runge-Kutta method is generally recommended in the literature for the generation of these additional initial conditions. However, numerical experiments by Singh and Kalra (1996) show that the higher order one step schemes are prone to numerical oscillations for differential-algebraic systems. Hence, we opt for the one step backward difference method with a reduced time step to generate additional starting values.

### 6. Error indicators

To measure the quality of the approximate solution, we need to utilize some appropriate norms. In the context of the boundary element analysis, the boundary  $L_2$  norm is usually preferred, as it can be easily evaluated from the boundary solution alone in contrast to the energy norm which requires solutions to be known at internal points as well (Rencis and Jong, 1989).

The absolute error in the approximate solution of function  $v$  is defined as

$$e_v(x, t) = v(x, t) - v_a(x, t), \quad (21)$$

where  $v(x, t)$  denotes the exact value and  $v_a(x, t)$  is the approximate value obtained from the boundary element analysis. The  $L_2$  global error norm is defined by

$$\|e_v\|_2^2 = \int_{\Gamma} e_v^2 d\Gamma = \sum_{i=1}^{N_e} \int_{\Gamma_i} e_v^2 d\Gamma, \quad (22)$$

where  $N_e$  is the total number of boundary elements. To obtain a more transparent measure of solution error, exact relative  $L_2$  error (in per cent) can be defined as (Rencis and Jong, 1989)

$$\eta_v = \frac{\|e_v\|_2}{\|v\|_2} \times 100, \quad (23)$$

in which

$$\|v\|_2^2 = \int_{\Gamma} v^2 d\Gamma.$$

For the computation of  $L_2$ -norms, we have used Gaussian quadrature with 24 integration points.

### 7. Numerical results

Let us consider the standard test problem of advection-diffusion of a sharp front along a line in uniform flow with the initial condition

$$\phi(x_1, 0) = 0 \quad x_1 \in [0, \infty), \quad (24) \quad \text{Dual reciprocity}$$

and the boundary conditions

$$\phi(0, t) = 1, \quad \phi(\infty, t) = 0. \quad (25)$$

With uniform advective velocity  $u$ , and absence of external or internal sources and reaction term, the exact solution of this problem is given by

$$\phi(x_1, t) = \frac{1}{2} \left[ \operatorname{erfc}(z_1) + \exp\left(\frac{ux_1}{D}\right) \cdot \operatorname{erfc}(z_2) \right], \quad (26)$$

where  $z_1 = (x_1 - ut)/\sqrt{4Dt}$  and  $z_2 = (x_1 + ut)/\sqrt{4Dt}$ . This problem is modelled as a two-dimensional problem over the rectangular domain  $\Omega$  defined as

$$\Omega = \{(x_1, x_2) : x_1 \in (0, 1), x_2 \in (0, 0.1)\}, \quad (27)$$

with the zero initial condition. Boundary conditions are:  $\phi(x, t) = 1$  on the boundary  $x_1 = 0$ ;  $q(x, t) = 0$  along upper ( $x_2 = 0.1$ ) and lower boundary ( $x_2 = 0$ ); and  $\phi(x, t) = 0$  on the boundary  $x_1 = 1$ . The last boundary condition represents an approximation of the boundary condition  $\phi(\infty, t) = 0$ .

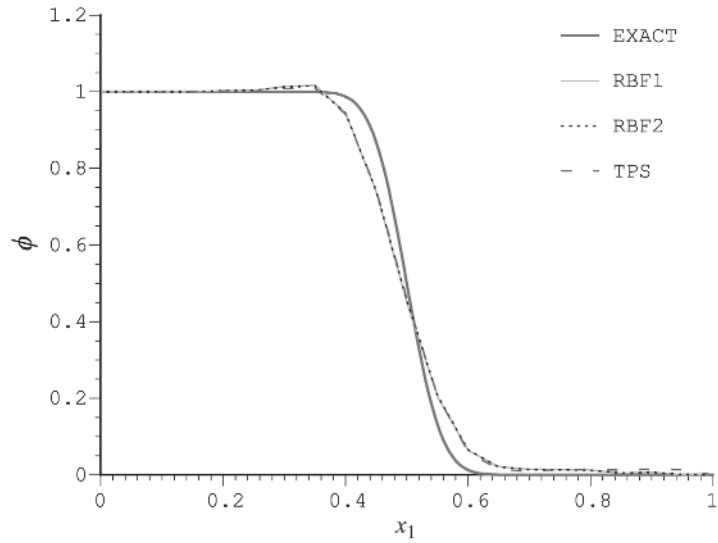
Equal linear elements ( $\Delta\Gamma = 0.05$ ) have been used for the discretisation of the boundary  $\Gamma$ , with partially discontinuous elements at the corners. We take  $u = 1.0$ , and thus with the unit value of the characteristic length  $L$ ,  $Pe = 1/D$ . We present results with two values of  $D$  which correspond to  $Pe = 500$ , and 1,000, respectively. These two cases represent moderate to heavily advection-dominated transport process.

We summarize the errors in the numerical solutions for both the cases for different sets of the coordinate functions in Table II. It can be observed that for both the problems, the higher order multistep methods produce very accurate results, and the three step backward difference scheme is the most accurate. Further, choice of augmented TPS as coordinate functions yields the most accurate results, whereas the previously used choice, RBF1, is the least accurate.

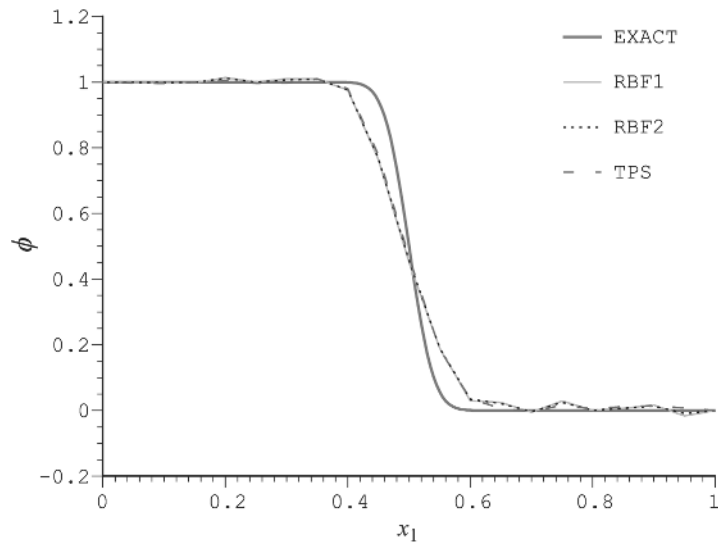
Figures 1 and 2 present the profile of the sharp front at  $t = 0.5$  with SS1B and SS3B, respectively. For both the cases, considerable damping of the front is observed with the one step backward difference method, whereas perceptible

Scheme	Relative $L_2$ error (per cent) with $\Delta t=0.005$					
	Pe = 500			Pe = 1,000		
	RBF1	RBF2	TPS	RBF1	RBF2	TPS
SS1B	6.11	6.07	5.96	8.15	8.06	7.72
SS1C	4.29	4.07	3.81	6.08	5.75	5.18
SS2B	3.88	3.68	3.41	5.81	5.50	4.97
SS3B	3.60	3.41	3.18	5.50	5.18	4.67

**Table II.**  
Errors in the boundary element solution of sharp front problem for Pe = 500 and 1,000 ( $t = 0.5$ )



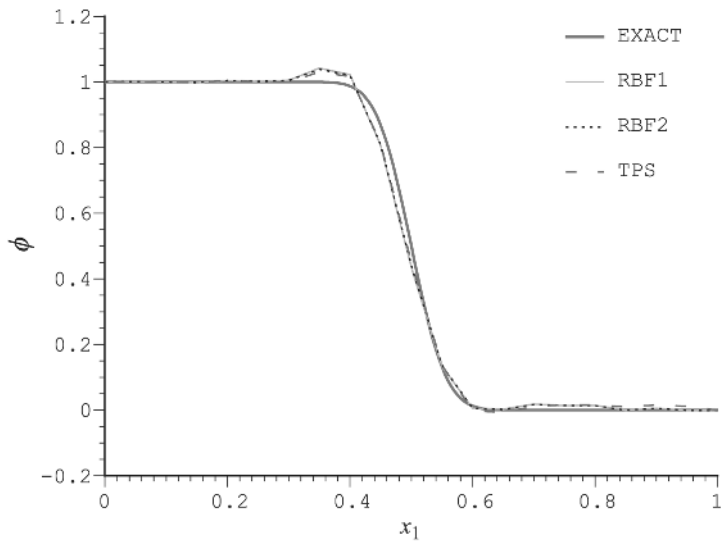
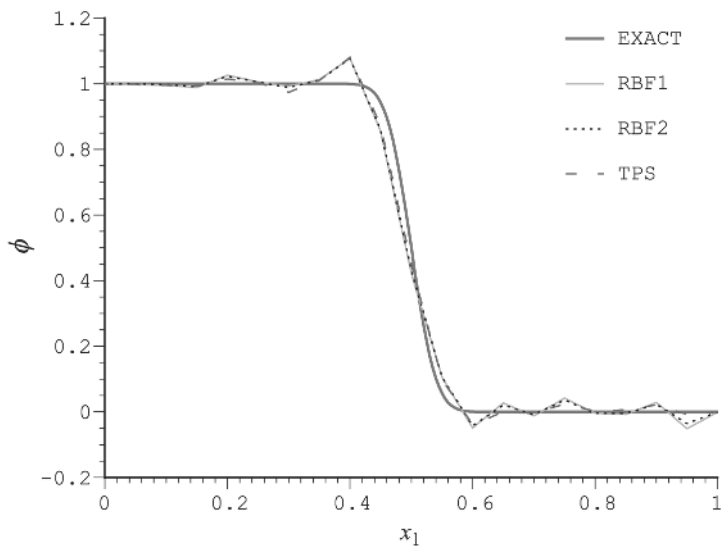
(a)  $Pe = 500$



(b)  $Pe = 1,000$

**Figure 1.**  
Profile of the sharp front  
at  $t = 0.5$  with SS1B and  
different coordinate  
functions. (a)  $Pe = 500$   
and (b)  $Pe = 1,000$   
( $\Delta t = 0.005$ )

---

(a)  $Pe = 500$ (b)  $Pe = 1,000$ 

**Figure 2.** Profile of the sharp front at  $t = 0.5$  with SS3B and different coordinate functions ( $\Delta t = 0.005$ )

numerical dispersion is present in the solution with SS3B (results with other two higher order schemes are very similar).

### 8. Concluding remarks

We have presented an application DRBEM to the transient advection-diffusion problems. In addition to the previously used set of coordinate functions of radial basis type, two more sets of coordinate functions – the radial basis and TPS type – have been evaluated. Of these, the use of the augmented TPS yields the most accurate results. Linear multistep methods have been used for time integration of the differential algebraic boundary element system. Of these, one step backward difference method produces considerable damping of the wave front. The higher order schemes yield good overall accuracy, although some numerical dispersion is present in the solution for the advection-dominated problems.

### References

- Aral, M.M. and Tang, Y. (1988), "A boundary only procedure for time-dependent diffusion equations", *Applied Mathematical Modelling*, Vol. 12, pp. 610-18.
- Aral, M.M. and Tang, Y. (1989), "A boundary-only procedure for transient transport problems with or without first-order chemical reaction", *Applied Mathematical Modelling*, Vol. 13, pp. 130-7.
- Brebbia, C.A. and Skerget, P. (1984), "Diffusion-convection problems using boundary elements", in Laible, J.P., Brebbia, C.A., Gray, W. and Pinder, G. (Eds), *Finite Elements in Water Resources V*, Springer-Verlag, Berlin, pp. 747-68.
- Carey, G.F. and Jiang, B.N. (1988), "Least-squares finite elements for first-order hyperbolic systems", *International Journal for Numerical Methods in Engineering*, Vol. 26, pp. 81-93.
- Celia, M.A., Herrera, I., Bouloutas, E.T. and Kindred, J.S. (1989), "A new numerical approach for the advective-diffusive transport equation", *Numerical Methods for Partial Differential Equations*, Vol. 5, pp. 203-26.
- Chen, C.J. and Chen, H.C. (1984), "Finite-analytic numerical method for unsteady two-dimensional Navier-Stokes equations", *Journal of Computational Physics*, Vol. 53, pp. 209-26.
- DeFigueiredo, D.B. and Wrobel, L.C. (1990), "A boundary element analysis of transient convection-diffusion problems", in Brebbia, C.A., Tanaka, M. and Honma, T. (Eds), *Boundary Elements XII*, Vol. 1, Computational Mechanics Publications, Southampton and Springer-Verlag, Berlin.
- Demkowicz, L. and Oden, J.T. (1986), "An adaptive characteristic Petrov-Galerkin finite element method for convection-dominated linear and nonlinear parabolic problems in one space variable", *Journal of Computational Physics*, Vol. 67, pp. 188-213.
- Ding, D. and Liu, P-F. (1989), "An operator-splitting algorithm for two-dimensional convection-dispersion-reaction problems", *International Journal for Numerical Methods in Engineering*, Vol. 28, pp. 1023-40.
- Donea, J., Giuliani, S., Laval, H. and Quartapelle, L. (1984), "Time-accurate solution of advection-diffusion problems by finite elements", *Computer Methods in Applied Mechanics and Engineering*, Vol. 45, pp. 123-45.

- Goldberg, M.A., Chen, C.S. and Karur, S.R. (1996), "Improved multiquadric approximation for partial differential equations", *Engineering Analysis with Boundary Elements*, Vol. 18, pp. 9-17.
- Goldberg, M.A., Chen, C.S., Bowman, H. and Power, H. (1998), "Some comments on the use of radial basis functions in the dual reciprocity method", *Computational Mechanics*, Vol. 21, pp. 141-8.
- Hughes, T.J.R. and Brooks, A. (1982), "A theoretical framework for Petrov-Galerkin methods with discontinuous weighting functions: application to the streamline-upwind procedure", in Gallagher, R.H., Norrie, D.H., Oden, J.T. and Zienkiewicz, O.C. (Eds), *Finite Elements in Fluids*, Vol. 4, Wiley, London, pp. 47-65.
- Ikeuchi, M. and Onishi, K. (1983), "Boundary elements in transient convective diffusive problems", in Brebbia, C.A., Futagami, T. and Tanaka, M. (Eds), *Boundary Elements V*, Springer-Verlag, Berlin, pp. 275-82.
- Ikeuchi, M. and Tanaka, M. (1985), "Boundary elements in travelling magnetic field problems", in Brebbia, C.A. and Maier, G. (Eds), *Boundary Elements VII*, Springer-Verlag, Berlin.
- Li, S-G., Ruan, F. and McLaughlin, D. (1992), "A space-time accurate method for solving solute transport problems", *Water Resources Research*, Vol. 28 No. 9, pp. 2297-306.
- Okamoto, N. (1989), "Unsteady numerical analysis of convective diffusion with chemical reaction by combined finite and boundary element methods", in Chung, T.J. and Karr, G.R. (Eds), *Finite Element Analysis in Fluids*, UAH Press, University of Alabama, Huntsville, USA, pp. 265-70.
- Okamoto, N. (1991), "Transient analysis by coupling method of finite and boundary elements using Laplace transform", *JASCOME: 8th Symposium on BEMs*, pp. 91-6.
- Park, N-S. and Liggett, J.A. (1990), "Taylor-least-squares finite element for two-dimensional advection-dominated unsteady advection-diffusion problems", *International Journal for Numerical Methods in Fluids*, Vol. 11, pp. 21-38.
- Partridge, P.W., Brebbia, C.A. and Wrobel, L.C. (1991), *The Dual Reciprocity Boundary Element Method*, Computational Mechanics Publications, Southampton and Elsevier Applied Science, London.
- Raithby, G.D. and Torrance, K.E. (1974), "Upstream-weighted differencing schemes and their application to elliptic problems involving fluid flow", *Computers and Fluids*, Vol. 2, pp. 191-206.
- Rencis, J.J. and Jong, K-Y. (1989), "Error estimation for boundary element analysis", *ASCE Journal of Engineering Mechanics*, Vol. 115 No. 9, pp. 1993-2010.
- Singh, K.M. and Kalra, M.S. (1996), "Time integration in the dual reciprocity boundary element analysis of transient diffusion", *Engineering Analysis with Boundary Elements*, Vol. 18, pp. 73-102.
- Singh, K.M. and Tanaka, M. (1998), "Dual reciprocity BEM for advection-diffusion problems: temporal discretization aspects", *Proceedings of the 8th BEM Technology Conference (BTEC-98)*, JASCOME, Tokyo, Japan, pp. 79-84.
- Spalding, D.B. (1972), "A novel finite difference formulation for differential expressions involving both first and second derivatives", *International Journal for Numerical Methods in Engineering*, Vol. 4, pp. 551-9.
- Taigbenu, A. and Liggett, J.A. (1986), "An integral solution for the diffusion-convection equation", *Water Resources Research*, Vol. 22 No. 8, pp. 1237-46.

---

HF  
13,5

Tanaka, Y., Honma, T. and Kaji, I. (1987), "Transient solution of a three dimensional diffusion equation using mixed boundary elements", in Cruse, T.A. (Ed.), *Advanced Boundary Element Methods*, Springer-Verlag, Berlin.

Westerink, J.J. and Shea, D. (1989), "Consistent higher degree Petrov-Galerkin methods for solution of the transient convection-diffusion equation", *International Journal for Numerical Methods in Engineering*, Vol. 29, pp. 1077-101.

646

Wood, W.L. (1990), *Practical Time-stepping Schemes*, Clarendon Press, Oxford.

---

Yu, C-C. and Heinrich, J.C. (1986), "Petrov-Galerkin methods for the time-dependent convective transport equation", *International Journal for Numerical Methods in Engineering*, Vol. 23, pp. 883-901.

Zienkiewicz, O.C., Wood, W.L., Hine, N.W. and Taylor, R.L. (1984), "A unified set of single step algorithms. Part 1: general formulation and applications", *International Journal for Numerical Methods in Engineering*, Vol. 20, pp. 1529-52.

## Awards for Excellence

**C. Nonino**

and

**G. Comini**

*Dipartimento di Energetica e Macchine, Università degli Studi di Udine, Udine, Italy*

are the recipients of the Journal's Outstanding Paper Award for Excellence for their paper

### **“Convective heat transfer in ribbed square channels”**

which appeared in *International Journal of Numerical Methods for Heat & Fluid Flow*, Vol. 12 No. 5, 2002

**Carlo Nonino** graduated in Chemical Engineering from the University of Trieste in 1980 and joined the University of Udine in 1981. In 2000, he was appointed as the Professor of Heat Transfer and Applied Thermodynamics at the University of Udine, and in 2001 he became Head of the Department of Energetics and Machines at the same University.

Professor Nonino has authored/co-authored a book on finite elements in heat transfer, one book chapter and over 60 research articles in various refereed journals and proceedings of international conferences. He is also a member of the editorial advisory board of the *International Journal of Numerical Methods for Heat & Fluid Flow*. He is currently active in the field of numerical simulation of forced convection flows in compact heat exchangers and micro-channels. His expertise also includes modeling of liquid-solid phase change and development of finite element codes for the numerical solution of conduction and convection problems.

**Gianni Comini** is the Professor of Heat Transfer and Applied Thermodynamics at the Engineering Faculty of the University of Udine. With the cooperation of Professors Del Giudice and Nonino, he has established in Udine a well known research group, very active in the development of thermal applications of the FEM. Currently, he is interested in FEM applications to the design of convection enhancing devices.

Professor Comini has authored/co-authored a book on finite elements in heat transfer, seven textbooks used in Italian Universities, several chapters in numerical heat transfer books, and over 100 research articles in various refereed journals and proceedings. His editorial activities include the membership of the editorial board of the *International Journal of Numerical Methods in Engineering*, and the editorial advisory boards of the *International Journal of Numerical Methods for Heat & Fluid Flow* and the *Numerical Heat Transfer – Part A and B* journals.